DISSERTATION
submitted
to the
Combined Faculty of the Natural Sciences and Mathematics
of
Heidelberg University, Germany
for the degree of
Doctor of Natural Sciences

Put forward by

M.Sc.: Pinyo Yonthanthum .....

Born in: Ranong, Thailand .....

Oral examination: .....

Mathematical Modeling and Simulation of the Photosynthesis in a Plant Leaf Cell

Supervisor: Prof. Dr. Dr. h. c. mult. Willi Jäger .....

Second supervisor: Prof. Dr. Dr. h. c. mult. Hans Georg Bock .....

Zusammenfassung

Die Photosynthese ist ein zentraler Prozess in Pflanzen, der in den Chloroblasten abläuft. Pflanzen nutzen die Energie von Photonen, um Wasser zu oxidieren, Sauerstoff und Wasserstoff-Ionen freizusetzen, die ihrerseits dazu beitragen, Kohlendioxid zu Zuckermolekülen zu konvertieren. Photosynthese ist ein komplexes Netzwerk physikalisch-chemischer Prozesse und besteht aus zwei Teilprozessen: Licht abhängige Reaktionen und Licht unabhängige Reaktionen. In dieser Untersuchung wird ein mathematisches Modell aufgestellt, analysiert und simuliert, das im Falle einer einzelnen Zelle eines Blattes einer C_3 Pflanze sowohl die zugrunde liegenden chemischen Reaktionen als auch die auftretenden Diffusions-Transport-Prozesse beschreibt. Dabei handelt es sich um ein Multi-Komponenten System, wobei die in den einzelnen unterschiedlichen Organellen, in den Chloroplasten, Mitochondrien, Vakuloen und Perisomen, ablaufenden Vorgänge gekoppelt werden. Vereinfachend wird angenommen, dass das Zellgebiet in fünf zeitlich fixierte Teilbereiche zerlegt ist. Diese entsprechen den Organellen, die durch das Zytoplasma miteinander verbunden werden. Die Prozesse in den einzelnen Kompartments werden durch Diffusions-Reaktions-Gleichungen beschrieben und mit Transmissionsbedingungen an den Grenzflächen Organellen-Zytoplasma gekoppelt. Es werden die Licht induzierten chemischen Reaktionen, der Calvin-Zyklus, die Stärke-Synthese, die Zucker-Synthese und die Photorespiration in einem Netzwerk zusammengefasst und untersucht. Das dabei so entstehende System von nichtlinearen partiellen Differentialgleichungen und entsprechenden Transmissionsbedingungen wird unter Einsatz eines dafür entwickelten Compilers aufgestellt und simuliert. Dazu wird eine Transformation der Differentialgleichungen auf eine schwache Formulierung vorgenommen, die es erlaubt Finite Elemente Verfahren anzuwenden. In dieser Arbeit wurde die Software Gascoigne verwendet. Eine Sensitivitätsanalyse wurde durchgeführt, deren Ergebnisse eine Reduktion des komplexen Systems erlaubt. Für dieses reduzierte System werden die räumlich zeitlich Entwicklung der wichtigsten Substanzen numerisch berechnet und diskutiert.

Abstract

Photosynthesis is a very important process in plants which occurs in chloroplasts. Plants use photon energy to oxidize water molecule, release oxygen, and convert carbon dioxide to sugar molecule. The process of photosynthesis contains two main parts: light dependent reactions and light independent reactions.

A mathematical model, which describes the diffusion-transport and related chemical reactions in a multi-component flow in a single C_3 plant leaf cell, is constructed. A sub-domain of a leaf cell is considered containing multiple organelles: chloroplast, mitochondria, vacuole, cytoplasm, and peroxisome. A typical distribution of a finite number of these organelles inside a cell is considered. The cell domain is decomposed in 5 sub-domains, separated by fixed interfaces. The interacting chemical reactions induced by light, of the Calvin cycle, the starch synthesis, sugar synthesis, respiration and photorespiration are investigated. A sensitivity analysis was performed, the results allows a reduction of the complex system. A system of partial differential equations, which describes the diffusion-transport and also related chemical reactions is formulated and simulated using the software Gascoigne. For the reduced system, the resulting flow of substances is analyzed.

Acknowledgments

This is a great opportunity to express my respect and thanks to all for the great support that make this Ph.D. research possible.

First of all, I would like to express my deepest gratitude to my supervisors, Prof. Dr. Dr. h. c. mult. Willi Jäger, Prof. Dr. Dr. h. c. mult. Hans Georg Bock, Faculty of Mathematics and Computer Science of Heidelberg University, and also Prof. Suchada Siripant, Department of Mathematics of Chulalongkorn University, for the excellent guidance, for the continuous strong support of my Ph.D study, and for providing me with the great atmosphere during my research. Thank you for all of the strong motivation, the valuable comment, and the fruitful discussion over the years of my study.

I heartily thank to all sponsors. I have been financially supported by the Ministry of Education of the Royal Thai Government, the Erasmus Mundus Mobility with Asia (EMMA), the German Research Foundation DFG (Deutsche Forschungsgemeinschaft), the Interdisciplinary Center for Scientific Computing (IWR), and the Center for Modelling and Simulation in the Biosciences (BIOMS). All of the financial supports and their contributions are gratefully acknowledged.

I would also like to take this opportunity to thank my colleagues at IWR's MathComp graduate school for their great assistant, guidance, help, and discussion. I would like to thank Dr. Michael J. Winckler for willing to help and for his best suggestions.

Many thanks to my dearest friends. All of you make my living and working experience in Heidelberg is wonderful. Special thanks to Mr. Chamroeun Khim, it would have been a lonely office and lab without him.

Finally, I would like to express my sincere gratitude to my family for their unconditional love, hearty encouragement, and endless strong support.

Pinyo Yonthanthum
Heidelberg, Germany
August 2016

Contents

Chapter 1

Introduction

State of the Art

(1) Process flow of photosynthesis

Photosynthesis is a biological process in which light energy is captured and stored by organisms in the chloroplast. The organism has a process to convert the energy of light into the biochemical energy by splitting the water molecule, transporting electrons through the organelle chain and pumping proton through the membrane. In the light-dependent reaction, oxygen (O_2) is released as a by-product. The biochemical energy, nicotinamide adenine dinucleotide phosphate-oxidase (NADPH) and adenosine triphosphate (ATP) are used to drive cellular processes [1]. The light-independent reaction includes three stages of the Calvin cycle: carboxylation, reduction and regeneration. Carbon dioxide CO_2 is captured during photosynthesis, either in the cytoplasm or chloroplast, depending on the metabolic pathway [2]. The crucial enzyme for C_3 plants, which converts CO_2 into an organic compound with 3-carbon atoms, is rubisco (ribulose-1, 5-bisphosphate carboxylase-oxygenase). Rubisco catalyzes the reaction of CO_2 with RuBP, the CO_2 acceptor. The product of the process splits into two molecules of PGA. PGA is reduced to triose phosphate in the reactions by using the product of the light-dependent reaction, ATP and NADPH [3]. Later, triose phosphate produced by the Calvin cycle are changed to a carbohydrate compound in chloroplast and sucrose in cytoplasm. Sugars produced by photosynthesis are diffused and transported from the source (leaf cells) to cells that use them for growth or

energy supply [4].

(2) Existing models

Models for chemical reactions: Several mathematical models for C_3 plant photosynthesis have been proposed. A computer model comprising light reactions, electron-proton transport, and reaction of enzymes of C_3 photosynthesis has been developed as a system of ordinary differential equations [5]. The model focuses on electron transport through photosystem II and photosystem I. Furthermore, the model also emphasises on the modeling of chlorophyll fluorescence and 810 nm absorptance signals. Caemmerer et al. [6] show that the rate of CO_2 assimilation is given as the minimum of a Rubisco limited rate, a RuBP saturating, or a chloroplast electron transport limited rate. A mathematical model was designed to interpret gas exchange measurements of CO_2 assimilation of a plant leaf. The model also represents C_3 photosynthesis in other systems such as stomatal control.

Models for radiation: Various methods have been developed to analyze the interaction of light with plant leaf elements. The Monte Carlo ray tracing method was used for the description and investigation of integrated characteristics of light scattering in a typical dicotyledon leaf. The three-dimensional internal cellular structure of the dicotyledon leaf tissues, including the epidermis, the palisade parenchyma, and the spongy mesophyll (but not including xylem, phloem, and stomata), is described and designed in [7]. The influence of the roughness of the epidermis on the reflection and absorption of light is investigated. The simulation results confirm that convex cells in the epidermis focus light on the palisade parenchyma and increase the absorption of radiation. The radiative transfer equation with a strongly anisotropic phase function of two-layer model of light scattering and absorption in plant phytoelements is constructed in [8]. In plants, light is absorb by pigments and water. Light is scattering by two type of particles: chloroplasts and intercellular spaces. An elementary light scattering event is described by the Mie theory.

Models for complex system: The diffusion of carbon dioxide from ambient air outside a plant leaf to the mesophyll cells through stomata and intercellular spaces is very important for modelling the photosynthesis process. The conductance of CO_2 from intercellular spaces to the sites of carboxylation is also limits the photosynthesis rate [9]. A numerical three-dimensional model

(3D) was developed to study CO_2 transport inside a birch leaf [10]. The structure of 3D model is including chloroplasts, palisade mesophyll cells, spongy mesophyll cells, airspaces, stomatal opening, and leaf boundary layers. This model focuses on the diffusion and transport of CO_2 in the liquid phase (mesophyll) and gaseous phase (airspaces). Evans et al. [11] show that leaves with high photosynthetic capacity per unit leaf area reduce mesophyll resistance by increasing the surface area of chloroplasts exposed to intercellular space per unit leaf area. In [12], the mathematical modeling of C_3 photosynthesis is developed and interpreted in form of carbon assimilation, or oxygen release (not sucrose or carbohydrate concentration). The photosynthesis rate depends not only on the difference of CO_2 partial gradient between inside and outside leaf, but also the stomatal conductance.

(3) Open problems

1. How is photosynthetically active radiation transfer and scattering in the C_3 plant leaf tissue?
2. How does CO_2 diffuse and react in the leaf tissue of C_3 plant?
3. How to derive a new mathematical model to describe the light-dependent reaction and the light-independent reaction for C_3 plant?
4. How is sugar transported from a leaf mesophyll cell to a leaf phloem cell?
5. How to model a three dimensional structure of C_3 plant leaf tissue including epidermis, stomata, palisade mesophyll cell, spongy mesophyll cell, intercellular space, phloem cell, and xylem cell?

According to the open problems above, these are some of the interesting question of this research:

1. *What is the dynamics of the products in the light reaction (O_2, NADPH, and ATP)?*
2. *What is the dynamics of the consumptions in the carbon reaction (CO_2)?*
3. *What is the dynamics of the products in the carbon reaction (PGAL or TP)?*

4. *What is the dynamics of the products in the starch reaction (starch)?*

5. *What is the dynamics of the products in the sugar reaction (sucrose)?*

Aim of the PhD thesis

The aim of this PhD thesis is to develop and to simulate a mathematical model for the photosynthesis process in plant leaves. The relevant sub-processes to be integrated in a sufficiently comprehensive model applicable to the real life situation in plant growth:

(1) *Chemical reactions*: chemical reactions involved in the conversion of carbon dioxide (CO_2) to 3-Phosphoglycerate (PGAL) and to triose sugar (3-carbon atoms or C_3)

(2) *Radiation*: radiation absorption and the activation of conversion process by light

(3) *Complex system*: integrated network of the chemical reactions for the multi-chemical species in the multi-compartments

Research results and contributions

Fixed domain model: A mathematical model for photosynthesis of a C_3 plant leaf cell describes the diffusion, reaction, and transport of the chemical species in each sub-domains at specific times. The light-dependent model describes the process of light absorption, water photolysis, electron transport chain, formulation of NADPH, and generation of ATP. The reaction-diffusion model describes the complex network of Calvin cycle, photorespiration reaction, starch synthesis and sucrose synthesis. Most of the chemical reactions are taking places in chloroplast. However for the photorespiration reactions, the chemical reactions are performed in 3 different compartments: chloroplast, mitochondria, and peroxisome. There are some chemical species transports from one compartment to another. Most of chemical species in C_3 photosynthesis are diffuse in the cell. Some of them are only exists in one compartment. So that, the coupling of the photorespiration have to taken to account for the modeling of photosynthesis for a C_3 plant leaf cell. The mathematical

model focuses on 5 sub-domains including chloroplast, mitochondria, peroxisome, cytoplasm, and vacuole. The appropriate initial-boundary conditions are derived for the model. The transmission conditions of some chemical species are depend on the difference in its concentration on the both sides the interface.

Weak form: A variational formulation of the light-dependent model and the reaction-diffusion model is derived. The initial-boundary and transmission conditions are also taken to account.

Photosynthesis in silico: A computer simulation for photosynthesis of a C_3 plant leaf cell focuses on 2 sub-models: the light-dependent model and the reaction-diffusion model. A dimensional cell and its organelles of a C_3 plant are represented in a squircle shape. The computational domain boundary and interfaces are continuous and smooth. The numerical simulation for photosynthesis of a plant leaf cell illustrates the concentration of each chemical species in the 2D domain at a specific time. Various of time step sizes and mesh refinement levels are applied to investigate the convergence of numerical solutions. As the results of the simulation, the dynamics of the productions and consumptions of the target chemical species: O_2, NADPH, ATP, CO_2, TP, starch, and sucrose, agreed with the biological observation.

Outline of this thesis

Chapter 2 provides a biological background about the anatomy of plant leaf cells and the physiological processes of plant leaf photosynthesis together with photorespiration, starch and sucrose synthesis.

In Chapter 3, a mathematical model for photosynthesis of a plant leaf cell is developed. The model is formulated on a fixed domain and describes the mechanism of chemical species in the light-dependent reaction, the light-independent reaction, the photorespiration process, the starch synthesis, and the sucrose synthesis. The 3 dimensional domain of a single cell containing with 5 sub-domains: Cytoplasm, Chloroplast, Peroxisome, Mitochondria and Vacuole are defined. In the sub-domains of plant leaf cell, the chemical reactions are taken to account to the model. By applying the the law of Mass Action Kinetics (MAK) or the Michaelis–Menten Kinetics (MMK), the reaction-diffusion equation of multi-chemical species are given for each sub-domains. A set of initial, boundary and transmission conditions with respect

to sub-domains are proposed.

Chapter 4, the variational formulation of the fixed domain model is derived.

In chapter 5 presents the numerical methods used to simulate the develop mathematical model. The numerical simulations are performed by using the finite element library Gascoigne. The numerical results are discussed and compared with the biological observation.

In Chapter 6 we present the discussions, summarize the conclusions, and also provide an outlook for the future research.

Chapter 2

Biological background

This chapter describes the structure of plant leaf and its physiology. In higher plants, the main function of a leaf is to produce food in the form of sugar molecules and distribute them to the rest of plant organs. In this chapter we aim to give take a closer look at the biological and chemical processes called photosynthesis and some related processes. First of all, we will start with the structure of plant leaf in Section 2.1, and in Section 2.2 we will introduce the process of photosynthesis from the light capture to the Calvin cycle in detail. Furthermore, we will next investigate the process that transforms photosynthetic products of the Calvin cycle to starch and sugar molecules in Section 2.3. After giving the details of photosynthesis and its final product process, we will finally identify the environment factors and the physiological process, called photorespiration, that affect the rate of photosynthesis in Section 2.4.

2.1 Plant leaf structure and function

Leaves are broad, flat and thin, which are found in various sizes and shapes. The plant leaf also contains several types of unique tissue structures that plays very specific roles (see also Figures 2.1 and 2.2). Most leaves have an upper (adaxial) and lower (abaxial) surfaces that differ in color, roughness and some other features. A leaf is an organ of a vascular plant that is made of many layers. The layers inside are sandwiched between two outermost layers, typically one cell thick, called epidermis. There is a thin, waxy multilayered structure

that covers the outer cell walls of the epidermis called a cuticle. A plant cuticle restricts the passage of water and gases into and out of the plant. The cuticle also protects the leaf from bacteria, insects, parasitic fungi, and other pests. Upper epidermis layer is a single layer of clear cells that allows light to pass through and prevents the loss of water. Lower epidermis layer is also a single layer of clear cells. A pairs of specialized cells called guard cells are found on the lower epidermis of the leaf. Each pair of guard cells forms a microscopic pore called stoma (plural stomata). Stomata on the leaf underside allow gas exchange (water, carbon dioxide and oxygen) of leaves by controlling the dimension of stomatal pore. Normally the stomata are open during the day and closed at night. [4, 13]
As mentioned previously, the epidermis is usually one cell layer thick. However, in some plants that live in very cold, very dry, or very hot conditions, the epidermis may be several layers thick to prevent a water loss from transpiration. The epidermis are more elongated in the leaves of monocot plants than in those of dicot plants. Between the upper and lower epidermal layers are layers of cells known as the mesophyll that consists of palisade parenchyma and spongy parenchyma. The palisade parenchyma (also called the palisade mesophyll) contains long column cells that are packed tightly together. Some plant species may be have more than one layers. The palisade mesophyll cells contain a vast number of chloroplasts and are the main cells where most of the photosynthesis takes place. The spongy mesophyll cells consist of irregularly shaped cells surrounded by large air spaces. The connection of the air spaces between spongy mesophyll cells allows gas exchange between stomata and photosynthetic cells. The leaf also contains vascular bundles tissue composed of phloem and xylem. The phloem transports the photosynthetic products (sugar ans starch) from the mature leaves to the area of growth and storage part of the plant. The xylem transports water and mineral ions to the leaves. [4, 13, 14]

A summary of the plant leaf structures and its functions is shown in Table 2.1.

Plant cell organelles and their functions

The plant cell contains various types of organelles (see also Figure 2.3). Each of them has a unique form and specific functions. All plant cells have the same basic eukaryotic organization: They contain a nucleus, a cytoplasm,

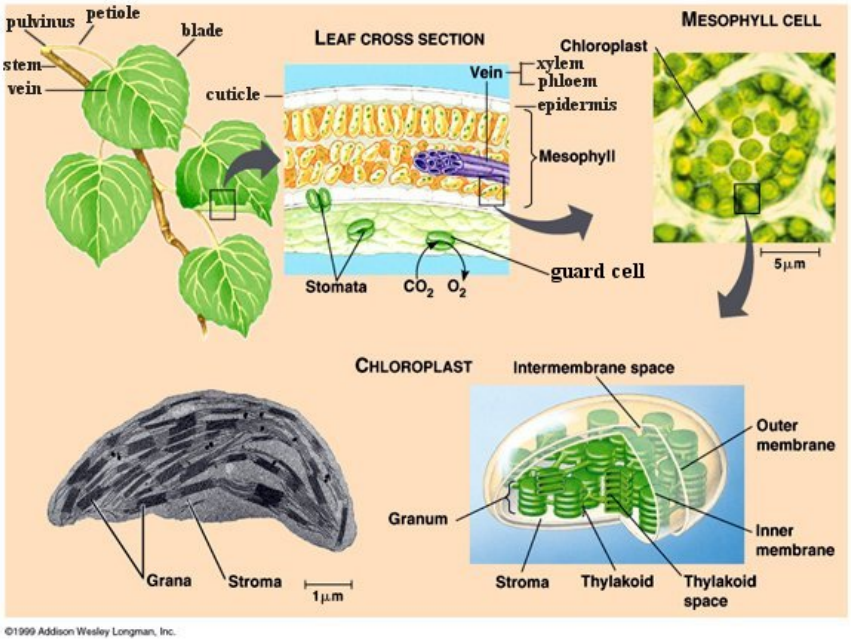

Figure 2.1: Cross section of a typical leaf, its external and internal structures (https://universe-review.ca)

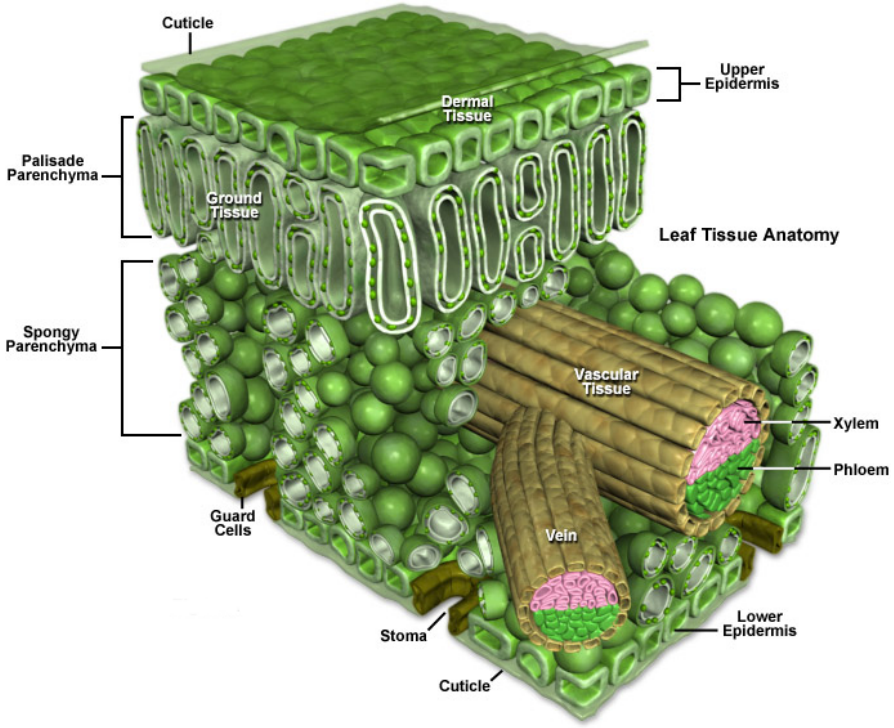

Figure 2.2: Leaf tissue anatomy (http://micro.magnet.fsu.edu)

Table 2.1: Plant leaf structure and its function

Layer & Adaptation	**Function**
Cuticle: Waterproof	The waxy, waterproof layer that cuts down the water lost by evaporation and protects against parasitic fungi.
Upper Epidermis: Transparent	A single layer of cells that are transparent and contain no chloroplast, allowing light to pass straight through.
Palisade Layer: Contains chloroplasts	This layer is made up of palisade cells, which contain chloroplasts. This is where most of the photosynthesis takes place.
Vein: vascular bundles	The vein contains tubes called the xylem and phloem. The xylem brings water and salts to the leaf for photosynthesis. The phloem transports the carbohydrates from the photosynthetic sites to the growing tissues and storage tissues.
Spongy Layer: Irregularly shaped cells with air spaces between them.	This layer consists of irregularly shaped cells with large air spaces between them allowing gas exchange (diffusion) between stomata and photosynthesising cells.
Lower Epidermis: Contains lots of tiny holes.	This layer contains lots of tiny pores called stomata at regular intervals. These allow gases to diffuse in and out of the leaf.

vacuole, and subcellular organelles. These organelles include structures such as chloroplasts, endoplasmic reticulum (ER), Golgi apparatus, mitochondria, and ribosomes. Plant cells are enclosed in membranes that define their boundaries. Like the fungi, plant cells have a cellulosic rigid cell surface structure called cell wall which supports the cell growth, protects the cell, and allows the gas and liquid diffusion between inside and outside the cell. Inside the cell wall, a thin layer of protein and fat also known as cell membrane are surrounds the cell. The cell membrane is semi-permeable, protects and controls movement of materials and substances into or out of the cell.

The nucleus is a large, oval shaped body surrounded by the nuclear membrane and contains many organelles, including one nucleolus or more. The nucleolus is a densely granular region that is the site of ribosome synthesis. The nucleus also controls the activities of the cell and contains the genetic information.

Cytoplasm is the jellylike cellular matter outside the cell nucleus in which the cytosol, the cytoskeleton fibers, and the membrane-limited organelles are located.

The vacuole is the largest membrane-bounded organelle in a plant that contains a fluid-filled sacs including water, inorganic ions, sugars, organic acids, pigments, metabolic and toxic wastes. It also helps maintain the shape of the cell.

Chloroplasts are the green round, oval, or disc-shaped organelles with a double membrane (inner and outer membrane) containing chlorophyll and other pigments. Between the outer and inner layers is a gap, called the intermembrane space. Chloroplasts are the site of photosynthesis in plants and other photosynthetic organisms. They are the most important characteristic structures of plants since their ability to captures the photon of light, converts light energy into chemical energy, and releases the oxygen gas. Chloroplasts also contain stroma and a stack of thylakoid disks, called granum (see also Figures 2.1 and 2.4). The connection between two granum is called stroma lamellae. Stroma is the fluid component surrounding the thylakoid membranes of the chloroplast containing dissolved enzymes and starch granules. The thylakoid discs are disc-shaped membrane structures that contain chlorophyll, carotenoids, and other pigments. The pigments are chemical compounds that reflect only certain wavelengths of visible light. Chlorophyll is a group of magnesium-based molecules able to captures the photon of light.

The endoplasmic reticulum is a network of sacs or membranes that connects to the nuclear envelope and cell membrane. It carries materials through the cell, and transports chemical compounds between inside and outside of the cell.

The Golgi apparatus (also called Golgi body or Golgi complex) is a layered, flattened organelle that look like a stack and is located near the nucleus. The golgi body is the distribution and shipping department for the cell's chemical products. It modifies proteins and carbohydrates for exporting them out of the cell.

Mitochondria are the spherical to rod-shaped organelles with a double membrane in the cytoplasm. These specialized structure is the site for most reactions in the aerobic cellular respiratory process. Mitochondria break down sugar (glucose) molecules and carbohydrate to energy, particularly when light is not available for the chloroplasts to produce energy. Ribosomes are the tiny organelles composed of proteins and ribosomal RNA that also are site of cellular protein synthesis. [4, 13, 14]

2.2 Plant photosynthesis

In plants and certain other organisms, photosynthesis is a very important process by which the solar light energy is transformed into chemical energy of organic compounds that can be later delivered to fuel of the living organisms activities. These chemical energy is stored in the bonds of sugar, which are synthesized from water, carbon dioxide, minerals, and energy-rich organic compounds. In plant photosynthesis, gaseous oxygen is also released as a by-product or waste product that is so vital to life on this planet. Plant leaf cells are the main sites where photosynthesis takes place. This process is performed differently by various plant species. However the first step always starts when a photon of light is absorbed by a reaction center complex, a group of proteins that receive energy and covert it to chemical energy [4]. In green plants, the proteins are embedded in the thylakoid of chloroplasts, which are plentiful in leaf cells. Photosynthesis includes two main biochemical processes: light reactions and dark reactions (see also Figure 2.5). The first process of photosynthesis also known as the energy transduction reactions or the light dependent reactions. During this step, solar energy is transacted to chemical energy in the form of nicotinamide adenine dinucleotide phosphate (NADPH) and

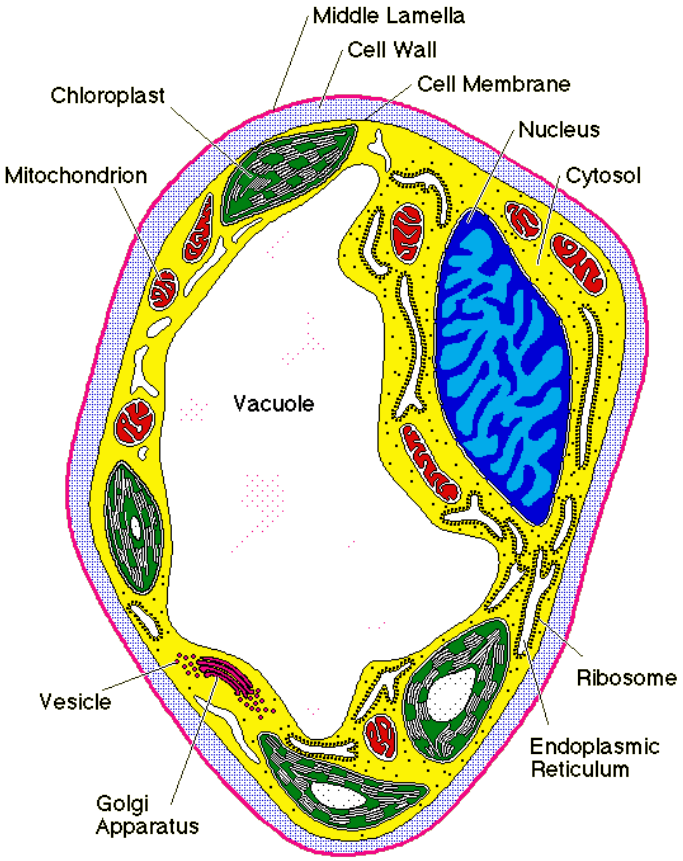

Figure 2.3: The cell organelles (http://plantphys.info)

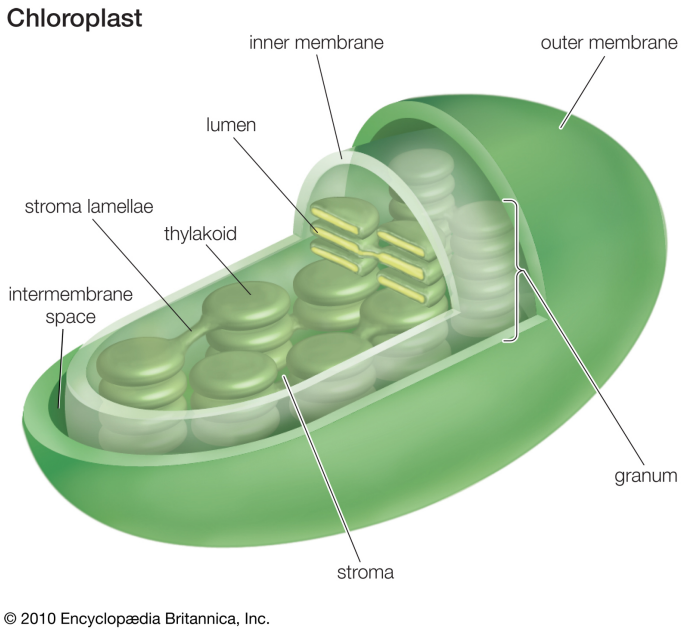

Figure 2.4: The structure of chloroplast (www.britannica.com)

adenosine triphosphate (ATP), molecular unit currency. The dark reactions are also known as the carbon assimilation reactions or the light-independent reactions. By using the ATP and NADPH, atmospheric carbon dioxide is fixed and reduced to organic compounds that later converts to carbohydrates and sugars. In general photosynthesis is the opposite of cellular respiration, in which glucose and other compounds are oxidized to produce carbon dioxide and water, and to release exothermic chemical energy to drive the organism's metabolism. In general, photosynthesis and cellular respiration (also called dark respiration) are almost the opposite process because dark respiration uses oxygen and glucose while photosynthesis produces oxygen and sugar. Moreover, cellular respiration releases carbon dioxide and water while photosynthesis uses them as the reactants.

The general chemical equation for photosynthesis:

$$6\,CO_2 + 6\,H_2O \xrightarrow[\text{chloroplast}]{\text{light energy}} C_6H_{12}O_6 + 6\,O_2$$

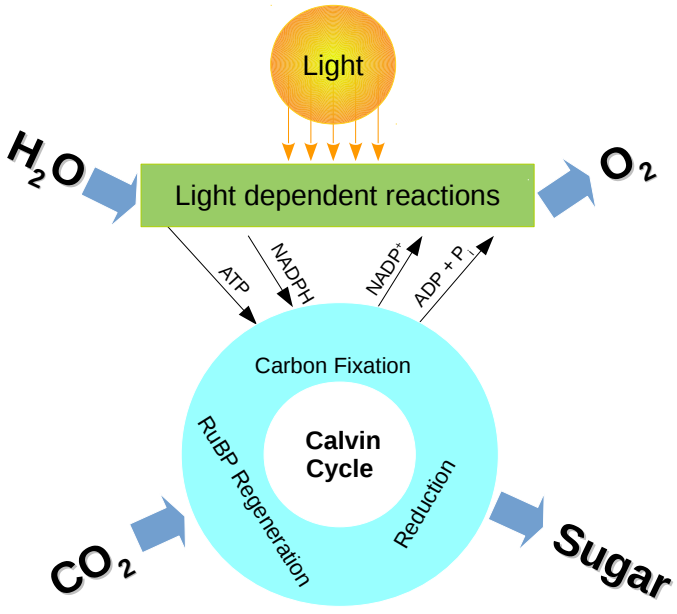

Figure 2.5: The overview of photosynthesis process

Light-dependent reactions

In plants, the general chemical equation for the light dependent reactions is:

$$2\,H_2O + 2\,NADP^+ + 3\,ADP + 3\,P_i \xrightarrow[\text{chloroplast}]{\text{light energy}} 2\,NADPH + 2\,H^+ + 3\,ATP + O_2$$

In details, the energy transduction reactions consist of four sub-processes including light harvesting, water photolysis, electron transport chain, and generation of NADPH and ATP (see also Figure 2.5). Next, we will discuss some of the mechanism, the biological and chemical process for each of the subprocess.

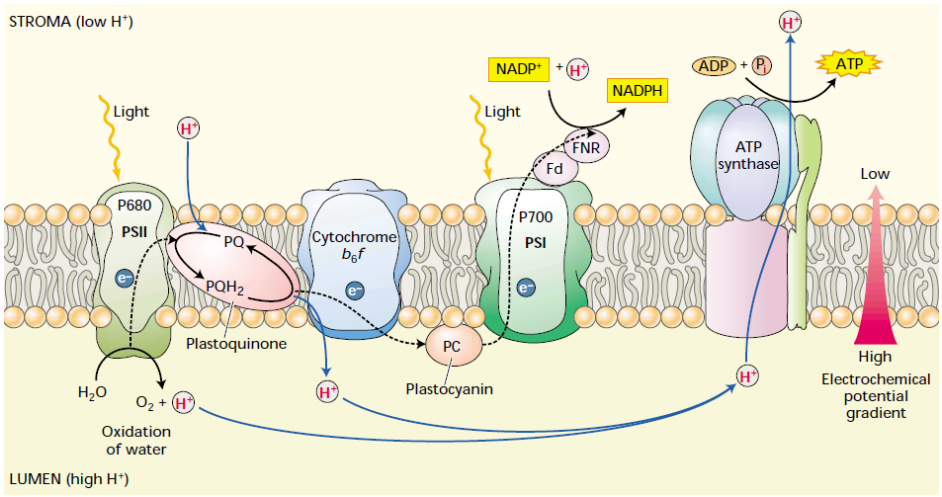

Figure 2.6: Light dependent reactions of photosynthesis at the thylakoid membrane (see also [4])

Light harvesting

All of higher plant have a system to collect the solar energy called antenna complex, a group of pigment molecules that cooperate to absorb light energy and transfer it to a reaction center complex [4]. The antenna complex collects light and transfers the energy to a neighboring group of proteins and pigments called the reaction center complex. In the light harvesting complex system, chlorophylls play an important role as a typical pigment of photosynthetic organisms. However, the light energy that is absorbed by carotenoids

is also transfered to chlorophyll; these activities make them into accessory pigments. In plants, the photosynthetic pigments absorb the light on specific wavelengths. With the absorption spectrum band between 400 and 700 nm, the chlorophylls absorb mainly blue and red wavelengths of light that make them appears green. Other accessory pigments include carotenoids, that present yellow, absorb photons from a broad range of violet and blue-green regions of the spectrum (between 420 and 480 nm). The antenna complex, chlorophyll molecules, accessory pigments, and reaction centers complex are organized into functional units called photosystems, which are located in the thylakoid membrane. After the photon energy is absorbed by antenna pigments, this energy is passed to another pigments by resonance energy transfer until it reaches to a specific chlorophyll molecule at the reaction center of the photosystem. Upon receipt of enough energy, an electron of the chlorophyll molecule turns from a ground state to an excited state, then ejects from the chlorophyll, and passes along to a protein that performs as a primary electron acceptor (see also Figure 2.7). For the photosynthesis of plants, there

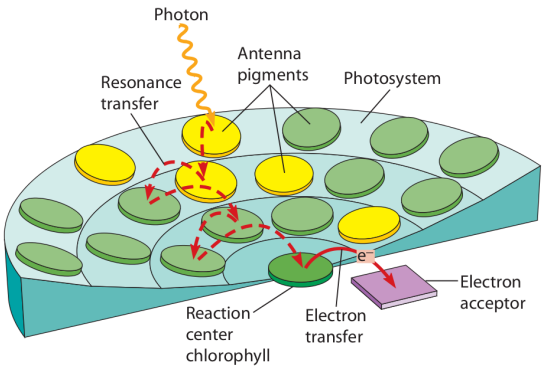

Figure 2.7: The energy transfer in the photosystem (see also [14])

are exist two distinct photochemical complexes also known as Photosystem I and II (PSI and PSII) that work together in series (see also Figure 2.6). Each photosynthesis system has a different an absorption maximum. Photosystem I can absorbs the far-red light of wavelengths more than 680 nm well, whereas photosystem II preferentially absorbs the red light of wavelength 680 nm. Moreover, photosystem II is also performs very poorly with the far-red light of wavelength greater than 690 nm. By the photon absorption, chlorophyll *a* molecules of the reaction center of each photosystem will be excited simultaneously. In Figure 2.6, P680 and P700 refer to the maximum absorption wavelength of the chlorophyll of the reaction center in photosystem II and I, respectively. The two photosystems also produce different products helping

them to work together. Photosystem I produces a strong reductant, capable of reducing $NADP^+$, and a weak oxidant. On the other hand, Photosystem II produces a very strong oxidant, capable of oxidizing water, and a weaker reductant than is produced by photosystem I.

Water photolysis

Since the photons of light strike photosystems I and II simultaneously, when the photons strike photosystem II, the energized electrons are passed from the reaction center of photosystem II to a primary electron acceptor molecule, pheohpytin (Pheo). The electrons lost by photosystem II are replaced back by a process called water photolysis or water splitting. By the photolysis process, two water molecules are oxidized by photosystem II, four hydrogen ions are released to the lumen of the thylakoid, free electrons are transfered to the reaction center of photosystem II, and one molecule of diatomic oxygen is produced as a by-product of light-dependent reactions (see also Figure 2.6). The general chemical equation for water photolysis is:

$$2\,H_2O \xrightarrow{\textbf{PSII}} O_2 + 4\,H^+ + 4\,e^-$$

Electron transport chains

According to the photon absorptions, electrons of the chlorophyll molecule of the reaction center in photosystem I are excited and then passed to the primary electron acceptor molecule called ferredoxin (Fd). These electrons are later transfered from ferredoxin to $NADP^+$ molecules by using a mobile carrier called ferredoxin-$NADP^+$ reductase (FNR). The electrons lost by photosystem I are replaced by the electrons from a series of protein carriers including pheohpytin, platoquinone (PQ), cytochrome b_6f complex (Cyt_{b_6f}), and plastocyanin (PC), respectively.

$$H_2O \rightarrow \textbf{PSII} \rightarrow \text{Pheo} \rightarrow \text{PQ} \rightarrow Cyt_{b_6f} \rightarrow \text{PC} \rightarrow \textbf{PSI} \rightarrow \text{FR} \rightarrow \text{FNR} \rightarrow NADP^+$$

A mechanisms of noncyclic electron is transported from H_2O molecule to $NADP^+$ molecule through the line of protein complexes as shown in Fig-

ure 2.6 also known as electron transport chains (ETC) or Z scheme. While cytochrome b_6f complex oxidizes plastohydroquinone (PQH_2) molecules that were reduced by PSII and delivers electrons to PSI, two hydrogen ions are transported from stroma to lumen space across the thylakoid membrane.

NADPH and ATP generations

According to the electron transport chain, two of the free electrons that are releases from ferredoxin-$NADP^+$ reductase combining with $NADP^+$ and H^+ generate one energy compound NADPH in the stroma.

$$\boxed{NADP^+ + 2\,e^- + H^+ \longrightarrow NADPH}$$

During the water photolysis, many proton ions are produced in the lumen of thylakoid. Moreover, the oxidizing of plastohydroquinone by cytochrome b_6f complex also moves proton ions from stroma (outside) to lumen (inside). As a results of two mechanisms, the different concentration of H^+ between two sides of thylakoid membrane generates the proton gradient force (inside is higher than outside). As protons pass through the thylakoid membrane (from lumen to stroma), a combination of adenosine diphosphate (ADP) molecules and phosphate ions produces chemical energy in the form of ATP and releases it into the stroma (see also Figure 2.6).

$$\boxed{ADP + P_i \longrightarrow ATP}$$

As a consequence of the light harvesting, water photolysis, electron transport chains, and generations of NADPH and ATP that efficiently working together, two water molecules and eight photons of light produces two molecules of NADPH, three molecules of ATP, and releases one molecule of diatomic oxygen.

Light-independent reactions

The light independent reactions of photosynthesis also known as the Calvin cycle-Benson or Calvin cycle, a chemical process that uses NADPH, ATP and some enzymes captures carbon dioxide, and produces sugar molecules.

Plants that fix carbon dioxide and convert it to three-carbon sugar molecules as a final product of photosynthesis are also called C_3 plant. In general, the chemical equation for the light-independent reactions is

$$3\,CO_2 + 9\,ATP + 6\,NADPH + 6\,H^+ \longrightarrow C_3H_6O_3 + 9\,ADP + 8\,P_i + 6\,NADP^+ + 3\,H_2O$$

Calvin cycle

With the discovery of the carbons assimilation reactions of photosynthesis by M. Calvin and colleagues in 1950, this cycle incorporated with the key enzyme called RuBisCO and the sugar molecule produced is called Glyceraldehyde 3-phosphate (G3P or PGAL) in the final step. The Calvin cycle takes place in the stroma of the chloroplast. In details, this cycle consists of three main phases including the carbon fixation phase, the reduction phase, and the RuBP regeneration phase (see also Figure 2.8). In this thesis we focus only on the photosynthesis of C_3 plants. Next, we will discuss the biological and chemical process for each sub-processes in detail.

The carbon fixation phase

The carbon fixation phase is also known as the carboxylation phase. In this phase, rubisco catalyzes the carboxylation of three molecules Ribulose 1,5-bisphosphate (RuBP) by dissolved CO_2 and water, yielding six molecules of 3-Phosphoglycerate (PGA).

$$3\,RuBP + 3\,CO_2 + 3\,H_2O \longrightarrow 6\,PGA + 6\,H^+$$

The reduction phase

In the second phase, 3-Phosphoglycerate is reduced to 1,3-Bisphosphoglycerate (BPGA) using six molecules of ATP. After phosphorylation of the carboxylic group, BPGA is transformed into six molecules of Glyceraldehyde 3-phosphate requiring six of NADPH. The product of this step is also referred to as 3-phosphoglyceraldehyde or, more generically, as triose phosphate (3-carbon carbohydrates).

$$6\,\mathrm{PGA} + 6\,\mathrm{ATP} \longrightarrow 6\,\mathrm{BPGA} + 6\,\mathrm{ADP}$$
$$6\,\mathrm{BPGA} + 6\,\mathrm{NADPH} + 6\,\mathrm{H^+} \longrightarrow 6\,\mathrm{PGAL} + 6\,\mathrm{NADP^+} + 6\,\mathrm{P_i}$$

The RuBP regeneration phase

In the final stage of the Calvin cycle, three molecules of RuBP is regenerated though a series of ten enzyme-catalyzed reactions using three molecules of ATP. The list of substances and products along this phase are Dihydroxyacetone phosphate (DHAP), Fructose-1,6-bisphosphatase (FBP), Fructose 6-phosphate (FP), Erythrose-4-phosphate (EP), Xylulose-5-phosphate (XP), Sedoheptulose-1,7-bisphosphate (SBP), Sedoheptulose-7-phosphate (SuP), Ribose-5-phosphate (RP), and Ribulose-5-phosphate (RuP), respectively.

$$2\,\mathrm{PGAL} \rightleftharpoons 2\,\mathrm{DHAP}$$
$$\mathrm{PGAL} + \mathrm{DHAP} \longrightarrow \mathrm{FBP}$$
$$\mathrm{FBP} + \mathrm{H_2O} \longrightarrow \mathrm{FP}$$
$$\mathrm{FP} + \mathrm{PGAL} \longrightarrow \mathrm{EP} + \mathrm{XP}$$
$$\mathrm{EP} + \mathrm{DHAP} \longrightarrow \mathrm{SBP}$$
$$\mathrm{SBP} + \mathrm{H_2O} \longrightarrow \mathrm{SuP} + \mathrm{P_i}$$
$$\mathrm{SuP} + \mathrm{PGAL} \longrightarrow \mathrm{RP} + \mathrm{XP}$$
$$2\,\mathrm{XP} \longrightarrow 2\,\mathrm{RuP}$$
$$\mathrm{RP} \longrightarrow \mathrm{RuP}$$
$$3\,\mathrm{RuP} + 3\,\mathrm{ATP} \longrightarrow 3\,\mathrm{RuBP} + 3\,\mathrm{ADP} + 3\,\mathrm{H^+}$$

2.3 Products of photosynthesis

The final products of the light-dependent reactions and the Calvin cycle are ATP, NADPH, and triose phosphate, respectively. As we have previously discussed, ATP and NADPH are used as an energy budget for the Calvin cycle. By partitioning off the final product of the Calvin cycle, some of triose phosphates are transported from stroma to cytosol. As a result, starch and sugar molecules are produced in the photosynthetic cells.

Starch synthesis

During the day times, the product of the Calvin cycle is converted to a polysaccharide carbohydrate consisting of a large number of glucose monosaccharide units joined together, known as starch. The chemical process that transformed triose phosphatase to starch molecule, called starch synthesis, takes place in the stroma of chloroplast. In order to form the soluble starch, Amylopactin (A), many substrates are involves including Dihydroxyacetone phosphate (DHAP), Glyceraldehyde 3-phosphate (PGAL), Fructose 1,6-bisphosphate (FBP), Fructose 6-phosphate (FP), Fructose 2,6-bisphosphate (FTBP), Glucose 6-phosphate (GSP), Glucose 1-phosphate (GP), Primer, and ADP-glucose (ADPG) (see also Figure 2.9). The list of chemical reactions of starch synthesis are collected and summarized in Table 2.2.

Sucrose synthesis

Triose phosphates are not only converted to starch molecules but also synthesized to one type of sugar molecules, a highly soluble disaccharide, called sucrose. As triose phosphates are transported from the stroma, sucrose synthesis takes place in the cytosol of the cells . Sucroses produced by photosynthesis are transported from the photosynthetic cells (source) to the nonphotosynthetic cells (sink); for example, stems, grains, and roots. In all plants, sucrose is made from two molecules of fructose 6-phosphate (FP). One molecule is activated with UDP and converted to UDP-glucose (UDPG). As the reactions of sucrose 6-phosphate reacts with UDP-glucose and fructose 6-phosphate, one molecule of sucrose 6^F-phosphate (SSP) is produced. In the final step, sucrose 6^F-phosphate reacts with phosphatase to generate sucrose (see also Figure 2.9 and table 2.2).

In plants, the photosynthesis process requires photons of light, water, carbon dioxide, and necessary substrates and enzymes to produces triose phosphate as a final product of carbon assimilation reactions. Triose phosphate later converts to starch in the stroma of the chloroplast and to sucrose in cytosol. However, there are some factors that directly affect to the rate of photosynthesis. In the next section, we will investigate the limiting factors of photosynthesis in C_3 plants.

2.4 Factors affecting photosynthesis

Before we consider the limiting factors, it is very important to know that how to measure the rates at which photosynthesis takes place. Due to the complexity of the photosynthesis process, there are many products released for each sub-processes. Some approaches have been developed to measure the photosynthesis rate; for example, gas exchange and biomass. For a scale of canopy or single leaf, the methods to calculate the rate of gas exchange include measuring the uptake of CO_2 and the production of O_2 as indicators of the photosynthesis rate. The amount of dry mass or fresh mass can be represented as the rate of photosynthesis. In a tissues or a single cell scale, measuring the increase or decrease of concentration for the chemical products, for example, ATP, NADPH, triose phosphate, carbohydrates, and sucrose, also show the photosynthesis rate in more precise calculations.

C_3 plants, the main factors affecting the photosynthesis rate are external and internal influences including light intensity and wavelength, temperature and carbon dioxide levels. F.F. Blackman (1905) shows that the rate of photosynthesis as a function of light intensity, temperature and CO_2 concentration [15].

Light intensity and temperature

According to the principle of the limiting factors [15, 16] states that the overall rate of photosynthesis is limited by the impact of the slowest factors; the slowest step or the shortest supply. At constant temperature, the rate of carbon assimilation varies with light intensity. The initial part, the rate of photosynthesis increases proportionally with light intensity. In strong light and limiting CO_2 concentrations, increasing temperature also increases the rate of photosynthesis. However, at higher light intensity, the rate of carbon assimilation reaches to a saturation point. At constant irradiance, increasing the temperature over a limited range increases the rate of photosynthesis. At low light intensity, increasing the temperature has small impact on the rate of photosynthesis. Moreover, there is no temperature effect at high CO_2 concentrations and low light intensity. In the complexity of light-dependent reactions of photosynthesis process we can see that another limiting factor is the wavelength of light.

Carbon dioxide levels

As the light-independent reactions occur, increasing of CO_2 concentrations also increases sugars until limited by other factors. In this case, the enzyme RuBisCO plays an important role to control the rate of photosynthesis. As we mentioned above, RuBisCO captures carbon dioxide in the Calvin cycle. However, at low CO_2 concentration, this enzyme will bind with oxygen instead of carbon dioxide. This process, known as photorespiration, requires ATP and releases CO_2 , but does not produce any sugars (see 2.10). The site of photorespiration involves in three organelles including chloroplasts, mitochondria and peroxisomes (see also Figure 2.11).

Photorespiration

Photorespiration also known as C_2 oxidative photosynthesis because the final product of this reactions is two-carbon sugar molecules, 2-Phosphoglycolate (PGC). This process involves a complex network of chemical reactions and many of chemical species including RuBP, 3-Phosphoglycerate (PGA), 2-Phosphoglycolate (PGC), Glycolate (GCL), Glyoxlate (GOL), Serine (Ser), Glycine (GC), 2-oxoglutarate (OGA), Methylene-[GDC] (MLG), Hydroxypyruvate (HDP), Glycerate (GA), Glutamate (GMa), Glutamine (GMi), Fd_{red} (Fdr), and Fd_{oxid} (Fdo). The details of chemical reactions show in Figure 2.11 and table 2.2. The reactions of photorespiration process are performs in 3 difference organelles including chloroplast, mitochondria, and peroxisome. Since sharing the same enzyme, photorespiration reduces the efficiency of photosynthesis.

2.5 Summary

As the complexity of the chemical process that occurs in different sub-domains, we will now summarize the complex network and the chemical reactions of C_3 plant photosynthesis, starch and sucrose synthesis, and photorespiration in the Table 2.2. According to chemical network and locations, it is easy to see that there are some chemical species moving in or out from one sub-domain to another neighborhood sub-domain. We have are now collected all of them and they are shown in figure 2.12 and Table 2.3.

Table 2.2: Chemical reactions of C_3 plant leaf photosynthesis, starch and sucrose synthesis, and photorespiration in Chloroplast, Mitochondria, Peroxisome, and Cytoplasm.

Line	Chemical reaction
	Photosynthesis: *Light dependent reactions*
1	$2\,H_2O \longrightarrow O_2 + 4\,H^+ + 4\,e^-$
2	$NADP^+ + 2\,e^- + H^+ \longrightarrow \mathbf{NADPH}$
3	$ADP + P_i \longrightarrow \mathbf{ATP}$
	Photosynthesis: *Calvin cycle*
4	$3\,RuBP + 3\,\mathbf{CO_2} + 3\,H_2O \longrightarrow 6\,PGA + 6\,H^+$
5	$6\,PGA + 6\,ATP \longrightarrow 6\,BPGA + 6\,ADP$
6	$6\,BPGA + 6\,NADPH + 6\,H^+ \longrightarrow 6\,\mathbf{PGAL} + 6\,NADP^+ + 6\,P_i$
7	$2\,PGAL \rightleftharpoons 2\,\mathbf{DHAP}$
8	$PGAL + DHAP \longrightarrow FBP$
9	$FBP + H_2O \longrightarrow FP + P_i$
10	$FP + PGAL \longrightarrow EP + XP$
11	$EP + DHAP \longrightarrow SBP$
12	$SBP + H_2O \longrightarrow SuP + P_i$
13	$SuP + PGAL \longrightarrow RP + XP$
14	$2\,XP \longrightarrow 2\,RuP$
15	$RP \longrightarrow RuP$
16	$3\,RuP + 3\,ATP \longrightarrow 3\,RuBP + 3\,ADP + 3\,H^+$
	Starch synthesis
17	$PGAL \rightleftharpoons DHAP$
18	$DHAP + PGAL \longrightarrow FBP$
19	$FBP + H_2O \longrightarrow FP + P_i$

Continued on next page

Table 2.2 – continued from previous page

Line	Chemical reaction
20	$FP + ATP \longrightarrow FBP + ADP$
21	$FP + PP_i \longrightarrow FBP + P_i$
22	$FP + ATP \longrightarrow FTBP + ADP$
23	$FTBP + H_2O \longrightarrow FP + P_i$
24	$FP \longrightarrow GSP$
25	$GSP \longrightarrow GP$
26	$GP + ATP \longrightarrow ADPG + PP_i$
27	$ADPG + Primer \longrightarrow \mathbf{A} + ADP,$ (**A**, starch)
	Sucrose synthesis
28	$PGAL \rightleftharpoons DHAP$
29	$DHAP + PGAL \longrightarrow FBP$
30	$FBP + H_2O \longrightarrow FP + P_i$
31	$FP + ATP \longrightarrow FBP + ADP$
32	$FP + PP_i \longrightarrow FBP + P_i$
33	$FP + ATP \longrightarrow FTBP + ADP$
34	$FTBP + H_2O \longrightarrow FP + P_i$
35	$FP \longrightarrow GSP$
36	$GSP \longrightarrow GP$
37	$GP + UDP \longrightarrow UDPG + PP_i$
38	$UDPG + FP \longrightarrow UDP + SSP$
39	$SSP + H_2O \longrightarrow \mathbf{S} + P_i,$ (**S**, sucrose)
	Photorespiration
40	$2\,RuBP + 2\,O_2 \longrightarrow 2\,PGC + 2\,PGA$
41	$2\,PGC + 2\,H_2O \longrightarrow 2\,GCL + 2\,P_i$
42	$2\,GCL + 2\,O_2 \longrightarrow 2\,GOL + H_2O_2$
43	$2\,H_2O_2 \longrightarrow 2\,H_2O + O_2$
44	$2\,GOL + 2\,GMa \longrightarrow GC + OGA$
45	$GC + NAD^+ + GDC \longrightarrow CO_2 + NH_4^+ + NADH + MLG$
46	$MLG + GL + H_2O \longrightarrow Ser + GDC$
47	$Ser + OGA \longrightarrow HDP + GDC$
48	$HDP + NADH + H^+ \longrightarrow GA + NAD^+$
49	$GA + ATP \longrightarrow PGAL + ADP$
50	$GMa + NH_4^+ + ATP \longrightarrow GMi + ADP + P_i$
51	$OGA + GMi + 2\,Fd_{red} + 2\,H^+ \longrightarrow 2\,GMa + 2\,Fd_{oxid}$

Group	From	To	Chemical species
1	Cytosol	Chloroplast	CO_2, GA, OGA, NH_4^+
2	Chloroplast	Cytosol	PGAL, DHAP, O_2, GCL, GMa
3	Cytosol	Mitochondria	GC, O_2
4	Mitochondria	Cytosol	CO_2, Ser, NH_4^+
5	Cytosol	Peroxisome	O_2, GCL, GMa, Ser
6	Peroxisome	Cytosol	GA, OGA, GC
7	Cytosol	Vacuole	S

Table 2.3: The transporting chemical species between two sub-domains

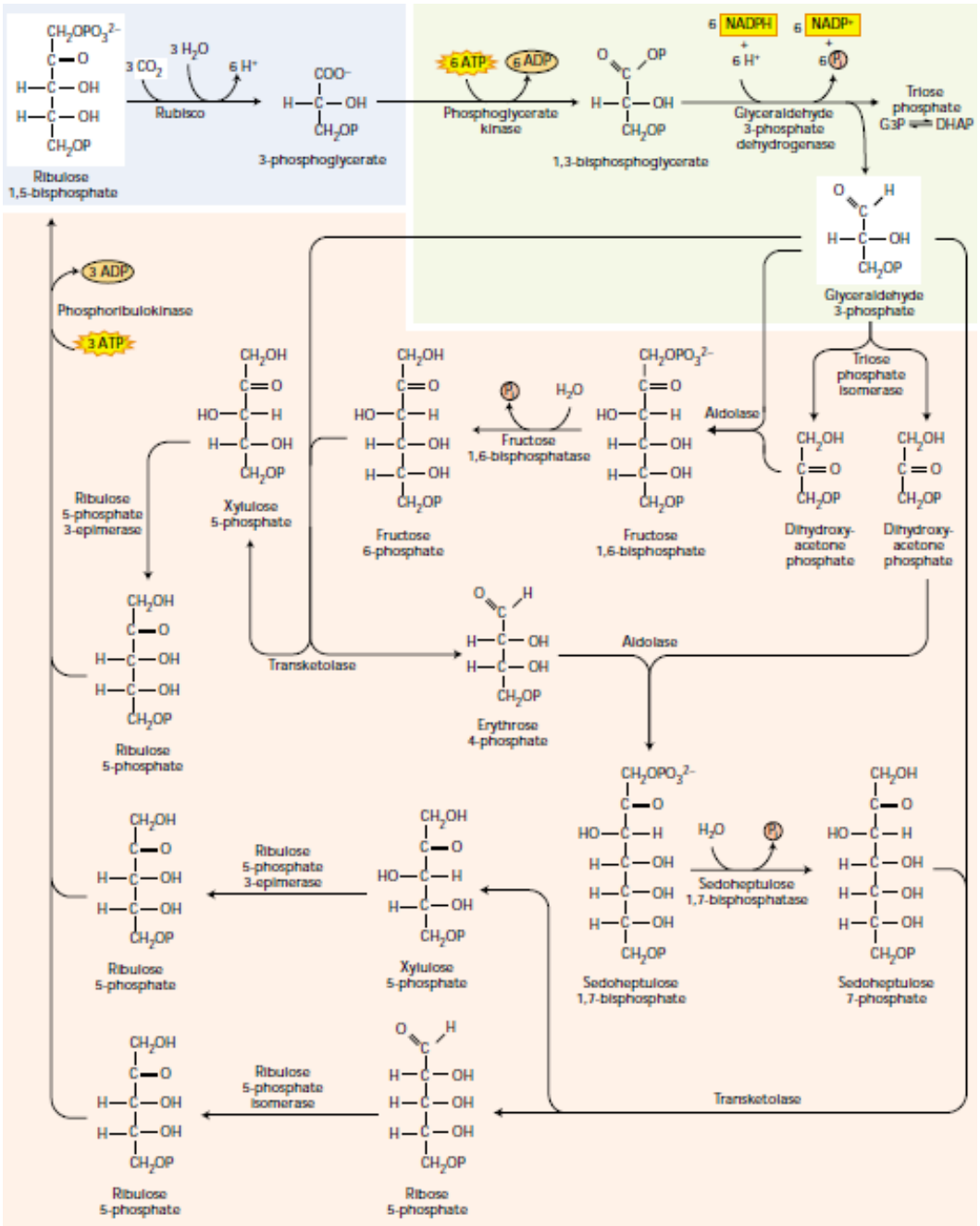

Figure 2.8: The Calvin cycle (see also [4])

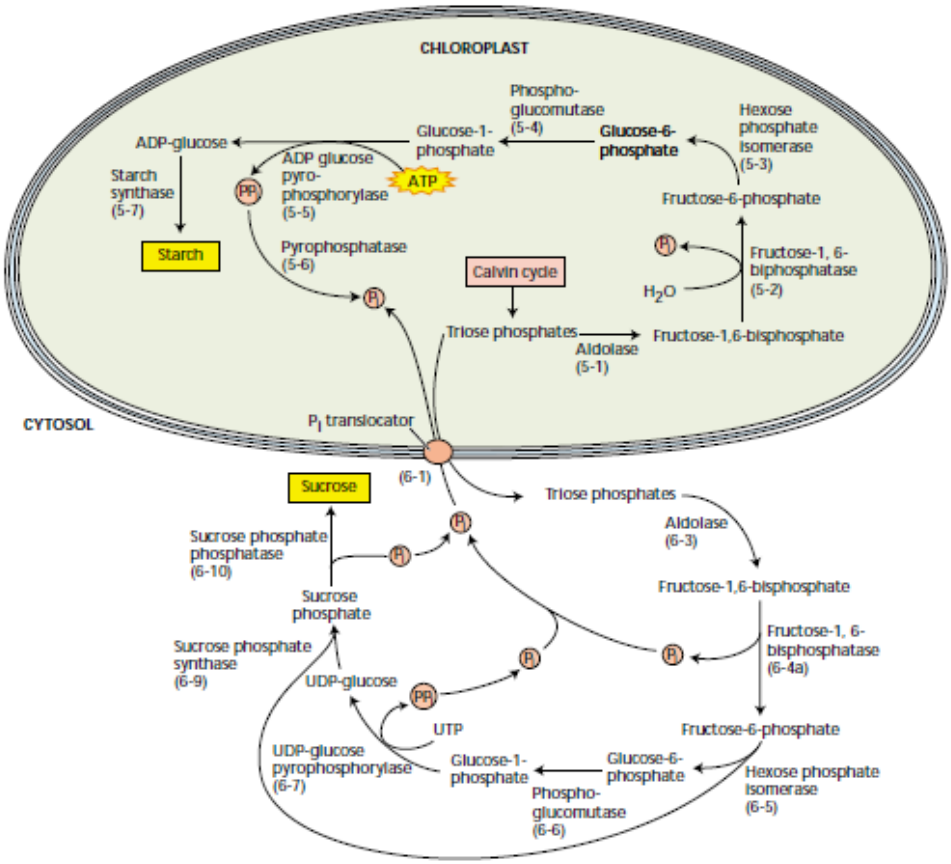

Figure 2.9: Starch and Sucrose synthesis diagram (see also [4])

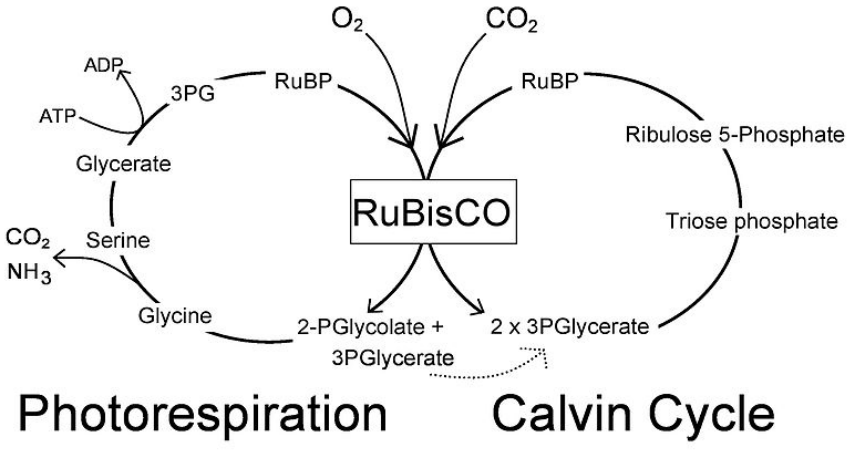

Figure 2.10: Simplified photorespiration and Calvin cycle (see also [4])

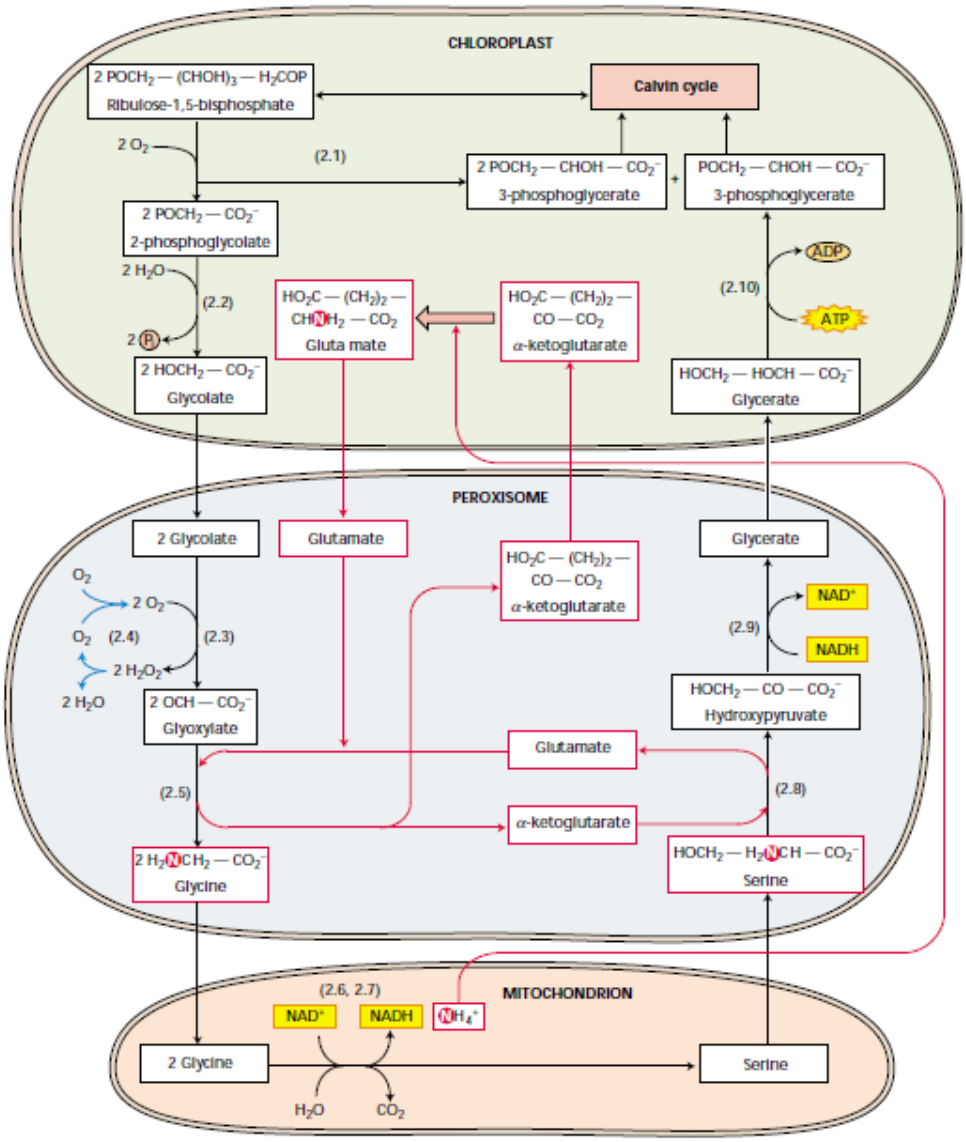

Figure 2.11: Photorespiration diagram (see also [4])

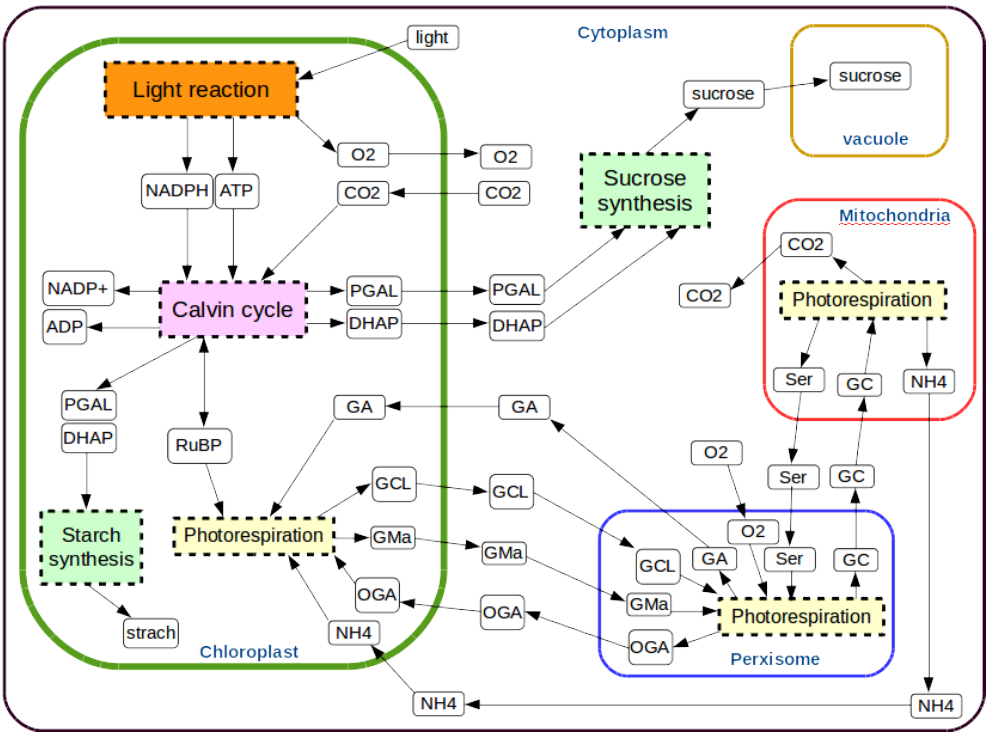

Figure 2.12: Network of chemical processes

Chapter 3

Mathematical model

In this chapter, the goal is to derive a mathematical model to describe the whole biophysical and biochemical process from light-dependent reaction to sucrose synthesis. As local chemical substances react, transform and spread out, we will concentrate on explaining how the concentration of the chemical substrates and products of a complicated system distributed in spaces changes in the chemical reaction and diffusion process. This mathematical model involves chemical processes including photosynthesis, photorespiration, starch and sucrose synthesis. Due to the complexity of the chemical network, a compartmental model is applied to each of sub-compartments: chloroplast, cytosol, mitochondria, peroxisome, and vacuole.

3.1 Overview of existing models

As we mentioned previously in Section 2.4, the measuring of the photosynthesis rate can be performed in various ways depending on how the product of photosynthesis is defined. In this section, we will discusses the mathematical model of photosynthesis in a level of a canopy, a single leaf, a tissue, and a single cell. There are now several existent mathematical models of plant photosynthesis concentrate on the Calvin cycle in the scale of single cell. Other contributions focus on the scale of a compartment or a leaf.

Photosynthesis models for leaf level

Currently, the biochemical models for the photosynthesis rate at the level of a single leaf have been developed [17–20]. Three basic concepts including the dynamic of the Rubisco enzyme, the capacity of an electron transport due to light harvesting, and the limitation of inorganic phosphate, have been applied to the mathematical model.

Farquhar et al. [17] proposed a mathematical model of C_3 plant leaf photosynthesis in form of the net assimilation rate of CO_2 for a single leaf that depends on the rate of carboxylation, the rate of oxygenation, and the evolution rate from mitochondria in the light. The photosynthesis rate is interpreted in terms of a gas exchange. In this model, some plant physiology processes including the photosynthetic electron transport, the ATP and NADPH productions, the simplified photosynthetic carbon reduction cycle, and the reduced photorespiratory carbon oxidation cycle are discussed. The chemical reactions terms are described with the Michaelis-Menten kinetics. Moreover, the net assimilation rate of CO_2 is limited by the temperature optimum. The model outputs can be compared with the measurements of gas exchange of the partial pressure of CO_2 and the temperature.

Sharkey et al. [19, 20] applied the Farquhar model to interpret C_3 leaf level photosynthesis. However, the chemical reactions of photosynthesis were considered as one of two distinct steady states: a rubisco-limited photosynthesis and a RuBP regeneration-limited photosynthesis. In the model, the limitation by rubisco occurs when the concentration of CO_2 is low. On the other hand, the condition for RuBP occurs at higher concentration of CO_2. The partial pressure of CO_2 at the sites of carboxylation and set of parameters were calculated and fitted with the experimental data.

For light limitation, Kull et al. [18] considers the impact of the photosynthetic photon flux density (PPFD) on the rate of light harvesting photosynthesis. The light condition is based on a heterogeneous environment of the chlorophyll and PPFD. Base on [17], Kull et al. also calculates the photosynthesis rate for a plant canopy by scaling from the smaller level.

Photosynthesis models for cell level

Several mathematical models for photosynthesis of C_3 plant leaf have been proposed [5, 21–32]. The complex system of photosynthesis have been discussed and studied in many directions and aspects.

Hahn [21–24] proposed a mathematical model of C_3 leaf carbon metabolism, involving the Calvin cycle, synthesis and degradation of starch and sucrose, and glycerate pathways of photorespiration, that is formulated in terms of a system of non-linear ordinary differential equations. An analytical steady-state solution with mathematical properties was derived. Due photorespiration, however the impact of the spatial factors, the transmission of the chemical species, and the conversion by light were not studied in this work.

The dynamical model for the Calvin cycle has been developed, Pettersson et al. [25] proposed a mathematical model for photosynthetic carbohydrate formation in C_3 plants under conditions of light and carbon dioxide saturation. The model of the Calvin cycle was represented in form of a system of ordinary differential equations. The enzyme kinetics were explained by the Michaelis-Menten kinetics. The main outputs of their model were triose phosphate and starch production. However, the impact of the spatial factors, the sucrose synthesis, and the transmission of the chemical species were not included.

Poolman et al. [26, 27] presented a model and computer simulation for a system of Calvin cycle in the chloroplast. In the mathematical model, the rate of chemical reaction was simply based on the law of Mass Action Kinetics. According to their computer modeling and experimental in [27], the results showed that there are exist two steady states in the photosynthetic Calvin cycle. However, the complex process of photorespiration, the conversion light, the impact of the spatial factors, and the carbohydrate process were not considered.

In the model of Laisk et al. [28] and Laisk et al. [5], the photosynthesis process of the C_3 plant cell was explained in form of a system of ordinary differential equations. The structure of the model in [28] consists of a photosynthetic carbon reduction (PCR) cycle, starch synthesis, and sucrose pathways. The Michaelis-Menten kinetics was applied for the rate of each chemical reaction. Later on the model in [5] comprised the light energy reactions, electron-proton transport and enzymatic reactions into the system of ordinary differential equation. Due photorespiration, the impact of the spatial factors was not

included. So that the exchange of the chemical species between the compartments was not involved in this work.

Zhu et al. [29–32] developed a dynamic model of C_3 plant leaf photosynthesis. The model concerned each of the discrete biochemical processes from light capture to carbohydrate synthesis. A system of ordinary differential equations was applied to interpret the chemical network in a cell. A chemical reaction term was generally modified from Laisk et al. also using the Michaelis-Menten kinetics. In [29, 30] the model described in details of the reactions from water splitting to PQH_2 formation, and the carbon metabolism. Zhu et al. [31] proposed a simplified model of the Calvin cycle and finally showed the Calvin cycle can reach to multiple steady states, but that only one of these is physiologically feasible. Recently, Zhu et al. [32] introduced a dynamic model of leaf photosynthesis that extended from their previous model. The complexity of the photorespiration that depend on the chemical reactions and the locations. In this simulation, however the impact of the spatial factors are not included. So that the exchange of the chemical species between the compartments were not involved.

3.2 Mathematical model

In this section we present a mathematical model of a plant leaf cell photosynthesis which incorporates some of the fundamental biological and chemical processes of the C_3 plant leaf physiology. As we explored before in Section 2.2, the most important part of light-dependent reactions is the conversion of light energy into chemical energy in the form of ATP and NADPH. According to RuBisCO consumption, photorespiration is one of the most significant factors that influence 3-Phosphoglycerate production. As an end-product of the Calvin cycle, triose phosphates play an important role in starch and sucrose synthesis. Therefore, we constructed 5 sub-models including the light-dependent reaction (LDR), the Calvin cycle (CC) or the light-independent reaction (LIR), the photorespiration reaction (PR), the starch synthesis (StS), and the sucrose synthesis (SuS), respectively (see also Table 3.1).
The system of partial differential equations describing the LDR, CC or LIR, PR, StS, and SuS, can be briefly represented as:

$$\frac{\partial u}{\partial t} = D\Delta u + R(t,u,p) \tag{3.1}$$

where each component of the vector $u(x,t)$ is the concentration of a substance, D denotes a diagonal matrix of diffusion coefficients, R elucidates a local chemical reactions, t is times, and p represents parameters or constants. The equation (3.1) also known as the reaction-diffusion equations (RDEs). For more details, the derivation of RDEs are provided in the Appendix A. If the chemical reactions do not occur, the substrates will accumulate and the products will be reduced.

Table 3.1: Sub-mathematical model with respect to the biochemical of plant physiology and the sub-compartments

Sub-model	**Physiology process**	**Sub-compartment**
RDEs of LDR	Photosynthesis	Chloroplast
RDEs of LIR	Photosynthesis	Chloroplast
RDEs of PR	Photorespiration	Chloroplast
		Peroxisome
		Mitochondria
RDEs of StS	Starch synthesis	Chloroplast
RDEs of SuS	Sucrose synthesis	Cytosol

3.3 Problem Domains

Before developing the mathematical model, we need to specify the spatial domain of the problem. For a parenchyma cell of a C_3 plant leaf, we consider a three dimensional closed and bounded domain ($\Omega \in \mathbb{R}^3$) embedding with a finite multi sub-domains so that

$$\Omega = \bigcup_{j=0}^{4} \Omega_j \in \mathbb{R}^3$$

where each of sub-domain is defined in Table 3.2.

For domain Ω, two perspectives are depicted in Figure 3.1 (above right) shows a three dimensional cell embedding a finite number of organelles, and Figure 3.1 (below left) shows a cross section (BEMH) of a cell, in which a simple distribution of the organelles inside is depicted. More precisely, all of the

Table 3.2: Sub-domain definitions

Sub-domain	Sub-compartment
Ω_0	a cytosol
Ω_1	all of the chloroplast
Ω_2	all of the mitochondria
Ω_3	all of the peroxisome
Ω_4	all of the vacuole

sub-domain are also closed and bounded. In addition, each of the sub-domain boundaries ($\partial\Omega_j$) is fixed in time and does not overlap any other sub-domain boundary ($\partial\Omega_j \cap \partial\Omega_p, j \neq p$). We are going to set up a reaction network representing the biochemical processes and taking into account the different compartments and their coupling. According to table 3.1 and table 3.2, the process of LDR have to be consider first, then LIR, PR, StS, and SuS will be taken into account later.

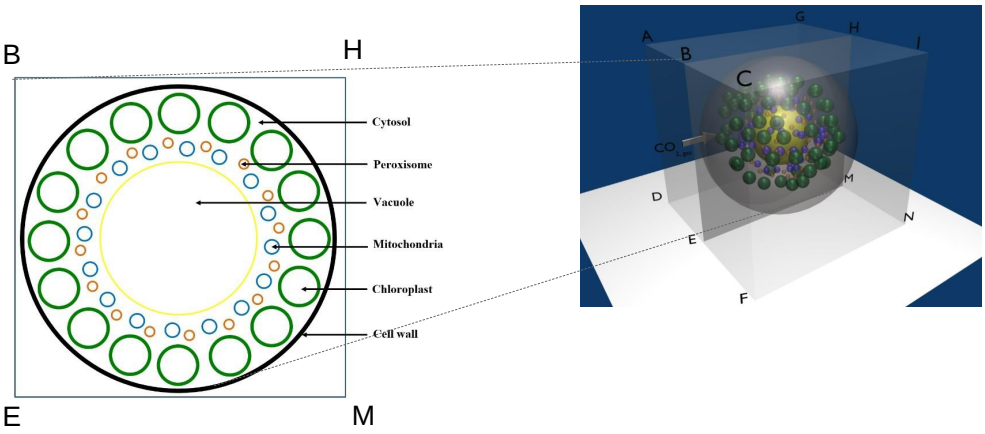

Figure 3.1: The distribution of the organelles inside a single cell.

3.4 Light-dependent model

We will now consider a mathematical relations representing the light-dependent reactions of C_3 plant photosynthesis. The energy transduction reactions of the photosynthesis process occur in the chloroplast thylakoids and include light

harvesting, electron transport chain from H_2O to NADPH with simultaneous proton pumping, and ATP synthesis. We will now explain the sub-processes: light absorption, water photolysis sub-process, electron transport chain, and generation of NADPH and ATP, in the form of the following a mathematical model.

Light absorption sub-process

When a photon is absorbed by a pigment (light absorbing molecule), such as chlorophyll, the energy of the photon is transferred to an electron, which is energized from its ground state in a low-energy orbital to an excited state in a high-energy orbital (see also [14]). The chlorophyll molecules in a photosystem (PS) can exist in three different states. In the ground state (Chl), all electrons are at their normal stable level. Chl in its lowest-energy or the ground state absorbs a photon ($h\nu$) of light and then makes a transition to a higher-energy or the lowest excited singlet state, (Chl^*) which is represented by equation (3.2). Loss of an electron (e^-) of Chl^* produces the electron-deficient or oxidized state (Chl^+) which is showed in equation (3.3) . The chlorophyll molecule in the oxidized state must be regenerated by receiving an electron from an electron donor (see also [33]).

$$Chl + h\nu \longrightarrow Chl^*, \tag{3.2}$$

$$Chl^* \longrightarrow Chl^+ + e^-. \tag{3.3}$$

We rewrite equations (3.2) and (3.3) in a short form (see also [34]):

$$Chl \xrightarrow{\gamma(h\nu)} Chl^+ + e^-. \tag{3.4}$$

Suppose that X_{PSII} and X^+_{PSII} are a concentration of the special pigment, chlorophylls P680, in a ground state and an oxidized state of the photosystem II (PSII), respectively. The light absorption of the pigment of PSII is represented in the following equation,

$$X_{PSII} \xrightarrow{\gamma_1(h\nu)} X^+_{PSII} + e^-_{PSII}. \tag{3.5}$$

We assume that a rate of light absorption,

$$\gamma_1(h\nu) = \alpha \cdot \Upsilon, \tag{3.6}$$

where

$$\Upsilon = \begin{cases} \frac{(E-E_{min})}{(E_{max}-E_{min})} & \text{if } E_{min} \leq E \leq E_{max}, \\ 0 & \text{otherwise,} \end{cases} \tag{3.7}$$

$$\alpha = \frac{1}{d} \cdot log \frac{T_0}{T}, \tag{3.8}$$

$$E = h\nu = \frac{hc}{\lambda}, \tag{3.9}$$

h is a Planck's constant, c is the speed of light, ν and λ is a frequency and a wavelength of the light, respectively. α is an absorption coefficient, d is the depth of the absorption cell, T_0 and T are a fluxes transmitted (light intensity) through to the incident surface and the absorption cell, respectively (see also [35]). E_{max} and E_{min} are maximum and minimum energy required for the transition of the pigment from a ground state to an oxidized state and releases one electron. The required energy for the transition of the pigment from a ground state to an oxidized state are shown in Table 3.3. The photosynthetic pigments can absorb photons of light well on a very specific wavelength. In photosystem II (PSII), a chlorophyll (Chl) *a* at a reaction centers of the photosynthetic center complex can absorb red light of 680 nm well but it is driven very poorly by far-red light (wavelength $>$ 680 nm). In the case of the fully absorption (100%), the maximum energy for the transition of the pigment of PSII is

$$\begin{aligned} E_{max} &= \frac{hc}{\lambda_{\text{PSII}}}, \\ &= \frac{(6.626 \times 10^{-34}\,\text{J s})(2.988 \times 10^{8}\,\text{m s}^{-1})}{680\,\text{nm}} \times \frac{1\,\text{eV}}{1.602 \times 10^{-19}\,\text{J}}, \qquad (3.10) \\ &= 1.82353\,\text{eV}, \qquad (3.11) \end{aligned}$$

where a photon with an energy 1 electron-volt (eV) = 1.602×10^{-19} joule (J). We consider the rate of electron excitation of PSII ($v_{e^-_{PSII}}$) in the following form:

$$v_{e^-_{PSII}} = \gamma_1(h\nu) X_{PSII}. \tag{3.12}$$

Similarly situation for the light absorption of the pigment molecule of the photosystem I (PSI):

$$\text{X}_{\text{PSI}} \xrightarrow{\gamma_2(h\nu)} \text{X}^+_{\text{PSI}} + \text{e}^-_{\text{PSI}}, \tag{3.13}$$

Table 3.3: The required energy for the transition of the pigment from a ground state to an oxidized state

Photosystem	Wavelength (nm)	Energy (eV)	
		E_{min}	E_{max}
PSII	680	E_{II}	1.82353
PSI	700	E_I	1.77143

where X_{PSI} and X^{+}_{PSI} are a concentration of the special pigment, chlorophylls P700, in a ground state and an oxidized state of PSI, respectively. The rate of electron excitation of PSI ($v_{e^{-}_{PSI}}$) reads

$$v_{e^{-}_{PSI}} = \gamma_2(h\nu)X_{PSI}. \tag{3.14}$$

Nevertheless, the minimum energy required for the transition of the pigment of PSI and PSII are defined by E_I, $E_{II} \in \mathbb{R}^{+}$, respectively. Each of E_{min} is a function dependent on the relative light absorption coefficient for a photosynthetic pigments.

Water photolysis sub-process

Photons of light strike photosystems I and II simultaneously. When the photons strike photosystem II, the energized electrons are passed from the reaction center of photosystem II to an electron transport chain. The electrons lost by photosystem II are replaced by a process called photolysis, which involves the oxidation of a water molecule, producing electrons, protons and oxygens. By the photolysis process free electrons are passed to the reaction center of photosystem II, proton ions are released to the lumen of thylakoid, and oxygen gas is produced as a by-product of photosynthesis:

$$2\,H_2O \xrightarrow{k} O_2 + 4\,H^{+}_{\text{lumen}} + 4\,e^{-}_{H_2O}. \tag{3.15}$$

The rate of water photolysis (v_{H_2O}) depends on the rate of electron excitation of PSII ($v_{e^{-}_{PSII}}$), so that we write

$$v_{H_2O} = v_1. \tag{3.16}$$

Electron transport chain sub-process

The process of photosynthetic electron transfer, a line of protein complexes that passes an electron of H_2O from one protein to another to put out at $NADP^+$, is like a bucket brigade (see also [36], Figure 2.6 and section 2.2 for details). During a cytochrome b_6f oxidize plastohydroquinone (PQH_2) molecule that was reduced by PSII and delivers an electron to PSI, one proton (H^+ ion) is also transported from stroma to lumen across the thylakoid membrane. So we rewrite the transportation of the electrons along the series of the carriers in the following form:

$$X^+_{\mathrm{PSII}} + e^-_{\mathrm{H_2O}} \xrightarrow{k_{LDR1}} X_{\mathrm{PSII}}, \tag{3.17}$$

$$X^+_{\mathrm{PSI}} + e^-_{\mathrm{PSII}} \xrightarrow{k_{LDR2}} X_{\mathrm{PSI}}. \tag{3.18}$$

The transition rate of the photosynthetic pigment molecule from the oxidized state to the ground state are assumed to be

$$v^{LDR}_{PSII} = k_{LDR1}\left[X^+_{PSII}\right]\left[e^-_{H_2O}\right] \quad \text{for PSII and,} \tag{3.19}$$

$$v^{LDR}_{PSI} = k_{LDR2}\left[X^+_{PSI}\right]\left[e^-_{PSII}\right] \quad \text{for PSI, respectively.} \tag{3.20}$$

Generation of NADPH and ATP sub-process

According to the electron transport chain, two of the free electrons that are released from PSI combining with $NADP^+$ and H^+ generate one energy compound NADPH in the stroma,

$$NADP^+ + 2\,e^-_{\mathrm{PSI}} + H^+_{\mathrm{stroma}} \xrightarrow{k_{LDR3}} NADPH. \tag{3.21}$$

In this case, we set up the generation rate of NADPH for the light-dependent reaction (LDR),

$$v^{LDR}_{NADPH} = v_2. \tag{3.22}$$

During the electron transport chain, the protons (H^+) are transported across a thylakoid membrane of the chloroplast. This creates an electrochemical proton gradient between inside (lumen) and outside (stroma). Transportation of H^+ back from lumen to stroma through a complex protein called ATP synthase generates chemical energy in the form of adenosine triphosphate (ATP) from ADP and P_i in the stroma,

$$ADP + P_i \xrightarrow{k_{LDR4}} ATP. \tag{3.23}$$

Suppose the concentration of H^+ in lumen is not less than the concentration of H^+ in stroma, that means the ATP synthase is still active. Then, the generation rate of ATP for the light-dependent reaction reads

$$v_{ATP}^{LDR} = v_3. \tag{3.24}$$

Since the water photolysis rate, the proton pumping rate, the generation rate of NADPH, and also the ATP synthesis rate are affected by the accumulation rate of the protons in lumen and stroma. So that we write these rates in the following form:

$$\begin{aligned} v_{H_{lumen}^+} &= 2v_{H_2O} + 2v_{e_{PSII}^-} - v_{ATP}^{LDR}, \\ &= 6v_{e_{PSII}^-} - v_{ATP}^{LDR}, \qquad (3.25) \\ v_{H_{stroma}^+} &= v_{ATP}^{LDR} - 2v_{e_{PSII}^-} - v_{NADPH}^{LDR}. \qquad (3.26) \end{aligned}$$

A Mathematical Model for Light-Dependent Reactions (LDR)

From equations (3.5), (3.13), (3.17), (3.18), (3.21) and (3.23), the light-dependent models are derived in the following form of the equations (3.27) to (3.41).

$$\begin{aligned} \frac{\partial [X_{PSII}]}{\partial t} &= -v_{e_{PSII}^-} + v_{PSII}^{LDR}, \qquad (3.27) \\ \frac{\partial [X_{PSII}^+]}{\partial t} &= v_{e_{PSII}^-} - v_{PSII}^{LDR}, \qquad (3.28) \\ \frac{\partial [e_{PSII}^-]}{\partial t} &= v_{e_{PSII}^-} - v_{PSI}^{LDR}, \qquad (3.29) \\ \frac{\partial [X_{PSI}]}{\partial t} &= -v_{e_{PSI}^-} + v_{PSI}^{LDR}, \qquad (3.30) \\ \frac{\partial [X_{PSI}^+]}{\partial t} &= v_{e_{PSI}^-} - v_{PSI}^{LDR}, \qquad (3.31) \\ \frac{\partial [e_{PSI}^-]}{\partial t} &= v_{e_{PSI}^-} - 2v_{NADPH}^{LDR}, \qquad (3.32) \end{aligned}$$

in $[0,T] \times \Omega_1$.

As we mentioned above, the rate of water photolysis depends on the rate of electron excitation of PSII ($v_{e^-_{PSII}}$). This facts also implies that the evolution rate of oxygen gas (O_2) and the rate of proton ions in lumen (H^+_{lumen}, due to water photolysis) are dependent on $v_{e^-_{PSII}}$ as well. In this work D_A denotes the diffusion coefficient of the chemical species A and Δ denotes the Laplacian.

$$\begin{aligned}
\frac{\partial [O_2]}{\partial t} &= D_{O_2}\Delta[O_2] + \frac{1}{2}v_{H_2O} - v^{dark}_{O_2}, \\
&= D_{O_2}\Delta[O_2] + v_{e^-_{PSII}} - v^{dark}_{O_2}, && (3.33)\\
\frac{\partial [H^+_{lumen}]}{\partial t} &= D_{H^+_{lumen}}\Delta[H^+_{lumen}] + 2v_{H_2O} + 2v_{e^-_{PSII}} - v^{LDR}_{ATP}, \\
&= D_{H^+_{lumen}}\Delta[H^+_{lumen}] + 6v_{e^-_{PSII}} - v^{LDR}_{ATP}, && (3.34)\\
\frac{\partial [e^-_{H_2O}]}{\partial t} &= 2v_{H_2O} - v^{LDR}_{PSII}, \\
&= 4v_{e^-_{PSII}} - v^{LDR}_{PSII}, && (3.35)
\end{aligned}$$

in $[0,T]\times\Omega_1$,

where $v^{dark}_{O_2} \in \mathbb{R}^+$ is the rate of a cellular respiration also called dark respiration. Moreover, we denote that the respiration rate of a cells (dark respiration rate) is simply a constants.

According to the generation of NADPH in the stroma, the mathematical model for NADPH, $NADP^+$, and proton ions in stroma (H^+_{stroma}) are

$$\begin{aligned}
\frac{\partial [NADP^+]}{\partial t} &= D_{NADP^+}\Delta[NADP^+] - 2v^{LDR}_{NADPH} + v^{calvin}_{NADPH}, && (3.36)\\
\frac{\partial [H^+_{stroma}]}{\partial t} &= D_{H^+_{stroma}}\Delta[H^+_{stroma}] + v^{LDR}_{ATP} - 2v_{e^-_{PSII}} - 2v^{LDR}_{NADPH} \\
&\quad + v^{calvin}_{NADPH}, && (3.37)\\
\frac{\partial [NADPH]}{\partial t} &= D_{NADPH}\Delta[NADPH] + 2v^{LDR}_{NADPH} - v^{calvin}_{NADPH}, && (3.38)
\end{aligned}$$

in $[0,T]\times\Omega_1$,

where v_{NADPH}^{calvin} is the rate of NADPH consumption in the Calvin cycle.
The generation rate of ATP and related species are defined by

$$\frac{\partial [ADP]}{\partial t} = D_{ADP}\Delta[ADP] - v_{ATP}^{LDR} + v_{ATP}^{calvin}, \tag{3.39}$$

$$\frac{\partial [P_i]}{\partial t} = D_{P_i}\Delta[P_i] - v_{ATP}^{LDR} + v_{ATP}^{calvin}, \tag{3.40}$$

$$\frac{\partial [ATP]}{\partial t} = D_{ATP}\Delta[ATP] + v_{ATP}^{LDR} - v_{ATP}^{calvin}, \tag{3.41}$$

$$\text{in} \quad [0,T] \times \Omega_1,$$

where v_{ATP}^{calvin} is the rate of ATP consumption in Calvin cycle.

The initial and boundary conditions for LDR

First of all we defined a set of the chemical species for LDR:

$$\begin{aligned}\mathbb{S}_{LDR} = \{&X_{PSII}, X_{PSII}^{+}, e_{PSII}^{-}, X_{PSI}, X_{PSI}^{+}, e_{PSI}^{-}, O_2, H_{lumen}^{+}, e_{H_2O}^{-}, \\ &NADP^{+}, H_{stroma}^{+}, NADPH, ADP, P_i, ATP\}.\end{aligned} \tag{3.42}$$

So that the initial conditions for the LDR are defined by

$$[u](x, t = t_0) = u_0 \in \mathbb{R}^{+} \cup \{0\} \quad \text{in} \quad \Omega_1. \tag{3.43}$$

For the chemical species in $\mathbb{S}_{LDR}$, there is no flux on the chloroplast membrane therefore the boundary conditions on the $\Gamma_1 = \partial\Omega_1$ for the LDR are defined by Neumann conditions:

$$\frac{\partial [u]}{\partial n}(x,t) = 0 \quad \text{on} \quad [0,T] \times \Gamma_1, \tag{3.44}$$

where $[u](x,t)$ represents a concentration of a chemical species $u \in \mathbb{S}_{LDR}$ at positions $x \in \mathbb{R}^3$ in times $t \in [0,T]$ and n is an outward normal vector to the boundary Γ_1 .

3.5 RDEs in sub-compartment

The chemical reaction of photosynthesis, starch synthesis, photorespiration and sucrose synthesis are take place in various sub-domains. Light-dependent

reaction, light-independent reaction, and also starch synthesis are all occur in the chloroplast (Ω_1). The photorespiration process is more complicated than other process. Their chemical reactions occur in three location including the chloroplast, the mitochondria (Ω_2), and the peroxisome (Ω_3). In order to fulfill photorespiration, many chemical species transports through the cytosol (Ω_4). In this work, the sucrose synthesis is considered only in the cytosol. Moreover, the diffusion of the final products of sucrose synthesis in form of sucrose concentration from the cytosol to the vacuole (Ω_5) must be discussed. In this section, we develop the mathematical model for each sub-domain in the framework of the reaction-diffusion equations (RDEs). For the simplicity, the RDEs are considered as 5 sub-Models: (1) all RDEs in the chloroplast, (2) all RDEs in the mitochondria, (3) all RDEs in the peroxisome, (4) all RDEs in the cytosol, and (5) RDEs in the vacuole.

Chemical reaction terms

In this work, there are two possible ways to generate a chemical reaction term, $R(t,u,p)$ in Equation (3.1). Generally, we can apply by the law of Mass Action Kinetics (MAK) or the Michaelis–Menten Kinetics (MMK). Suppose now we consider the following set of chemical reactions:

$$\boxed{\begin{aligned} &\mathrm{A} \xrightarrow{k_1} \mathrm{B}+\mathrm{C} \\ &\mathrm{B}+\mathrm{E} \xrightarrow{k_2} \mathrm{A}+\mathrm{C}. \end{aligned}}$$

According to the law of Mass Action Kinetics, the rate of chemical reactions is represented by

$$\begin{aligned} r_1^{MAK} &= k_1[A], \\ \text{and} \quad r_2^{MAK} &= k_2[B][E], \end{aligned}$$

where k_1 and k_2 are the rate constants, respectively; $[A]$, $[B]$ and $[E]$ are the concentrations of the substrate A, B and E, respectively. In addition, the rate of chemical reactions that obey on the Michaelis–Menten Kinetics are defined in the following form:

$$\begin{aligned} r_1^{MMK} &= V_{1max}\frac{[A]}{[A]+K_{mA}}, \\ \text{and} \quad r_2^{MMK} &= V_{2max}\frac{[B][E]}{([B]+K_{m2B})([E]+K_{m2E})}, \end{aligned}$$

where K_{m2A}, K_{m2B} and K_{m2E} are the Michaelis–Menten constants of substrate A, B and E, respectively; V_{1max} and V_{2max} represents the maximum rate achieved by these chemical reactions. Therefore, the reaction-diffusion equations for the previous system can be written the form:

$$\begin{aligned}
\frac{\partial [A]}{\partial t} &= D_A \Delta [A] - r_1 + r_2 \\
\frac{\partial [B]}{\partial t} &= D_B \Delta [B] + r_1 - r_2 \\
\frac{\partial [C]}{\partial t} &= D_C \Delta [C] + r_1 + r_2 \\
\frac{\partial [E]}{\partial t} &= D_E \Delta [E] - r_2
\end{aligned}$$

From the list of chemical reaction equations (see Table 2.2), we summarize a chemical rate for each process in Table 3.4. In order to form a system of RDEs from a very large set of the chemical reactions, we have been developed a supplement tool as a computer program called chemToRDE. The main purpose of this software is to convert a set of chemical reactions to a system of RDEs. For more details, the algorithm and user manual of software chemToRDE are proposed in Appendix B).

3.6 List of chemical reaction rate

Table 3.4: List of chemical reaction rates with respect to the photosynthesis, starch and sucrose synthesis, and photorespiration in Chloroplast, Mitochondria, Peroxisome, and Cytoplasm: 1. Mass action kinetics and 2. Michaelis–Menten kinetics

Chemical reaction	Rate	Mass action	Michaelis–Menten
Photosynthesis: *Light dependent reactions*			
$2\,H_2O \longrightarrow O_2 + 4\,H^+ + 4\,e^-$	v_1	$2\gamma_1(h\nu)u_1$	$\frac{2V_{1max}u_1}{(u_1+K_{m1,1})}$
$NADP^+ + 2\,e^- + H^+ \longrightarrow NADPH$	v_2	$k_3(u_6)^2u_{12}u_{18}$	$\frac{V_{2max}(u_6)^2u_{12}u_{18}}{(u_6+K_{m2,1})^2(u_{12}+K_{m2,2})(u_{18}+K_{m2,3})}$
$ADP + P_i \longrightarrow ATP$	v_3	$k_4(u_7-u_{12})_+u_{15}u_{19}$	$\frac{V_{3max}(u_7-u_{12})_+u_{15}u_{19}}{(u_{15}+K_{m3,1})(u_{19}+K_{m3,2})}$
Photosynthesis: *Calvin cycle*			
$3\,RuBP + 3\,CO_2 + 3\,H_2O \longrightarrow 6\,PGA + 6\,H^+$	v_4	$k_5u_9u_{10}$	$\frac{V_{4max}u_9u_{10}}{(u_9+K_{m4,1})(u_{10}+K_{m4,2})}$
$6\,PGA + 6\,ATP \longrightarrow 6\,BPGA + 6\,ADP$	v_5	$k_6u_{11}u_{13}$	$\frac{V_{5max}u_{11}u_{13}}{(u_{11}+K_{m5,1})(u_{13}+K_{m5,2})}$
$6\,BPGA + 6\,NADPH + 6\,H^+ \longrightarrow 6\,PGAL + 6\,NADP^+ + 6\,P_i$	v_6	$k_7u_{12}u_{14}u_{16}$	$\frac{V_{6max}u_{12}u_{14}u_{16}}{(u_{12}+K_{m6,1})(u_{14}+K_{m6,2})(u_{16}+K_{m6,3})}$
$2\,PGAL \rightleftharpoons 2\,DHAP$	v_7	$k_8u_{17} - k_9u_{20}$	$\frac{V_{7max}u_{17}}{(u_{17}+K_{m7,1})} - \frac{V_{7max}u_{20}}{(u_{20}+K_{m7,2})}$
$PGAL + DHAP \longrightarrow FBP$	v_8	$k_{10}u_{17}u_{20}$	$\frac{V_{8max}u_{17}u_{20}}{(u_{17}+K_{m8,1})(u_{20}+K_{m8,2})}$

Continued on next page

Table 3.4 – continued from previous page

Chemical reaction	Rate	Mass action	Michaelis–Menten
$FBP + H_2O \longrightarrow FP + P_i$	v_9	$k_{11}u_{21}$	$\frac{V_{9max}u_{21}}{u_{21}+K_{m9,1}}$
$FP + PGAL \longrightarrow EP + XP$	v_{10}	$k_{12}u_{17}u_{22}$	$\frac{V_{10max}u_{17}u_{22}}{(u_{17}+K_{m10,1})(u_{22}+K_{m10,2})}$
$EP + DHAP \longrightarrow SBP$	v_{11}	$k_{13}u_{20}u_{23}$	$\frac{V_{11max}u_{20}u_{23}}{(u_{20}+K_{m11,1})(u_{23}+K_{m11,2})}$
$SBP + H_2O \longrightarrow SuP + P_i$	v_{12}	$k_{14}u_{25}$	$\frac{V_{12max}u_{25}}{u_{25}+K_{m12,1}}$
$SuP + PGAL \longrightarrow RP + XP$	v_{13}	$k_{15}u_{17}u_{26}$	$\frac{V_{13max}u_{17}u_{26}}{(u_{17}+K_{m13,1})(u_{26}+K_{m13,2})}$
$2\,XP \longrightarrow 2\,RuP$	v_{14}	$k_{16}u_{24}$	$\frac{V_{14max}u_{24}}{u_{24}+K_{m24,1}}$
$RP \longrightarrow RuP$	v_{15}	$k_{17}u_{27}$	$\frac{V_{15max}u_{27}}{u_{27}+K_{m15,1}}$
$3\,RuP + 3\,ATP \longrightarrow 3\,RuBP + 3\,ADP + 3\,H^+$	v_{16}	$k_{18}u_{13}u_{28}$	$\frac{V_{16max}u_{13}u_{28}}{(u_{13}+K_{m16,1})(u_{28}+K_{m16,2})}$
Starch synthesis			
$PGAL \rightleftharpoons DHAP$	v_{17}	$k_{19}u_{13} - k_{20}u_{20}$	$\frac{V_{17max}u_{13}}{(u_{13}+K_{m17,1})} - \frac{V_{17max}u_{20}}{(u_{20}+K_{m17,2})}$
$DHAP + PGAL \longrightarrow FBP$	v_{18}	$k_{21}u_{17}u_{20}$	$\frac{V_{18max}u_{17}u_{20}}{(u_{17}+K_{m18,1})(u_{20}+K_{m18,2})}$
$FBP + H_2O \longrightarrow FP + P_i$	v_{19}	$k_{22}u_{21}$	$\frac{V_{19max}u_{21}}{u_{21}+K_{m19,1}}$

Continued on next page

Table 3.4 – continued from previous page

Chemical reaction	Rate	Mass action	Michaelis–Menten
$FP + ATP \longrightarrow FBP + ADP$	v_{20}	$k_{23}u_{13}u_{22}$	$\frac{V_{20max}u_{13}u_{22}}{(u_{13}+K_{m20,1})(u_{22}+K_{m20,2})}$
$FP + PP_i \longrightarrow FBP + P_i$	v_{21}	$k_{24}u_{22}u_{39}$	$\frac{V_{21max}u_{22}u_{39}}{(u_{22}+K_{m21,1})(u_{39}+K_{m21,2})}$
$FP + ATP \longrightarrow FTBP + ADP$	v_{22}	$k_{25}u_{13}u_{22}$	$\frac{V_{22max}u_{13}u_{22}}{(u_{13}+K_{m22,1})(u_{22}+K_{m22,2})}$
$FTBP + H_2O \longrightarrow FP + P_i$	v_{23}	$k_{26}u_{40}$	$\frac{V_{23max}u_{40}}{u_{40}+K_{m23,1}}$
$FP \longrightarrow GSP$	v_{24}	$k_{27}u_{22}$	$\frac{V_{24max}u_{22}}{u_{22}+K_{m24,1}}$
$GSP \longrightarrow GP$	v_{25}	$k_{28}u_{41}$	$\frac{V_{25max}u_{41}}{u_{41}+K_{m25,1}}$
$GP + ATP \longrightarrow ADPG + PP_i$	v_{26}	$k_{29}u_{13}u_{42}$	$\frac{V_{26max}u_{13}u_{42}}{(u_{13}+K_{m26,1})(u_{42}+K_{m26,2})}$
$ADPG + Primer \longrightarrow A + ADP$	v_{27}	$k_{30}u_{43}u_{44}$	$\frac{V_{27max}u_{43}u_{44}}{(u_{43}+K_{m27,1})(u_{44}+K_{m27,2})}$
Sucrose synthesis			
$PGAL \rightleftharpoons DHAP$	v_{28}	$k_{43}u_{13} - k_{44}u_{20}$	$\frac{V_{28max}u_{13}}{(u_{13}+K_{m28,1})} - \frac{V_{28max}u_{20}}{(u_{20}+K_{m28,2})}$
$DHAP + PGAL \longrightarrow FBP$	v_{29}	$k_{45}u_{17}u_{20}$	$\frac{V_{29max}u_{17}u_{20}}{(u_{17}+K_{m29,1})(u_{20}+K_{m29,2})}$
$FBP + H_2O \longrightarrow FP + P_i$	v_{30}	$k_{46}u_{21}$	$\frac{V_{30max}u_{21}}{u_{21}+K_{m30,1}}$

Continued on next page

Table 3.4 – continued from previous page

Chemical reaction	Rate	Mass action	Michaelis–Menten
$FP + ATP \longrightarrow FBP + ADP$	v_{31}	$k_{47}u_{13}u_{22}$	$\frac{V_{31max}u_{13}u_{22}}{(u_{13}+K_{m31,1})(u_{22}+K_{m31,2})}$
$FP + PP_i \longrightarrow FBP + P_i$	v_{32}	$k_{48}u_{22}u_{39}$	$\frac{V_{32max}u_{22}u_{39}}{(u_{22}+K_{m32,1})(u_{39}+K_{m32,2})}$
$FP + ATP \longrightarrow FTBP + ADP$	v_{33}	$k_{49}u_{13}u_{22}$	$\frac{V_{33max}u_{13}u_{22}}{(u_{13}+K_{m33,1})(u_{22}+K_{m33,2})}$
$FTBP + H_2O \longrightarrow FP + P_i$	v_{34}	$k_{50}u_{40}$	$\frac{V_{34max}u_{40}}{u_{40}+K_{m34,1}}$
$FP \longrightarrow GSP$	v_{35}	$k_{51}u_{22}$	$\frac{V_{35max}u_{22}}{u_{22}+K_{m35,1}}$
$GSP \longrightarrow GP$	v_{36}	$k_{52}u_{41}$	$\frac{V_{36max}u_{41}}{u_{41}+K_{m36,1}}$
$GP + UDP \longrightarrow UDPG + PP_i$	v_{37}	$k_{53}u_{42}u_{53}$	$\frac{V_{37max}u_{42}u_{53}}{(u_{42}+K_{m37,1})(u_{53}+K_{m37,2})}$
$UDPG + FP \longrightarrow UDP + SSP$	v_{38}	$k_{54}u_{22}u_{54}$	$\frac{V_{38max}u_{22}u_{54}}{(u_{22}+K_{m38,1})(u_{54}+K_{m38,2})}$
$SSP + H_2O \longrightarrow S + P_i$	v_{39}	$k_{55}u_{55}$	$\frac{V_{39max}u_{55}}{u_{55}+K_{m39,1}}$
Photorespiration			
$2\,RuBP + 2\,O_2 \longrightarrow 2\,PGC + 2\,PGA$	v_{40}	$k_{31}u_{10}u_{29}$	$\frac{V_{40max}u_{10}u_{29}}{(u_{10}+K_{m40,1})(u_{29}+K_{m40,2})}$
$2\,PGC + 2\,H_2O \longrightarrow 2\,GCL + 2\,P_i$	v_{41}	$k_{32}u_{30}$	$\frac{V_{41max}u_{30}}{u_{30}+K_{m41,1}}$

Continued on next page

Table 3.4 – continued from previous page

Chemical reaction	Rate	Mass action	Michaelis–Menten
$2\,GCL + 2\,O_2 \longrightarrow 2\,GOL + H_2O_2$	v_{42}	$k_{38}u_{29}u_{31}$	$\frac{V_{42max}u_{29}u_{31}}{(u_{29}+K_{m42,1})(u_{31}+K_{m42,2})}$
$2\,H_2O_2 \longrightarrow 2\,H_2O + O_2$	v_{43}	$k_{39}u_{58}$	$\frac{V_{43max}u_{58}}{u_{58}+K_{m43,1}}$
$2\,GOL + 2\,GMa \longrightarrow GC + OGA$	v_{44}	$k_{40}u_{33}u_{57}$	$\frac{V_{44max}u_{33}u_{57}}{(u_{33}+K_{m44,1})(u_{57}+K_{m44,2})}$
$GC + NAD^+ + GDC \longrightarrow CO_2 + NH_4^+ + NADH + MLG$	v_{45}	$k_{36}u_{46}u_{47}u_{48}$	$\frac{V_{45max}u_{46}u_{47}u_{48}}{(u_{46}+K_{m45,1})(u_{47}+K_{m45,2})(u_{48}+K_{m45,3})}$
$MLG + GL + H_2O \longrightarrow Ser + GDC$	v_{46}	$k_{37}u_{50}u_{51}$	$\frac{V_{46max}u_{50}u_{51}}{(u_{50}+K_{m46,1})(u_{51}+K_{m46,2})}$
$Ser + OGA \longrightarrow HDP + GDC$	v_{47}	$k_{41}u_{36}u_{52}$	$\frac{V_{47max}u_{36}u_{52}}{(u_{36}+K_{m47,1})(u_{52}+K_{m47,2})}$
$HDP + NADH + H^+ \longrightarrow GA + NAD^+$	v_{48}	$k_{42}u_{12}u_{49}u_{59}$	$\frac{V_{48max}u_{12}u_{49}u_{59}}{(u_{12}+K_{m48,1})(u_{49}+K_{m48,2})(u_{59}+K_{m48,3})}$
$GA + ATP \longrightarrow PGAL + ADP$	v_{49}	$k_{33}u_{13}u_{32}$	$\frac{V_{49max}u_{13}u_{32}}{(u_{13}+K_{m49,1})(u_{32}+K_{m49,2})}$
$GMa + NH_4^+ + ATP \longrightarrow GMi + ADP + P_i$	v_{50}	$k_{34}u_{13}u_{33}u_{34}$	$\frac{V_{50max}u_{13}u_{33}u_{34}}{(u_{13}+K_{m50,1})(u_{33}+K_{m50,2})(u_{34}+K_{m50,3})}$
$OGA + GMi + 2\,Fd_{red} + 2\,H^+ \longrightarrow 2\,GMa + 2\,Fd_{oxid}$	v_{51}	$k_{35}u_{12}u_{35}u_{36}u_{38}$	$\frac{V_{51max}u_{12}u_{35}u_{36}u_{38}}{(u_{12}+K_{m51,1})(u_{35}+K_{m51,2})(u_{36}+K_{m51,3})(u_{38}+K_{m51,3})}$

Sub-Model I

The RDEs for Calvin cycle, photorespiration, and starch synthesis in the chloroplast (Ω_1) are represented in the following forms (equations (3.45) to (3.81))

$$\frac{\partial [CO_2]}{\partial t} = D_{CO_2}\Delta[CO_2] - v_4 \tag{3.45}$$

$$\frac{\partial [RuBP]}{\partial t} = D_{RuBP}\Delta[RuBP] - v_4 + v_{16} - v_{40} \tag{3.46}$$

$$\frac{\partial [PGA]}{\partial t} = D_{PGA}\Delta[PGA] + 2v_4 - v_5 + v_{40} + v_{49} \tag{3.47}$$

$$\frac{\partial [H^+_{stroma}]}{\partial t} = D_{H^+_{st}}\Delta[H^+] + v_1 - v_2 + 2v_4 - v_6 + v_{16} - v_{51} \tag{3.48}$$

$$\begin{aligned}\frac{\partial [ATP]}{\partial t} =& D_{ATP}\Delta[ATP] + v_3 - v_5 - v_{16} - v_{20} - v_{22} - v_{26} \\ & - v_{49} - v_{50}\end{aligned} \tag{3.49}$$

$$\frac{\partial [BPGA]}{\partial t} = D_{BPGA}\Delta[BPGA] + v_5 - v_6 \tag{3.50}$$

$$\begin{aligned}\frac{\partial [ADP]}{\partial t} =& D_{ADP}\Delta[ADP] - v_3 + v_5 + v_{16} + v_{20} + v_{22} + v_{27} \\ & + v_{49} + v_{50}\end{aligned} \tag{3.51}$$

$$\frac{\partial [NADPH]}{\partial t} = D_{NADPH}\Delta[NADPH] + v_2 - v_6 \tag{3.52}$$

$$\frac{\partial [PGAL]}{\partial t} = D_{PGAL}\Delta[PGAL] + v_6 - v_7 - v_8 - v_{10} - v_{13} - v_{17} - v_{18} \tag{3.53}$$

$$\frac{\partial [NADP^+]}{\partial t} = D_{NADP^+}\Delta[NADP^+] - v_2 + v_6 \tag{3.54}$$

$$\begin{aligned}\frac{\partial [P_i]}{\partial t} =& D_{P_i}\Delta[P_i] - v_3 + v_6 + v_9 + v_{12} + v_{19} + v_{21} + v_{23} \\ & + v_{41} + v_{50}\end{aligned} \tag{3.55}$$

$$\frac{\partial [DHAP]}{\partial t} = D_{DHAP}\Delta[DHAP] + v_7 - v_8 - v_{11} + v_{17} - v_{18} \tag{3.56}$$

$$\frac{\partial [FBP]}{\partial t} = D_{FBP}\Delta[FBP] + v_8 - v_9 + v_{18} - v_{19} + v_{20} + v_{21} \tag{3.57}$$

$$\begin{aligned}\frac{\partial [FP]}{\partial t} =& D_{FP}\Delta[FP] + v_9 - v_{10} + v_{19} - v_{20} - v_{21} - v_{22} \\ & + v_{23} - v_{24}\end{aligned} \tag{3.58}$$

$$\frac{\partial [EP]}{\partial t} = D_{EP}\Delta[EP] + v_{10} - v_{11} \tag{3.59}$$

The RDEs for Calvin cycle, photorespiration, and starch synthesis in the chloroplast (continued from previous page)

$$\frac{\partial[XP]}{\partial t} = D_{XP}\Delta[XP] + v_{10} + v_{13} - v_{14} \tag{3.60}$$
$$\frac{\partial[SBP]}{\partial t} = D_{SBP}\Delta[SBP] + v_{11} - v_{12} \tag{3.61}$$
$$\frac{\partial[SuP]}{\partial t} = D_{SuP}\Delta[SuP] + v_{12} - v_{13} \tag{3.62}$$
$$\frac{\partial[RP]}{\partial t} = D_{RP}\Delta[RP] + v_{13} - v_{15} \tag{3.63}$$
$$\frac{\partial[RuP]}{\partial t} = D_{RuP}\Delta[RuP] + v_{14} + v_{15} - v_{16} \tag{3.64}$$
$$\frac{\partial[O_2]}{\partial t} = D_{O_2}\Delta[O_2] + v_1 - v_{40} \tag{3.65}$$
$$\frac{\partial[PGC]}{\partial t} = D_{PGC}\Delta[PGC] + v_{40} - v_{41} \tag{3.66}$$
$$\frac{\partial[GCL]}{\partial t} = D_{GCL}\Delta[GCL] + v_{41} \tag{3.67}$$
$$\frac{\partial[GA]}{\partial t} = D_{GA}\Delta[GA] - v_{49} \tag{3.68}$$
$$\frac{\partial[GMa]}{\partial t} = D_{GMa}\Delta[GMa] - v_{50} + 2v_{51} \tag{3.69}$$
$$\frac{\partial[NH_4^+]}{\partial t} = D_{NH_4^+}\Delta[NH_4^+] - v_{50} \tag{3.70}$$
$$\frac{\partial[GMi]}{\partial t} = D_{GMi}\Delta[GMi] + v_{50} - v_{51} \tag{3.71}$$
$$\frac{\partial[OGA]}{\partial t} = D_{OGA}\Delta[OGA] - v_{51} \tag{3.72}$$
$$\frac{\partial[Fd_{ox}]}{\partial t} = D_{Fd_{ox}}\Delta[Fd_{ox}] + 2v_{51} \tag{3.73}$$
$$\frac{\partial[Fd_{red}]}{\partial t} = D_{Fd_{red}}\Delta[Fd_{red}] - 2v_{51} \tag{3.74}$$
$$\frac{\partial[PP_i]}{\partial t} = D_{PP_i}\Delta[PP_i] - v_{21} + v_{26} \tag{3.75}$$
$$\frac{\partial[FTBP]}{\partial t} = D_{FTBP}\Delta[FTBP] + v_{22} - v_{23} \tag{3.76}$$
$$\frac{\partial[GSP]}{\partial t} = D_{GSP}\Delta[GSP] + v_{24} - v_{25} \tag{3.77}$$
$$\frac{\partial[GP]}{\partial t} = D_{GP}\Delta[GP] + v_{25} - v_{26} \tag{3.78}$$

The RDEs for Calvin cycle, photorespiration, and starch synthesis in the chloroplast (continued from previous page)

$$\frac{\partial [ADPG]}{\partial t} = D_{ADPG}\Delta[ADPG] + v_{26} - v_{27} \tag{3.79}$$
$$\frac{\partial [Primer]}{\partial t} = D_{Primer}\Delta[Primer] - v_{27} \tag{3.80}$$
$$\frac{\partial [A]}{\partial t} = D_{A}\Delta[A] + v_{27} \tag{3.81}$$
$$\text{in} \quad [0,T] \times \Omega_1.$$

Sub-Model II

The RDEs for photorespiration in the mitochondria are read (equations (3.82) to (3.90))

$$\frac{\partial [GC]}{\partial t} = D_{GC}\Delta[GC] - v_{45} \tag{3.82}$$
$$\frac{\partial [NAD^+]}{\partial t} = D_{NAD^+}\Delta[NAD^+] - v_{45} \tag{3.83}$$
$$\frac{\partial [GDC]}{\partial t} = D_{GDC}\Delta[GDC] - v_{45} + v_{46} \tag{3.84}$$
$$\frac{\partial [CO_2]}{\partial t} = D_{CO_2}\Delta[CO_2] + v_{45} \tag{3.85}$$
$$\frac{\partial [NH_4^+]}{\partial t} = D_{NH_4^+}\Delta[NH_4^+] + v_{45} \tag{3.86}$$
$$\frac{\partial [NADH]}{\partial t} = D_{NADH}\Delta[NADH] + v_{45} \tag{3.87}$$
$$\frac{\partial [MLG]}{\partial t} = D_{MLG}\Delta[MLG] - v_{46} \tag{3.88}$$
$$\frac{\partial [GL]}{\partial t} = D_{GL}\Delta[GL] - v_{46} \tag{3.89}$$
$$\frac{\partial [Ser]}{\partial t} = D_{Ser}\Delta[Ser] + v_{46} \tag{3.90}$$
$$\text{in} \quad [0,T] \times \Omega_2.$$

Sub-Model III

The RDEs for photorespiration in the peroxisome are defined by (equations (3.91) to (3.103))

$$\frac{\partial[GCL]}{\partial t} = D_{GCL}\Delta[GCL] - v_{42} \tag{3.91}$$
$$\frac{\partial[O_2]}{\partial t} = D_{O_2}\Delta[O_2] - v_{42} + v_{43} \tag{3.92}$$
$$\frac{\partial[GOL]}{\partial t} = D_{GOL}\Delta[GOL] + v_{42} - v_{44} \tag{3.93}$$
$$\frac{\partial[H_2O_2]}{\partial t} = D_{H_2O_2}\Delta[H_2O_2] + v_{42} - 2v_{43} \tag{3.94}$$
$$\frac{\partial[GMa]}{\partial t} = D_{GMa}\Delta[GMa] - v_{44} \tag{3.95}$$
$$\frac{\partial[GC]}{\partial t} = D_{GC}\Delta[GC] + v_{44} \tag{3.96}$$
$$\frac{\partial[OGA]}{\partial t} = D_{OGA}\Delta[OGA] + v_{44} - v_{47} \tag{3.97}$$
$$\frac{\partial[Ser]}{\partial t} = D_{Ser}\Delta[Ser] - v_{47} \tag{3.98}$$
$$\frac{\partial[HDP]}{\partial t} = D_{HDP}\Delta[HDP] + v_{47} - v_{48} \tag{3.99}$$
$$\frac{\partial[NADH]}{\partial t} = D_{NADH}\Delta[NADH] - v_{48} \tag{3.100}$$
$$\frac{\partial[H^+]}{\partial t} = D_{H^+}\Delta[H^+] - v_{48} \tag{3.101}$$
$$\frac{\partial[GA]}{\partial t} = D_{GA}\Delta[GA] + v_{48} \tag{3.102}$$
$$\frac{\partial[NAD^+]}{\partial t} = D_{NAD^+}\Delta[NAD^+] + v_{48} \tag{3.103}$$

in $[0,T] \times \Omega_3$.

Sub-Model IV

The RDEs for sucrose synthesis in the cytosol is represent by (equations (3.104) to (3.127))

$$\frac{\partial[DHAP]}{\partial t} = D_{DHAP}\Delta[DHAP] - v_{28} - v_{29} \tag{3.104}$$
$$\frac{\partial[PGAL]}{\partial t} = D_{PGAL}\Delta[PGAL] + v_{28} - v_{29} \tag{3.105}$$
$$\frac{\partial[FBP]}{\partial t} = D_{FBP}\Delta[FBP] + v_{29} - v_{30} + v_{31} + v_{32} \tag{3.106}$$
$$\frac{\partial[FP]}{\partial t} = D_{FP}\Delta[FP] + v_{30} - v_{31} - v_{32} - v_{33} + v_{34} - v_{35} - v_{38} \tag{3.107}$$
$$\frac{\partial[ATP]}{\partial t} = D_{ATP}\Delta[ATP] - v_{31} - v_{33} \tag{3.108}$$
$$\frac{\partial[ADP]}{\partial t} = D_{ADP}\Delta[ADP] + v_{31} + v_{33} \tag{3.109}$$
$$\frac{\partial[PP_i]}{\partial t} = D_{PP_i}\Delta[PP_i] - v_{32} + v_{37} \tag{3.110}$$
$$\frac{\partial[P_i]}{\partial t} = D_{P_i}\Delta[P_i] + v_{30} + v_{32} + v_{34} + v_{39} \tag{3.111}$$
$$\frac{\partial[FTBP]}{\partial t} = D_{FTBP}\Delta[FTBP] + v_{33} - v_{34} \tag{3.112}$$
$$\frac{\partial[GSP]}{\partial t} = D_{GSP}\Delta[GSP] + v_{35} - v_{36} \tag{3.113}$$
$$\frac{\partial[GP]}{\partial t} = D_{GP}\Delta[GP] + v_{36} - v_{37} \tag{3.114}$$
$$\frac{\partial[UDP]}{\partial t} = D_{UDP}\Delta[UDP] - v_{37} + v_{38} \tag{3.115}$$
$$\frac{\partial[UDPG]}{\partial t} = D_{UDPG}\Delta[UDPG] + v_{37} - v_{38} \tag{3.116}$$
$$\frac{\partial[SSP]}{\partial t} = D_{SSP}\Delta[SSP] + v_{38} - v_{39} \tag{3.117}$$
$$\frac{\partial[S]}{\partial t} = D_{S}\Delta[S] + v_{39} \tag{3.118}$$
$$\frac{\partial[CO_2]}{\partial t} = D_{CO_2}\Delta[CO_2] \tag{3.119}$$
$$\frac{\partial[O_2]}{\partial t} = D_{O_2}\Delta[O_2] \tag{3.120}$$
$$\frac{\partial[GCL]}{\partial t} = D_{GCL}\Delta[GCL] \tag{3.121}$$
$$\frac{\partial[GA]}{\partial t} = D_{GA}\Delta[GA] \tag{3.122}$$
$$\frac{\partial[GMa]}{\partial t} = D_{GMa}\Delta[GMa] \tag{3.123}$$

The RDEs for sucrose synthesis in the cytosol (continued from previous page)

$$\frac{\partial [NH_4^+]}{\partial t} = D_{NH_4^+} \Delta [NH_4^+] \tag{3.124}$$

$$\frac{\partial [GC]}{\partial t} = D_{GC} \Delta [GC] \tag{3.125}$$

$$\frac{\partial [OGA]}{\partial t} = D_{OGA} \Delta [OGA] \tag{3.126}$$

$$\frac{\partial [Ser]}{\partial t} = D_{Ser} \Delta [Ser] \tag{3.127}$$

in $[0,T] \times \Omega_0$.

Sub-Model V

According to the fact that sucrose is the final product transported from cytosol to vacuole. Moreover, the vacuole is a location to stored the sucrose. We will therefore only consider the diffusion of sucrose in the vacuole. So that a mathematical model is simply defined by

$$\frac{\partial [S]}{\partial t} = D_S \Delta [S] \quad \text{in} \quad [0,T] \times \Omega_4. \tag{3.128}$$

In the next step, we need to develop a initial conditions, boundary conditions, and transmission conditions for each Sub-Model. Before forming any conditions, we need to give some definitions about the set of the chemical species in each sub-domains.

Set of the chemical species

Suppose a set of the chemical species are designed as follows:

$$\begin{aligned}\mathbb{S}_0 = \{&DHAP, PGAL, FBP, FP, ATP, PP_i, P_i, FTBP, GSP, GP,\\ &UDP, UDPG, SSP, S, CO_2, O_2, GCL, GA, GMa, NH_4^+,\\ &GC, OGA, Ser\}. \end{aligned} \tag{3.129}$$

$$\begin{aligned}\mathbb{S}_1 = \{&CO_2, RuBP, PGA, H^+_{stroma}, ATP, BPGA, ADP, NADPH, PGAL,\\ &NADP^+, P_i, DHAP, FBP, FP, EP, XP, SBP, SuP, RP, RuP, O_2,\\ &PGC, GCL, GA, GMa, NH_4^+, GMi, OGA, Fd_{oxid}, Fd_{red}, PP_i,\\ &FTBP, GSP, GP, ADPG, Primer, A, X_{PSII}, X^+_{PSII}, X_{PSI}, X^+_{PSI},\\ &H^+_{lumen}, e^-_{PSII}, e^-_{PSI}, e^-_{H2O}\}. \end{aligned} \tag{3.130}$$

$$\mathbb{S}_2 = \{GC, NAD^+, GDC, CO_2, NH_4^+, NADH, MLG, Ser\}. \tag{3.131}$$

$$\begin{aligned}\mathbb{S}_3 = \{&GCL, O_2, GOL, H_2O_2, GMa, GC, OGA, Ser, HDP, NADH,\\ &H^+_{stroma}, GA, NAD^+\}. \end{aligned} \tag{3.132}$$

$$\mathbb{S}_4 = \{S\}, \tag{3.133}$$

where $\mathbb{S}_0, \mathbb{S}_1, \mathbb{S}_2, \mathbb{S}_3, \mathbb{S}_4$ are sets of the chemical species in cytosol ($j = 0$), chloroplast ($j = 1$), mitochondria ($j = 2$), peroxisome ($j = 3$), and vacuole ($j = 4$), respectively.

According to transmission of some chemical species between cytosol and others sub-domains (see Table 2.3). Therefore, the sets of transmitting chemical species across the interfaces are shown in the following forms:

$$\mathbb{T}_{01} = \{CO_2, GA, OGA, NH_4^+\}, \tag{3.134}$$

$$\mathbb{T}_{10} = \{PGAL, DHAP, O_2, GCL, GMa\}, \tag{3.135}$$

$$\mathbb{T}_{02} = \{GC\}, \tag{3.136}$$

$$\mathbb{T}_{20} = \{CO_2, Ser, NH_4^+\}, \tag{3.137}$$

$$\mathbb{T}_{03} = \{O_2, GCL, GMa, Ser\}, \tag{3.138}$$

$$\mathbb{T}_{30} = \{GA, OGA, GC\}, \tag{3.139}$$

$$\mathbb{T}_{04} = \{S\}, \tag{3.140}$$

where $\mathbb{T}_{01}$ represents the chemical species transporting from cytosol (Ω_0) to chloroplast (Ω_1), and vice versa for $\mathbb{T}_{10}$. Consequently, the same idea can be applied to $\mathbb{T}_{02}, \mathbb{T}_{20}, \mathbb{T}_{03}, \mathbb{T}_{30}$, and $\mathbb{T}_{04}$, respectively.
For the simplicity, we also defined the following sets:

$$\mathbb{T}_1 = \mathbb{T}_{01} \cup \mathbb{T}_{10}, \tag{3.141}$$
$$\mathbb{T}_2 = \mathbb{T}_{02} \cup \mathbb{T}_{20}, \tag{3.142}$$
$$\mathbb{T}_3 = \mathbb{T}_{03} \cup \mathbb{T}_{30}, \tag{3.143}$$
$$\mathbb{T}_4 = \mathbb{T}_{04}. \tag{3.144}$$

Moreover, we denoted that a set of all chemical species in Ω by

$$\mathbb{S} = \cup_{j=1}^{4} (\mathbb{S}_0 \cup \mathbb{S}_j) \setminus \mathbb{T}_j. \tag{3.145}$$

Discussion of the boundary and the transmission conditions

The boundary of $\partial\Omega$ the region Ω is a disjoint union of Γ_j, where $\Gamma_j = \partial\Omega_j$ for $j = 1,\ldots,4$ and $\Gamma_0 = \partial\Omega_o \cup_{0<j} \Gamma_j$ is the outer boundary of Ω_0. In order to determine the solutions of the system of partial differential equations we need boundary conditions on Γ_0 respectively for all substances with no direct coupling on Γ_j of their distributions in Ω_0 and in Ω_j. In this case of impermeability the no flux condition

$$D_i^j \frac{\partial u_i^j(t,x)}{\partial n} = 0 \quad \text{on} \quad \Gamma_j, \tag{3.146}$$

is set. $\partial/\partial n$ is the outward normal derivative on the boundary.

In the other cases a transmission condition has to be chosen. Here we consider as a general assumption
(1) continuity of the fluxes

$$D_i^0 \frac{\partial u_i^0(t,x)}{\partial n} + D_i^j \frac{\partial u_i^j(t,x)}{\partial n} = 0 \quad \text{on} \quad \Gamma_j, \tag{3.147}$$

assuming that there are no processes are taking place on the interfaces.
(2) An additional assumption has to made. Here we consider two possibilities
(i) Continuity also of the concentrations is described:

$$u_i^0(t,x) = u_i^j(t,x) \quad \text{on} \quad \Gamma_j. \tag{3.148}$$

We remark that a more general relation between the values on both sides on Γ_j might come up. However, here only this simpler condition is posed.

(ii) The flux of the substances through the interface is described as a function of the concentration on both sides.

$$D_i^0 \frac{\partial u_i^j(t,x)}{\partial n} = \varphi_i^j(u_i^0, u_i^j) \tag{3.149}$$

Here in we are considering for permeable case

$$\varphi_i^j(u_i^0, u_i^j) = \zeta_i^j(u_i^0 - u_i^j), \tag{3.150}$$

for the semi-permeable case

$$\begin{aligned} \varphi_i^j(u_i^0, u_i^j) &= \zeta_i^j(u_i^0 - u_i^j)^+ \quad \text{respectively,} \\ &= \zeta_i^j(u_i^0 - u_i^j)^-. \end{aligned} \tag{3.151}$$

Here ζ_i^j is a nonnegative number.

Together with the initial conditions:

$$u_i^j(t = t_0, x) = u_0, \in \mathbb{R}^+ \cup \{0\} \quad \text{in} \quad \Omega_j, \quad \forall u_i^j \in \mathbb{S}_j. \tag{3.152}$$

We can formulate an initial-boundary value problem with transmission conditions. The analytic problem arises, under which conditions this system has for nonnegative initial data a unique, nonnegative solution, which is sufficiently smooth and exists for all time. Also for smaller sizes of the system this is posing a challenge to mathematical theory due to the fact the system has different diffusion conditions and that in particular in case of mass-reaction kinetics explosion might happen in finite times. The transmission conditions add further difficulties. Before starting a detailed analysis to solve this problem, the complex model set up in this investigation should be simulated and the results should be discussed and its relevance checked. Solving also the analytic problem without making too strong and non-realistic assumptions, is out off the scope of this thesis.

Chapter 4

Variational Formulation

First of all we consider a domain $\Omega = \cup\Omega_j$. The boundary of the domain is denoted by $\partial\Omega$ and the closure $\Omega \cup \partial\Omega$ is denoted by $\overline{\Omega}$. Consider the following system of the initial boundary value problem with Neumann and transmission conditions where a given function $f_i^j \in L^2\left(]0,T[;L^2\left(\Omega_j\right)\right)$. We are looking for a function $u_i^j : C^1\left([0,\infty],H^{1,2}(\Omega_j)\right)$ such that

$$\begin{aligned} \partial_t u_i^j - L_i u_i^j = \quad & f_i^j(t,x,u^j), \quad u^j = (u_1^j,\ldots,u_m^j), \quad i = 1,\ldots,m \\ t \in (0,T]\,, x \in \Omega & \end{aligned} \tag{4.1}$$

where $m \in \mathbb{N}$, L_i are the operators in the following form

$$L_i \equiv D_i^j \Delta, \quad i = 1,\ldots,m \tag{4.2}$$

$D_i^j \in \mathbb{R}^+ \cup \{0\}$, and Δ is the Laplacian. Considering (4.1) and (4.2) together with the following initial conditions, boundary conditions, and transmission conditions:

The initial conditions
For $u_i^0 \in \mathbb{S}_0$ (in cytosol),

$$u_i^0(t = t_0, x) = u_{i,t=0}^0 \in \mathbb{R}^+ \cup \{0\} \quad \text{in} \quad \Omega_0, \tag{4.3}$$

For $u_i^j \in \mathbb{S}_j$ (in each organelle),

$$u_i^j(t = t_0, x) = u_{i,t=0}^j \in \mathbb{R}^+ \cup \{0\} \quad \text{in} \quad \Omega_j, \tag{4.4}$$

where $j = 1,\ldots,4$.

The Neumann boundary conditions

For some chemical species in the cytosol that do not move cross the organelle membrane (Γ_j), $u_i \in \mathbb{S}_0 \setminus \mathbb{T}_j$ and there are no chemical species transported out of the cell:

$$D_i \frac{\partial u_i(t,x)}{\partial n} = 0 \quad \text{on} \quad \Gamma_j, \tag{4.5}$$

where $j = 0,\ldots,4$ and $\partial/\partial n$ is the outward normal derivative on the boundary.

Similar to the chemical species in each sub-domain that diffusion is only inside the organelle: $u_i \in \mathbb{T}_j$, $(j = 1,\ldots,4)$

$$D_i \frac{\partial u_i(t,x)}{\partial n} = 0 \quad \text{on} \quad \Gamma_j, \tag{4.6}$$

Transmission conditions and continuity of flux

For the chemical species that is transported from the cytosol (Ω_0) across the organelle membrane: $u_i \in \mathbb{T}_{0j}$,

$$D_i^0 \frac{\partial u_i^0(t,x)}{\partial n} + D_i^j \frac{\partial_n u_i^j(t,x)}{\partial n} = 0 \quad \text{on} \quad \Gamma_j, \tag{4.7}$$

$$D_i^0 \frac{\partial u_i^0(t,x)}{\partial n} = -\zeta_i^j (u_i^0(t,x) - u_i^j(t,x)) \quad \text{on} \quad \Gamma_j, \tag{4.8}$$

where $j = 1,\ldots,4$. $u_i^0(t,x), u_i^j(t,x)$ are a concentration of a chemical species i in a compartment 0 and j, respectively. On the other hand, there are some chemical species moving across the membrane from inside of the organelle to the cytosol: $u_i \in \mathbb{T}_{j0}$,

$$D_i^j \frac{\partial_n u_i^j(t,x)}{\partial n} + D_i^0 \frac{\partial u_i^0(t,x)}{\partial n} = 0 \quad \text{on} \quad \Gamma_j, \tag{4.9}$$

$$D_i^0 \frac{\partial u_i^j(t,x)}{\partial n} = -\zeta_i^j (u_i^j(t,x) - u_i^0(t,x)) = 0 \quad \text{on} \quad \Gamma_j, \tag{4.10}$$

where $j = 1,\ldots,4$. However the semi-permeability do not included in this part.

For the simplicity, we give the index i for each chemical species as in the Table 4.1.

4.1 Variational formulation

In this section we present the derivation of the variational (or weak) formulation of the mathematical model in the previous chapter: Given a function

Table 4.1: The chemical species

Index i	Chemical species
1	X_{PSII}
2	X^{+}_{PSII}
3	e^{-}_{PSII}
4	X_{PSI}
5	X^{+}_{PSI}
6	e^{-}_{PSI}
7	$e^{-}_{H_2O}$
8	H^{+}_{lumen}
9	CO_2
10	$RuBP$
11	PGA
12	H^{+}_{stroma}
13	ATP
14	$BPGA$
15	ADP
16	$NADPH$
17	$PGAL$
18	$NADP^{+}$
19	P_i
20	$DHAP$
21	FBP
22	FP
23	EP
24	XP
25	SBP
26	SuP
27	RP
28	RuP
29	O_2
30	PGC

Index i	Chemical species
31	GCL
32	GA
33	GMa
34	NH^{+}_{4}
35	GMi
36	OGA
37	Fd_{oxid}
38	Fd_{red}
39	PP_i
40	$FTBP$
41	GSP
42	GP
43	$ADPG$
44	$Primer$
45	A
46	GC
47	NAD^{+}
48	GDC
49	$NADH$
50	MLG
51	GL
52	Ser
53	UDP
54	$UDPG$
55	SSP
56	S
57	GOL
58	H_2O_2
59	HDP

$f_i^j : \Omega \to \mathbb{R}$, find a function $u : [0,\infty) \times \overline{\Omega} \to \mathbb{R}$. In order to formulate problem (4.1-4.10) in a weak sense, we assume that $f_i^j \in L^2\left(]0,T[;L^2\left(\Omega_j\right)\right)$ and $u_{i,t=0}^j \in H^{1,2}(\Omega_j)$. We consider an arbitrary $v_i \in H_0^1(\Omega)$ as so-called *test functions*. Multiply a test function v_i^j to (4.1-4.2) and integrate over the domain Ω, so that we obtain

$$\int_\Omega \partial_t u_i^j v_i^j dx - \int_\Omega D_i^j \Delta u_i^j v_i^j dx = \int_\Omega f_i v_i dx, \tag{4.11}$$

and by applying *Green's formula*, we get

$$\int_\Omega \partial_t u_i^j v_i^j dx + \int_\Omega D_i^j \nabla u_i^j \cdot \nabla v_i^j dx - \int_{\partial\Omega} D_i^j \frac{\partial u_i^j}{\partial n} \cdot v_i^j d\sigma = \int_\Omega f_i^j v_i^j dx. \tag{4.12}$$

Suppose that we define a real-valued mapping a by

$$a(u,v) := \int_\Omega D_i^j \nabla u(x) \cdot \nabla v(x) dx, \tag{4.13}$$

where $u \in C^1(\overline{\Omega}), v \in H_0^1(\Omega)$, then the solution of the initial boundary value problem satisfies

$$\boxed{(\partial_t u_i^j, v_i^j) + a(u_i^j, v_i^j) = (f_i^j, v_i^j) + \int_{\partial\Omega} D_i^j \frac{\partial u_i^j}{\partial n} \cdot v_i^j d\sigma} \tag{4.14}$$

where

$$(u,v) = \int_\Omega uv dx$$

and

$$\partial\Omega = \Gamma = \bigcup_{j=0}^{4} \Gamma_j$$

together with the initial-boundary conditions in (4.3-4.10). From the weak formulation problem (4.14), we next write down the weak form of our mathematical model from Chapter 3. According to the boundary conditions and transmissions above, we are considering a weak form for a chemical species in a specific sub-compartment.

Weak formulation for a chemical species in Ω_0

In sub-domain Ω_0, the weak formulation for each chemical specie $u_i^0 \in \mathbb{S}_0$ is corresponds to the following form

$$(\partial_t u_i^0, v_i^0) + a(u_i^0, v_i^0) = (f_i^0, v_i^0) + \sum_{j=0}^{4} \int_{\Gamma_j} D_i^0 \partial_n u_i^0 \cdot v_i^0 d\sigma \tag{4.15}$$

Considering the second term of the right hand side of equation (4.15), we see that

$$\int_{\Gamma_0} D_i^0 \partial_n u_i^0 \cdot v_i^0 d\sigma \quad = \quad 0 \quad \forall u_i^0 \in \mathbb{S}_0, \tag{4.16}$$

and

$$\int_{\Gamma_j} D_i^0 \partial_n u_i^0 \cdot v_i^0 d\sigma = \begin{cases} 0 & \forall u_i^0 \in \mathbb{S}_0 \setminus \mathbb{T}_j, \\ \int_{\Gamma_j} \zeta_i^j (u_i^j - u_i^0) \cdot v_i d\sigma & \forall u_i \in \mathbb{T}_{0j}, \end{cases} \tag{4.17}$$

where $j = 1, \ldots, 4$.

In agreement with the complexity of the chemical network, there are 7 groups of chemical species in the sub-domain Ω_0 transporting across membranes to another sub-domain:

(1) CO_2 $(i = 9)$ and NH_4^+ $(i = 34)$ moving from Ω_2 to Ω_0 and from Ω_0 to Ω_1, so that a weak formulation for CO_2 and NH_4^+ is

$$\begin{aligned} (\partial_t u_i^0, v_i^0) + a(u_i^0, v_i^0) \quad &= \quad (f_i^0, v_i^0) + \int_{\Gamma_1} \zeta_i^j (u_i^1 - u_i^0) \cdot v_i^0 d\sigma \\ &\quad + \int_{\Gamma_2} \zeta_i^j (u_i^0 - u_i^2) \cdot v_i^0 d\sigma \quad \text{in} \quad \Omega_0. \end{aligned} \tag{4.18}$$

(2) GA $(i = 32)$ and OGA $(i = 36)$ moving from Ω_3 to Ω_0 and from Ω_0 to Ω_1, then the weak formulation for GA and OGA is

$$\begin{aligned} (\partial_t u_i^0, v_i^0) + a(u_i^0, v_i^0) \quad &= \quad (f_i^0, v_i^0) + \int_{\Gamma_1} \zeta_i^j (u_i^1 - u_i^0) \cdot v_i^0 d\sigma \\ &\quad + \int_{\Gamma_3} \zeta_i^j (u_i^0 - u_i^3) \cdot v_i^0 d\sigma \quad \text{in} \quad \Omega_0. \end{aligned} \tag{4.19}$$

(3) O_2 $(i = 29)$, GCL $(i = 31)$, and GMa $(i = 33)$ moving from Ω_1 to Ω_0 and from Ω_0 to Ω_3, therefore the weak formulation for O_2, GCL, and GMa is

$$\begin{aligned} (\partial_t u_i^0, v_i^0) + a(u_i^0, v_i^0) \quad &= \quad (f_i^0, v_i^0) + \int_{\Gamma_1} \zeta_i^j (u_i^0 - u_i^1) \cdot v_i^0 d\sigma \\ &\quad + \int_{\Gamma_3} \zeta_i^j (u_i^3 - u_i^0) \cdot v_i^0 d\sigma \quad \text{in} \quad \Omega_0. \end{aligned} \tag{4.20}$$

(4) Ser $(i = 52)$ moving from Ω_2 to Ω_0 and from Ω_0 to Ω_3, then the weak formulation for Ser is

$$\begin{aligned} (\partial_t u_i^0, v_i^0) + a(u_i^0, v_i^0) \quad &= \quad (f_i^0, v_i^0) + \int_{\Gamma_2} \zeta_i^j (u_i^0 - u_i^2) \cdot v_i^0 d\sigma \\ &\quad + \int_{\Gamma_3} \zeta_i^j (u_i^3 - u_i^0) \cdot v_i^0 d\sigma \quad \text{in} \quad \Omega_0. \end{aligned} \tag{4.21}$$

(5) *GC* ($i = 46$) moving from Ω_3 to Ω_0 and from Ω_0 to Ω_2, so that the weak formulation for *GC* is

$$\begin{aligned}(\partial_t u_i^0, v_i^0) + a(u_i^0, v_i^0) &= (f_i^0, v_i^0) + \int_{\Gamma_2} \zeta_i^j (u_i^2 - u_i^0) \cdot v_i^0 d\sigma \\ &\quad + \int_{\Gamma_3} \zeta_i^j (u_i^0 - u_i^3) \cdot v_i^0 d\sigma \quad \text{in} \quad \Omega_0. \quad (4.22)\end{aligned}$$

(6) Since *S* ($i = 56$) moving from Ω_0 to Ω_4, thus the weak formulation for *S* is

$$(\partial_t u_i^0, v_i^0) + a(u_i^0, v_i^0) = (f_i^0, v_i^0) + \int_{\Gamma_4} \zeta_i^j (u_i^4 - u_i^0) \cdot v_i^0 d\sigma \quad \text{in} \quad \Omega_0. \quad (4.23)$$

(7) *PGAL* ($i = 17$) and *DHAP* ($i = 20$) moving from Ω_1 to Ω_0, therefore the weak formulation for *PGAL*, and *DHAP* is

$$(\partial_t u_i^0, v_i^0) + a(u_i^0, v_i^0) = (f_i^0, v_i^0) + \int_{\Gamma_1} \zeta_i^j (u_i^0 - u_i^1) \cdot v_i^0 d\sigma \quad \text{in} \quad \Omega_0. \quad (4.24)$$

For all chemical species ($u_i^0 \in \mathbb{S}_0 \setminus (\bigcup_{j=1}^4 \mathbb{T}_j)$) that only diffusion-transport in Ω_0, the weak formulation is defined as follows

$$(\partial_t u_i^0, v_i^0) + a(u_i^0, v_i^0) = (f_i^0, v_i^0) \quad \text{in} \quad \Omega_0. \quad (4.25)$$

Weak formulation for a chemical species in Ω_j

In sub-domain Ω_j ($j = 1, \ldots, 4$), there are chemical species diffusing and transporting in Ω_j, and also some species transmitting through Γ_j. Therefore, the weak formulation for chemical species $u_i^j \in \mathbb{S}_j$ is defined by

(1) for the species that only diffuse-transport in Ω_j,

$$(\partial_t u_i^j, v_i^j) + a(u_i^j, v_i^j) = (f_i^j, v_i^j) \quad \text{in} \quad \Omega_j, \quad \forall u_i^j \in \mathbb{S}_j \setminus \mathbb{T}_j, \quad (4.26)$$

(2) for the species that diffuse-transport in Ω_j, and transmit across membrane in Γ_j,

$$(\partial_t u_i^j, v_i^j) + a(u_i^j, v_i^j) = (f_i^j, v_i^j) + \int_{\Gamma_j} \zeta_i^j (u_i^j - u_i^0) \cdot v_i^j d\sigma \quad \text{in} \quad \Omega_j, \quad \forall u_i^j \in \mathbb{T}_{0j} \quad (4.27)$$

and

$$(\partial_t u_i^j, v_i^j) + a(u_i^j, v_i^j) = (f_i^j, v_i^j) + \int_{\Gamma_j} \zeta_i^j (u_i^0 - u_i^j) \cdot v_i^j d\sigma \quad \text{in} \quad \Omega_j, \quad \forall u_i^j \in \mathbb{T}_{j0}. \quad (4.28)$$

4.2 Summary

In this section, we summarize the weak formulation for the mathematical model. If we let

$$\int_{\Gamma_j} u_i^j \cdot v_i^j d\sigma = < u_i^j, v_i^j > |_{\Gamma_j},$$

then the variational form of the mathematical model is considered in a following form:

$$(\partial_t u_i^j, v_i^j) + a(u_i^j, v_i^j) - (f_i^j, v_i^j) = \mathscr{B}(\zeta_i^j, u_i^j, v_i^j) \quad \text{in} \quad \Omega_i \quad i = 0, \ldots, 4, \tag{4.29}$$

where $\mathscr{B}(\zeta_i^j, u_i^j, v_i^j)$ is defined in each sub-domain.

(1) In the sub-domain Ω_0,

$$\mathscr{B}(\zeta_i^j, u_i^j, v_i^j) = 0 \quad \text{for } i = 13, 19, 21, 22, 39, 40, 41, 42, 53, 54, 55, \tag{4.30}$$

$$\mathscr{B}(\zeta_i^j, u_i^j, v_i^j) = < \zeta_i^j (u_i^1 - u_i^0), v_i^j > |_{\Gamma_1} + < \zeta_i^j (u_i^0 - u_i^2), v_i^j > |_{\Gamma_2} \quad \text{for } i = 9, 34, \tag{4.31}$$

$$\mathscr{B}(\zeta_i^j, u_i^j, v_i^j) = < \zeta_i^j (u_i^0 - u_i^1), v_i^j > |_{\Gamma_1} \quad \text{for } i = 17, 20, \tag{4.32}$$

$$\mathscr{B}(\zeta_i^j, u_i^j, v_i^j) = < \zeta_i^j (u_i^0 - u_i^1), v_i^j > |_{\Gamma_1} + < \zeta_i^j (u_i^3 - u_i^0), v_i^j > |_{\Gamma_3} \quad \text{for } i = 29, 31, \tag{4.33}$$

$$\mathscr{B}(\zeta_i^j, u_i^j, v_i^j) = < \zeta_i^j (u_i^1 - u_i^0), v_i^j > |_{\Gamma_1} + < \zeta_i^j (u_i^0 - u_i^3), v_i^j > |_{\Gamma_3} \quad \text{for } i = 32, 36, \tag{4.34}$$

$$\mathscr{B}(\zeta_i^j, u_i^j, v_i^j) = < \zeta_i^j (u_i^2 - u_i^0), v_i^j > |_{\Gamma_2} + < \zeta_i^j (u_i^0 - u_i^3), v_i^j > |_{\Gamma_3} \quad \text{for } i = 46, \tag{4.35}$$

$$\mathscr{B}(\zeta_i^j, u_i^j, v_i^j) = < \zeta_i^j (u_i^0 - u_i^2), v_i^j > |_{\Gamma_2} + < \zeta_i^j (u_i^3 - u_i^0), v_i^j > |_{\Gamma_3} \quad \text{for } i = 52, \quad \text{and} \tag{4.36}$$

$$\mathscr{B}(\zeta_i^j, u_i^j, v_i^j) = < \zeta_i^j (u_i^4 - u_i^0), v_i^j > |_{\Gamma_4} \quad \text{for } i = 56. \tag{4.37}$$

(2) In the sub-domain Ω_1,

$$\mathscr{B}(\zeta_i^j, u_i^j, v_i^j) = 0 \quad \text{for } i = 1, \ldots, 8, 10, \ldots, 19, 21, \ldots, 30, 35, 37, \ldots, 45 \tag{4.38}$$

$$\mathscr{B}(\zeta_i^j, u_i^j, v_i^j) = < \zeta_i^j (u_i^1 - u_i^0), v_i^j > |_{\Gamma_1} \quad \text{for } i = 9, 32, 34, 36, \quad \text{and} \tag{4.39}$$

$$\mathscr{B}(\zeta_i^j, u_i^j, v_i^j) = < \zeta_i^j (u_i^0 - u_i^1), v_i^j > |_{\Gamma_1} \quad \text{for } i = 17, 20, 29, 31, 33. \tag{4.40}$$

(3) In the sub-domain Ω_2,

$$\mathscr{B}(\zeta_i^j, u_i^j, v_i^j) = 0 \quad \text{for } i = 46, \ldots, 50, \tag{4.41}$$

$$\mathscr{B}(\zeta_i^j, u_i^j, v_i^j) = < \zeta_i^j (u_i^2 - u_i^0), v_i^j > |_{\Gamma_2} \quad \text{for } i = 46, \quad \text{and} \tag{4.42}$$

$$\mathscr{B}(\zeta_i^j, u_i^j, v_i^j) = < \zeta_i^j (u_i^0 - u_i^2), v_i^j > |_{\Gamma_2} \quad \text{for } i = 9, 34, 52. \tag{4.43}$$

(4) In the sub-domain Ω_3,

$$\mathscr{B}(\zeta_i^j, u_i^j, v_i^j) = 0 \quad \text{for } i = 12, 47, 49, 57, 58, 59 \tag{4.44}$$

$$\mathscr{B}(\zeta_i^j, u_i^j, v_i^j) = < \zeta_i^j (u_i^3 - u_i^0), v_i^j > |_{\Gamma_3} \quad \text{for } i = 29, 31, 33, 52, \quad \text{and} \tag{4.45}$$

$$\mathscr{B}(\zeta_i^j, u_i^j, v_i^j) = < \zeta_i^j (u_i^0 - u_i^3), v_i^j > |_{\Gamma_3} \quad \text{for } i = 32, 36, 46. \tag{4.46}$$

(5) In the sub-domain Ω_4,

$$\mathscr{B}(\zeta_i^j, u_i^j, v_i^j) = < \zeta_i^j (u_i^4 - u_i^0), v_i^j > |_{\Gamma_4} \quad \text{in} \quad \Omega_4 \quad \text{for } i = 56. \tag{4.47}$$

However, the general form of the weak formulation reads:

$$\boxed{\sum (\partial_t u_i^j, v_i^j) + \sum a_i^j (u_i^j, v_i^j) = \sum (f_i^j, v_i^j) + \sum_{j=1}^{4} \int_{\Gamma_j} \varphi_i^j (u_i^0, u_i^j) \cdot n}, \quad \text{in} \quad \Omega. \tag{4.48}$$

Chapter 5

Numerical simulation

This chapter is devoted to the approximation of the solution of our mathematical model that represents in a form of time-dependent partial differential equations by finite elements method. From the previous chapter, the strong form of the continuous problems (4.1 - 4.10) is converted to the variational or weak form (4.29 - 4.47). According to the variational formulation of the continuous problems from the previous chapter: Given a function $f_i : \Omega_j \to \mathbb{R}$, where $f_i \in L^2(]0,T[;H^{-1}(\Omega_j))$. We looking for a function $u_i : [0,\infty) \times \overline{\Omega}_j \to \mathbb{R}$, where $u_{i,t=0} \in L^2(\Omega_j)$ and $v_i \in H_0^1(\Omega_j)$ such that

$$\begin{aligned} (\partial_t u_i, v_i) + a(u_i, v_i) - (f_i, v_i) &= \mathscr{B}(\zeta_i^j, u_i, v_i) \quad \text{in} \quad \Omega_j \times \mathbb{R}_+, \\ u_i &= 0, \quad \text{in} \quad \Gamma_j \times \mathbb{R}_+, \\ u_i(\cdot, t=0) &= u_0^i \quad \text{in} \quad \Omega_j, \end{aligned} \tag{5.1}$$

where $i = 1,\ldots,m$, $j = 0,\ldots,4$, and $t > 0$. By using a variational formulation of our problem, we define an approximation of the solution u_i of (5.1) as a function u_i^h that belongs to a finite dimensional linear space S_h of a functions of x for each t. This function will be a solution of a finite system of a linear algebraic equation. From the weak form, we then proceed to discretize the problem (5.1) in the next step. In order to get the fully discrete approximation for discretization processes we first discretize in the spatial variable x and then discretize in the temporal variable t. The approximate solution $u_i^h(t)$ of the finite element space S_h, for each $t > 0$ is a solution of an initial value problem for a finite-dimensional system of an ordinary differential equation.

To solve numerically the variational equation for the photosynthesis model, we are using the Rothe method. The arising elliptic system is discretized by a Galerkin approach. A Newton method is used to solve the non-linear discrete system. To carry out this out step, sketched in the following, the software Gascoigne is used.

Corresponding to a properly chosen rectangular grid of scale h we define the Finite Element space S_h generated by a base $\{\phi_l^h\}$.

Let $u : [0,\infty[\to H^{1,2}(\Omega,\mathbb{R}^M)$ be the solution to variational equation (5.1) which is of the form

$$(\partial_t u, v) + a(u,v) =< r(u), v > \tag{5.2}$$

where $< r(u), v >$ is include the information about the remaining terms and the transmission conditions.

Discretize time and set $U^n := u(t_n,\cdot)$. Projecting U^n on S_h , we define

$$U^n := \sum_l \alpha_l^{n,h}\phi_l^h. \tag{5.3}$$

Set $\alpha^{n,h} := (\alpha_l^{n,h})$. Consider the in time discretized version of (5.2)

$$(\frac{U^n - U^{n-1}}{k}, v) + a(U^n, v) =< r(u), v > \tag{5.4}$$

Projection this equation down to S_h and replacing $r(U^n)$ by $r(U^{n,h})$, we obtain after some calculations an equation for $\alpha_l^{n,h}$ of the type

$$\sum_l B_{jl}^h \alpha_l^{n,h} + k\sum_l A_{jl}^h \alpha_l^{n,h} = k r_j^h(\alpha_l^{n,h}) + k\sum_l B_{jl}^h \alpha_l^{n-1,h}. \tag{5.5}$$

By inversion we can obtain $\alpha_l^{n,h}$ as a linear function of the right hand side. We finally get a nonlinear equation of the following type

$$\alpha_l^{n,h} = F_l^h(\alpha^{n,h}, \alpha^{n-1,h}, k). \tag{5.6}$$

This nonlinear discrete system is solved by Newton Method iteratively.

In this work, the system of time-dependent diffusion-reaction equations was discretized in space with the polynomial Q1 finite element method.

5.1 Numerical simulation tools

In this section, we introduce three parts of a numerical simulation tool including Pre-processor tools, Finite element method tools, and Post-processor tools. In this work, various types of the open source software in Linux platform are required. For the pre-processor tools, we develop a simple C++ code to generate many structures of a 2D and 3D coarse mesh for a domain of the problem and also embed with its organelles (or sub-compartments). To create the coarse mesh, we define a simple algorithm and implement an Object-Oriented Programming (OOP) with *Eclipse IDE for C/C++*. The result of the program is export as an **inp**-files, a coarse mesh describing the domain Ω. For the numerical simulation, we use *gedit* for the text editor and implement with a finite element library called *Gascoigne3D*. As we mention above, the *file.inp* format is a necessary input for the finite element process with the library Gascoigne3D. For the post-processor tools and visualization we use *Gnuplot* and *ParaView* to show the numerical results in 2D, 3D, and also 4D. In this section, we will introduce the development and the implementation with Gascoigne3D for a similar problem in the two dimensional case.

Introduction of Gnuplot and ParaView

In Linux and many platforms, Gnuplot is a portable command-line driven graphing utility that supports many types of plots in 2D and 3D. It also can draw in various form, and shape by using points, lines, and others [37]. An open source so-called *ParaView* is a multiple-platform application for interactive, scientific visualization. This software uses the Visualization Toolkit (VTK) as its data processing and also rendering engine and can, therefore, read any data in VTK format. For the data exploration, its can be done interactively in two and three dimensions. Moreover, we can explore and analyze the data programmatically using ParaView's batch processing capabilities [38]

Introduction of Gascoigne3D

In this work, all of the numerical simulation are performed by using the high-performance adaptive finite element toolkit Gascoigne3D. Gascoigne3D is a open source C++ software library in Linux platform for solving the partial differential equations. The main focus of these software is to provide

a framework for the efficient simulation of complex systems of equations. Various applications can be applied by Gascoigne3D including diffusion and transport processes, chemical reactions, flow problems, time-dependent problem, and also the system of partial differential equations. Moreover there are some library of Gascoigne3D for mesh handling includes definition of the domain, managing of the curve boundaries, refinement of meshes, input and output of meshes in the **inp**-format and **gup**-format. In 2D and 3D case, the *file.inp* is very easy and convenient to visualize and analyze with *ParaView*. In Gascoigne3D, the time discretization is also based on the general θ*-scheme* [39, 40].

5.2 Photosynthesis of plant leaf cell in *silico*

In this section, we present the results of the numerical simulations of the model by using the C++ library Gascoigne3D. According to a complexity of the mathematical model for photosynthesis in chapter 3, some certain assumptions will be made for the numerical experiment.

A computational domain

First of all, we need to design a virtual plant leaf cell as a two-dimensional domain containing multi-organelles inside. For our mathematical model, the computational domain that we are considering is a closed connected 2D domain with fixed boundary as a plant cell. Inside of the computational domain contain 4 finite sub-compartments representing the cell organelles: chloroplast, mitochondria, peroxisome, and vacuole. For the sake of simplicity, we assume that all of the organelles inside a cell have a fixed boundary. Furthermore, we are also considering that the interfaces of two organelles are not overlapped. A shape of C_3 plant leaf cell can be represented as a shape of a *Rectellipse*,

$$\left|\frac{x}{a}\right|^n + \left|\frac{y}{b}\right|^n = 1, \text{ where } n = 4, \quad a,b \in \mathbb{R}^+, \text{ and } (x,y) \in \mathbb{R}^2.$$

In our numerical simulation, we are then the define a following function

$$f(x,y) := -(x-m_x)^4 - (y-m_y)^4 - r^4$$

for representing a 2D plant cell, where m_x, m_y is a midpoint, r is a radius.

For a structure and configuration of the organelles, we can be defined as a shape of a *Circle*, an *Oval* or a *Squircle*. Similar to the example case above, we then construct the coarse mesh for the this case. First of all, we start with a square size 10×10 as a beginning coarse mesh (see also figure 5.1a). Then in order to indicate the embedding fixed sub-compartments or the organelles (red boxes in figure 5.1b), 4 of squares (size 2×2) inside this domain are labeled with difference colors of the interfaces. By modified some parts of the program from the previous example, the structures of a two-dimensional domain are now replotted as the Squircle shape together with four of squircle shape sub-compartments inside. For the coarse mesh output, multiple options of views and visualizes for the 2D computational plant leaf cell in *ParaView* are shown in figure 5.2a and 5.2b. By assigning the data including a mathematical model (system of the reaction-diffusion equation), initial-boundary conditions, continuity of flux, transmission condition, and the parameter set then we can continue to find the approximate solutions of the system.

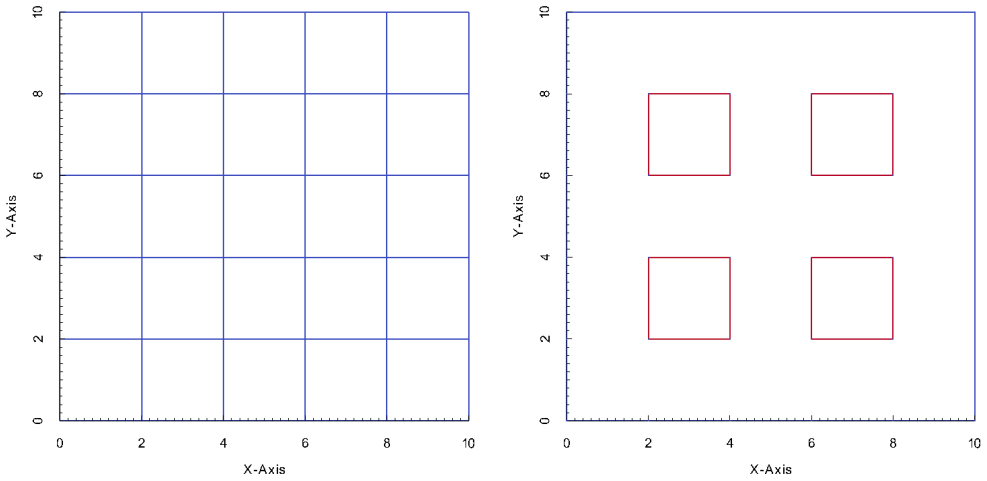

(a) Surface and edge.

(b) Sub-compartments.

Figure 5.1: A cube size 10×10 as a beginning coarse mesh (a) View as a surface and edge. (b) Sub-compartments.

In the next section, we focus on the numerical simulation of the mathematical model of plant leaf cell photosynthesis. Since, the biochemical of plant photosynthesis have been investigated and the full system of plant leaf cell photosynthesis have been proposed in the previous chapter. The biochemical schemes of the mathematical modeling include the complex processes of light-dependent reactions, light-independent reactions, photorespi-

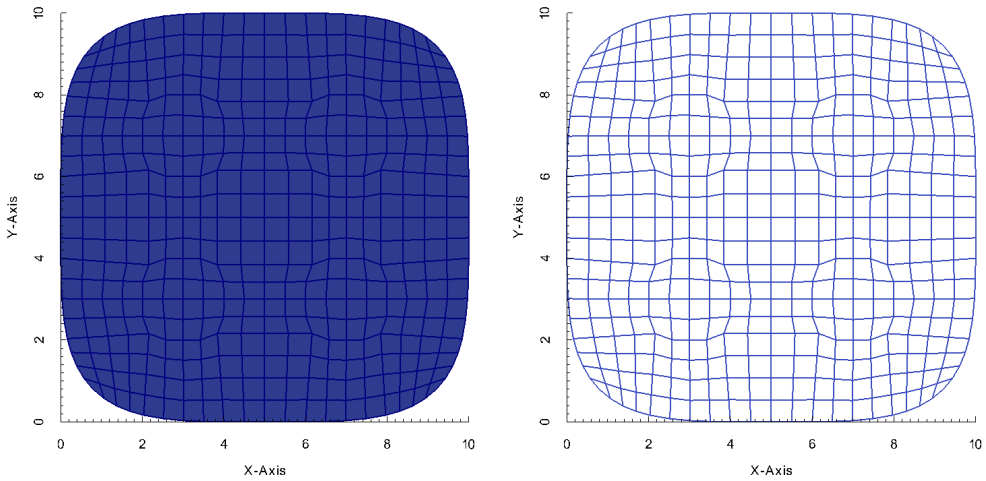

(a) Surface and edge. (b) Wireframe.

Figure 5.2: The computational domain (after the prerefinement) as a finite element coarse mesh (a) View as a surface and edge. (b) View as wireframe.

ration, starch synthesis, and sucrose synthesis. The chemical reactions are also performed in various sub-compartments including the chloroplast, mitochondria, peroxisome, cytoplasm, and vacuole. There are many chemical species transport across the sub-compartment interface, for instance, CO_2, O_2, and sucrose. According to the complexity of the network of the biochemical system, the computer experiments for a sub-network have been developed and analyzed.

Assumptions

In [41], the time sequence of the sub-processes of photosynthesis are perform in difference time scales. The light absorption is the first step that occur in 10^{-15} sec. The carbohydrate formation is the last act in photosynthesis. The enzymes reactions in starch reactions may take several seconds. Furthermore, Karmen [42] has divided the various times scale of the process of photosynthesis into difference eras (see also in Table 5.1).

Base on the investigation about the time sequence above, we have been designed the numerical simulation for C_3 plant leaf cell photosynthesis, also called C_3 photosynthesis in *silico*. The photosynthesis in *silico* is first performed in two parts including the numerical simulation I and II.

Table 5.1: Eras of time sequence

Eras	Actions	Time scales
Radiation Physics	light absorption, excitation energy transfer, trapping of excitation energy	10^{-15} to 10^{-6}
Photochemistry	primary oxidation-reduction reactions,	10^{-10} to 10^{-3}
Biochemistry	Oxygen evolution, Generation of ATP and NADPH, Carbon fixation	10^{-4} to 10^{-2}

In numerical simulation I, we consider only the process of light dependent reactions (LDR) consisting the process of light absorption, water photolysis, electron transport chain, formulation of NADPH, and generation of ATP. Then the coupling process of the light independent reactions (LIR), the photorespiration reactions (PR), and the product of photosynthesis are taken into account for numerical simulation II (see also Table 5.2). Corresponding to the computational domain, the numerical simulation I and II are directly refers to the C_3 plant cell photosynthesis. In this work, we considered that the dynamical products of LDR: O_2, NADPH, and ATP, in the last time step of numerical simulation I are the initial conditions of LIR, PR, and StS in numerical simulation II.

Table 5.2: Overview of the numerical simulation

Simulations	Processes	Input	Output
I	LDR	Light	ATP, NADPH, O_2
II	LIR, PR,	CO_2, ATP, NADPH	PGAL, DHAP
	StS, SuS	PGAL, DHAP	Starch, Sucrose

Next step, our numerical simulations made further assumptions about the computational domain, and the photorespiration process.

First, there was only 4 non-overlapping, closed, and bounded sub-domains embedding inside the domain, i.e. the sub-domain represents all of chloroplast, all of peroxisome, all of mitochondria, all of vacuole compartment, and cytoplasm.

Second, the spatial differentiation between peroxisome, mitochondria, chloroplast and cytosol were considered so that there was a limitation to metabolite

Table 5.3: The transport directions of the chemical species

Processes	Chemical species	Directions
LDR,	CO_2	Mitochondria → Cytosol → Chloroplast
LIR,	GC	Peroxisome → Cytosol → Mitochondria
PR,	NH_4^+	Mitochondria → Cytosol → Chloroplast
and StS	Ser	Mitochondria → Cytosol → Peroxisome
	GCL	Chloroplast → Cytosol → Peroxisome
	O_2	Chloroplast → Cytosol → Peroxisome
	GMa	Chloroplast → Cytosol → Peroxisome
	OGA	Peroxisome → Cytosol → Chloroplast
	GA	Peroxisome → Cytosol → Chloroplast
SuS	PGAL	Chloroplast → Cytosol
	DHAP	Chloroplast → Cytosol
	S	Cytosol → Vacuole

transporting from one sub-compartment to another. Moreover, the directions of the transmission conditions of the chemical species are summarized in table 5.3.

Third, the chemical reactions rate can considered by the law of mass actions or the Michaelis-Menten kinetics. However for the simplicity, in this numerical simulation the rate equations of all chemical reactions in LIR, PR, StS, and SuS were followed Michaelis-Menten kinetics [30]. The rate equations used for describing all of chemical reactions in the numerical simulations of C_3 plant leaf cell photosynthesis are listed in the table 3.4. Nevertheless, the transmission rate of the chemical species transmitting between cytosol and sub-compartment was assumed to follow the difference of their concentrations between both sides of the interface.

Parameters and constants

As the number of variables in the mathematical model is large so that the simulation also needs a large set of parameters and constants, for example the Michaelis-Menten constants and the maximal enzyme activities. However, there is no constants and parameters set for any single plant species was available. Similarly, a set of maximum enzyme activities for all enzymes in LDR, LIR, PR, StS, and SuS is not consist yet. Therefore, the constants and pa-

rameters is obtained by surveying peer-reviewed studies from different plant species [17, 22, 26, 28, 30, 34]. However, the diffusion coefficients for some chemical species are still missing. Then, in this work we will calculate the diffusion coefficients for all chemical species by the following equation [43]:

$$D_i = \frac{1.70 \cdot 10^{-7} \cdot T}{\eta \cdot M_i^{0.41}} \qquad (cm^2 \cdot s) \tag{5.7}$$

where D_i is the diffusion coefficient of the chemical species i, T is the temperature at 25°C (or 298.15 K), M_i is the molecular weight $(g \cdot mol^{-1})$ of the chemical species i, and η is the viscosity (mPa·s) of the solution.

The viscosity of the solution in cytoplasm is roughly the same as pure water [44]. In [45], the viscosity value of the solute in peroxisome assumed to be 0.06 (Pa·s). The viscosity is of the protein concentration in the stroma is sixty-nine times higher relative to water [46]. In [47], the viscosity value of the solution in the vacuole is 1.22 (mPa·s). Therefore, in this work the viscosity value of the solution in each of the sub-domain are assumed and shown in Table 5.4.

Table 5.4: List of viscosity values

Sub-domians	Viscosity (η)
Chloroplast	61.4376
Peroxisome	60.0
Cytoplasm	0.8904
Mitochondria	60.0
Vacuole	1.22

For example, the diffusion coefficients of Glutamate (GMa) and Glycerate (GA) are calculated and shown in Table 5.5.

The diffuse coefficients and the kinetic parameters of the enzymes of the light dependent reactions (LDR), which a system illustrated in Figures 2.6 and 2.7. are listed in Table 5.6.

The diffuse coefficients, the Michaelis-Menten constants and the kinetic parameters of the enzymes of the light independent reactions (LIR), which a network showed in Figure 2.8, are collected in Tables 5.7 and 5.8.

The diffuse coefficients, the Michaelis-Menten constants and the kinetic parameters of the enzymes of the photorespiration reactions (PR) illustrated in Figure 2.11 are listed in Tables 5.9 and 5.10.

Table 5.5: Diffusion coefficients of GMa and GA

Chemical Species	Molecular Weights	η (mPa·s)	D_i ($cm^2\cdot$ s)
GMa	147.13	61.4376 (in chloroplast)	1.066×10^{-7}
($C_5H_9NO_4$)	147.13	0.894 (in cytoplasm)	7.354×10^{-6}
	147.13	60.00 (in peroxisome)	1.091×10^{-7}
GA	105.07	61.4376 (in chloroplast)	1.224×10^{-7}
($C_3H_5O_4$)	105.07	0.894 (in cytoplasm)	8.443×10^{-6}
	105.07	60.00 (in peroxisome)	1.253×10^{-7}

Table 5.6: The parameters for LDR in numerical simulation I

Reactions	Parameters	Values	Units
$X_{PSII} \longrightarrow X^+_{PSII} + e^-_{PSII}$	$D_{X_{PSII}}, D_{X^+_{PSII}}, D_{e^-_{PSII}}$	0.0	$m^2\ s^{-1}$
$X_{PSI} \longrightarrow X^+_{PSI} + e^-_{PSI}$	$D_{X_{PSI}}, D_{X^+_{PSI}}, D_{e^-_{PSI}}$	0.0	$m^2\ s^{-1}$
$X^+_{PSII} + e^-_{H_2O} \xrightarrow{k_{LDR1}} X_{PSII}$	$D_{e^-_{H_2O}}$	0.0	$m^2\ s^{-1}$
	k_{LDR1}	1.0×10^2	
$X^+_{PSI} + e^-_{PSII} \longrightarrow X_{PSI}$	k_{LDR2}	1.0×10^2	
$2H_2O \longrightarrow O_2 + 4H^+_{lumen}$	$D_{H^+_{lumen}}$	8.224×10^{-7}	$m^2\ s^{-1}$
$+ 4e^-_{H_2O}$	D_{O_2}	1.992×10^{-7}	$m^2\ s^{-1}$
$NADP^+ + 2e^-_{PSI} + H^+_{stroma}$	k_{LDR3}	0.460×10^{-1}	
$\longrightarrow$ NADPH	$D_{H^+_{stroma}}$	8.224×10^{-7}	$m^2\ s^{-1}$
	D_{NADP^+}	5.495×10^{-8}	$m^2\ s^{-1}$
	D_{NADPH}	5.483×10^{-8}	$m^2\ s^{-1}$
$ADP + P_i \longrightarrow ATP$	k_{LDR4}	0.460×10^{-1}	
	D_{ADP}	6.905×10^{-8}	$m^2\ s^{-1}$
	D_{ATP}	6.417×10^{-8}	$m^2\ s^{-1}$
	D_{P_i}	2.019×10^{-7}	$m^2\ s^{-1}$

The diffuse coefficients, the Michaelis-Menten constants and the kinetic parameters of the enzymes of the starch synthesis (StS) in the chloroplast and the sucrose synthesis (SuS) in the cytosol, which their system showed in Figure 2.9, are listed in Tables 5.11 to 5.14.

Table 5.7: The parameters for LIR in numerical simulation II

Reactions	Parameters	Values	Units
$3\,\mathrm{RuBP} + 3\,\mathrm{CO_2} + 3\,\mathrm{H_2O} \longrightarrow$ $6\,\mathrm{PGA} + 6\,\mathrm{H^+_{stroma}}$	D_{RuBP}	7.851×10^{-8}	$\mathrm{m^2\ s^{-1}}$
	D_{CO_2}	1.748×10^{-7}	$\mathrm{m^2\ s^{-1}}$
	D_{PGA}	9.680×10^{-8}	$\mathrm{m^2\ s^{-1}}$
	$D_{H^+_{stroma}}$	8.224×10^{-7}	$\mathrm{m^2\ s^{-1}}$
	V_{4max}	1.0	
	$K_{m4,1}$ (RuBP)	0.2	mM
	$K_{m4,2}$ (CO_2)	0.115	mM
$6\,\mathrm{PGA} + 6\,\mathrm{ATP} \longrightarrow 6\,\mathrm{BPGA} + 6\,\mathrm{ADP}$	D_{ATP}	6.417×10^{-8}	$\mathrm{m^2\ s^{-1}}$
	D_{BPGA}	8.360×10^{-8}	$\mathrm{m^2\ s^{-1}}$
	D_{ADP}	6.905×10^{-8}	$\mathrm{m^2\ s^{-1}}$
	V_{5max}	10.3	
	$K_{m5,1}$ (PGA)	0.24	mM
	$K_{m5,2}$ (ATP)	0.39	mM
$6\,\mathrm{BPGA} + 6\,\mathrm{NADPH} + 6\,\mathrm{H^+_{stroma}} \longrightarrow$ $6\,\mathrm{PGAL} + 6\,\mathrm{NADP^+} + 6\,\mathrm{P_i}$	D_{NADPH}	5.483×10^{-8}	$\mathrm{m^2\ s^{-1}}$
	D_{PGAL}	1.004×10^{-7}	$\mathrm{m^2\ s^{-1}}$
	D_{NADP^+}	5.495×10^{-8}	$\mathrm{m^2\ s^{-1}}$
	D_{P_i}	2.019×10^{-7}	$\mathrm{m^2\ s^{-1}}$
	V_{6max}	1.39	
	$K_{m6,1}$ (BPGA)	0.004	mM
	$K_{m6,2}$ (NADPH)	0.1	mM
	$K_{m6,3}$ (H^+_{stroma})	0.5	mM
$2\,\mathrm{PGAL} \rightleftharpoons 2\,\mathrm{DHAP}$	D_{DHAP}	1.004×10^{-8}	$\mathrm{m^2\ s^{-1}}$
	$V_{7max,1}$ (PGAL)	0.3	
	$V_{7max,2}$ (DHAP)	0.31	
	$K_{m7,1}$ (PGAL)	0.05	mM
	$K_{m7,2}$ (DHAP)	0.05	mM
$\mathrm{PGAL} + \mathrm{DHAP} \longrightarrow \mathrm{FBP}$	D_{FBP}	7.596×10^{-8}	$\mathrm{m^2\ s^{-1}}$
	V_{8max}	0.42	
	$K_{m8,1}$ (PGAL)	0.3	mM

Numerical simulation I

In this simulation, we perform and focus on the numerical simulation only in the part of light-dependent reaction (LDR), LDR in *silico*. Since all the biochemical sub-processes of LDR operates in the same sub-compartment

Table 5.8: The parameters for LIR in numerical simulation II (Cont'd)

$PGAL + DHAP \longrightarrow FBP$	$K_{m8,2}$ (DHAP)	0.3	mM
$FBP + H_2O \longrightarrow FP$	D_{FP}	8.438×10^{-8}	$m^2\ s^{-1}$
	V_{9max}	0.25	
	$K_{m9,1}$ (FBP)	0.33	mM
$FP + PGAL \longrightarrow EP + XP$	D_{EP}	9.396×10^{-8}	$m^2\ s^{-1}$
	D_{XP}	8.905×10^{-8}	$m^2\ s^{-1}$
	V_{10max}	1.07	
	$K_{m10,1}$ (FP)	0.7	mM
	$K_{m10,2}$ (PGAL)	0.1	mM
$EP + DHAP \longrightarrow SBP$	D_{SBP}	7.334×10^{-8}	$m^2\ s^{-1}$
	V_{11max}	0.42	
	$K_{m11,1}$ (EP)	0.2	mM
	$K_{m11,2}$ (DHAP)	0.4	mM
$SBP + H_2O \longrightarrow SuP + P_i$	D_{SuP}	8.068×10^{-8}	$m^2\ s^{-1}$
	V_{12max}	0.11	
	$K_{m12,1}$ (SBP)	0.05	mM
$SuP + PGAL \longrightarrow RP + XP$	D_{RP}	8.873×10^{-8}	$m^2\ s^{-1}$
	V_{13max}	1.07	
	$K_{m13,1}$ (SuP)	0.46	mM
	$K_{m13,1}$ (PGAL)	0.072	mM
$2\,XP \longrightarrow 2\,RuP$	D_{RuP}	8.873×10^{-8}	$m^2\ s^{-1}$
	V_{14max}	0.2	
	$K_{m14,1}$ (XP)	0.67	mM
$RP \longrightarrow RuP$	V_{15max}	0.2	
	$K_{m15,1}$ (RP)	0.4	mM
$3\,RuP + 3\,ATP \longrightarrow$ $3\,RuBP + 3\,ADP + 3\,H^+_{stroma}$	V_{16max}	0.1	
	$K_{m16,1}$ (RuP)	0.05	mM
	$K_{m16,2}$ (ATP)	0.059	mM

(chloroplast). So that there are no need to discuss about the simulation in the sub-compartment of the mitochondria, the peroxisome, and the vacuole. However, there are some chemical species transports from the chloroplast to the cytoplasm but we are not focus about them in this simulation.

The chemical species that we interesting in this computer experiment is the products of the LDR including ATP, NADPH, and O_2. To dealing with this situation, there are some assumptions have been made for the simulation. The

Table 5.9: The parameters for PR in numerical simulation II

Reactions	Parameters	Values	Units
$2\,\mathrm{RuBP} + 2\,\mathrm{O_2} \longrightarrow 2\,\mathrm{PGC} + 2\,\mathrm{PGA}$	D_{PGC}	1.049×10^{-7}	$\mathrm{m^2\ s^{-1}}$
	V_{37max}	0.24	
	$K_{m37,1}$ (RuBP)	0.2	mM
	$K_{m37,2}$ (O_2)	0.222	mM
$2\,\mathrm{PGC} + 2\,\mathrm{H_2O} \longrightarrow 2\,\mathrm{GCL} + 2\,\mathrm{P_i}$	D_{GCL}	1.405×10^{-7}	$\mathrm{m^2\ s^{-1}}$
	V_{38max}	1.80	
	$K_{m38,1}$ (PGC)	0.26	mM
$2\,\mathrm{GCL} + 2\,\mathrm{O_2} \longrightarrow 2\,\mathrm{GOL} + \mathrm{H_2O_2}$	D_{GOL}	1.454×10^{-7}	$\mathrm{m^2\ s^{-1}}$
	$D_{H_2O_2}$	1.990×10^{-7}	$\mathrm{m^2\ s^{-1}}$
	V_{39max}	0.45	
	$K_{m39,1}$ (GCL)	0.1	mM
	$K_{m39,2}$ (O_2)	0.222	mM
$2\,\mathrm{H_2O_2} \longrightarrow 2\,\mathrm{H_2O} + \mathrm{O_2}$	V_{40max}	0.2	
	$K_{m40,1}$ (H_2O_2)	0.1	mM
$2\,\mathrm{GOL} + 2\,\mathrm{GMa} \longrightarrow \mathrm{GC} + \mathrm{OGA}$	D_{GMa}	1.091×10^{-7}	$\mathrm{m^2\ s^{-1}}$
	D_{GC}	1.438×10^{-7}	$\mathrm{m^2\ s^{-1}}$
	D_{OGR}	1.101×10^{-7}	$\mathrm{m^2\ s^{-1}}$
	V_{41max}	0.2	
	$K_{m41,1}$ (GOL)	0.15	mM
	$K_{m41,2}$ (GMa)	1.7	mM
$\mathrm{GC} + \mathrm{NAD^+} + \mathrm{GDC} \longrightarrow$ $\mathrm{CO_2} + \mathrm{NH_4^+} + \mathrm{NADH} + \mathrm{MLG}$	D_{NAD^+}	5.889×10^{-8}	$\mathrm{m^2\ s^{-1}}$
	D_{GDC}	9.659×10^{-8}	$\mathrm{m^2\ s^{-1}}$
	$D_{NH_4^+}$	2.580×10^{-7}	$\mathrm{m^2\ s^{-1}}$
	D_{NADH}	5.886×10^{-7}	$\mathrm{m^2\ s^{-1}}$
	D_{MLG}	6.855×10^{-8}	$\mathrm{m^2\ s^{-1}}$
	V_{42max}	0.86	
	$K_{m42,1}$ (GC)	6.0	mM
	$K_{m42,2}$ (NAD^+)	2.5	mM
	$K_{m42,3}$ (GDC)	3.5	mM
$\mathrm{MLG} + \mathrm{GL} + \mathrm{H_2O} \longrightarrow \mathrm{Ser} + \mathrm{GDC}$	D_{GL}	1.437×10^{-7}	$\mathrm{m^2\ s^{-1}}$
	D_{SR}	1.253×10^{-7}	$\mathrm{m^2\ s^{-1}}$
	V_{43max}	0.4	
	$K_{m43,1}$ (MLG)	4.0	mM
	$K_{m43,2}$ (GL)	3.7	mM
$\mathrm{Ser} + \mathrm{OGA} \longrightarrow \mathrm{HDP} + \mathrm{GDC}$	D_{HDP}	1.263×10^{-7}	$\mathrm{m^2\ s^{-1}}$
	V_{44max}	1.13	
	$K_{m44,1}$ (SR)	2.7	mM
	$K_{m44,2}$ (OGR)	0.15	mM

Table 5.10: The parameters for PR in numerical simulation II (Cont'd)

$HDP + NADH + H^+_{stroma} \longrightarrow GA + NAD^+$	D_{GA}	1.253×10^{-7}	$m^2\ s^{-1}$
	V_{45max}	3.44	
	$K_{m45,1}$ (HDP)	0.09	mM
	$K_{m45,2}$ (NADH)	0.1	mM
	$K_{m45,3}$ (H^+_{stroma})	0.5	mM
$GA + ATP \longrightarrow PGAL + ADP$	V_{46max}	1.96	
	$K_{m46,1}$ (GA)	0.25	mM
	$K_{m46,2}$ (ATP)	0.21	mM
$GMa + NH_4^+ + ATP \longrightarrow GMi + ADP + P_i$	D_{GMi}	1.069×10^{-7}	$m^2\ s^{-1}$
	V_{47max}	0.4	
	$K_{m47,1}$ (GMa)	1.7	mM
	$K_{m47,2}$ (NH_4^+)	0.1	mM
	$K_{m47,3}$ (ATP)	0.05	mM
$OGA + GMi + 2Fd_{red} + 2H^+_{stroma} \longrightarrow 2GMa + 2Fd_{oxid}$	$D_{Fd_{red}}$	8.250×10^{-7}	$m^2\ s^{-1}$
	$D_{Fd_{oxid}}$	8.250×10^{-7}	$m^2\ s^{-1}$
	V_{48max}	0.4	
	$K_{m48,1}$ (OGR)	0.15	mM
	$K_{m48,2}$ (GMi)	1.5	mM
	$K_{m48,3}$ (Fd_{red})	1.2	mM
	$K_{m48,4}$ (H^+_{stroma})	0.5	mM

Table 5.11: The parameters for StS in numerical simulation II

Reactions	Parameters	Values	Units
$FP + ATP \longrightarrow FBP + ADP$	V_{17max}	0.5	
	$K_{m17,1}$ (FP)	0.2	mM
	$K_{m17,2}$ (ATP)	0.2	mM
$FP + PP_i \longrightarrow FBP + P_i$	D_{PP_i}	1.520×10^{-7}	$m^2\ s^{-1}$
	V_{18max}	0.2	
	$K_{m18,1}$ (FP)	0.15	mM

mathematical model, which is showed in equations (3.27) to (3.41), is based on C_3 plant photosynthetic pathway. We consider that the percentage of light absorption (see also in figure 5.3) is simply estimated by the following function:

$$\alpha(\lambda) = a_s + b_s\lambda + c_s\lambda^2 + d_s\lambda^3, \quad s = 1, \ldots, 6.$$

Table 5.12: The parameters for StS in numerical simulation II (Cont'd)

$FP + PP_i \longrightarrow FBP + P_i$	$K_{m18,2}$ (PP_i)	0.25	mM
$FP + ATP \longrightarrow FTBP + ADP$	D_{FTBP}	7.559×10^{-8}	$m^2\ s^{-1}$
	V_{19max}	0.55	
	$K_{m19,1}$ (FP)	0.21	mM
	$K_{m19,2}$ (ATP)	0.22	mM
$FTBP + H_2O \longrightarrow FP + P_i$	V_{20max}	0.35	
	$K_{m20,1}$ (FTBP)	0.23	mM
$FP \longrightarrow GSP$	D_{GSP}	8.465×10^{-8}	$m^2\ s^{-1}$
	V_{21max}	0.15	
	$K_{m21,1}$ (FP)	0.1	mM
$GSP \longrightarrow GP$	D_{GP}	8.438×10^{-8}	$m^2\ s^{-1}$
	V_{22max}	0.2	
	$K_{m22,1}$ (GSP)	0.2	mM
$GP + ATP \longrightarrow ADPG + PP_i$	D_{ADGP}	6.034×10^{-8}	$m^2\ s^{-1}$
	V_{23max}	0.2	
	$K_{m23,1}$ (GP)	0.2	mM
	$K_{m23,2}$ (ATP)	0.2	mM
$ADPG + Primer \longrightarrow A + ADP$	D_{Primer}	9.192×10^{-8}	$m^2\ s^{-1}$
	D_A	6.782×10^{-8}	$m^2\ s^{-1}$
	V_{24max}	0.2	
	$K_{m24,1}$ (ADPG)	0.2	mM
	$K_{m24,2}$ (Primer)	0.2	mM

where λ is a wavelength (nm) and the coefficients a_s, b_s, c_s, and $d_s, s = 1, \ldots, 6$ are summarized in Table 5.16.

In this simulation, we consider that the photosynthetic pigments in photosystem I and II are absorb light in the same wavelength. The follow numerical simulation is calculated on the wavelength $\lambda = 600\,\text{nm}$ and temperature at 25°C. Moreover, list of parameters for this numerical simulation are provided in Table 5.6.

This computer simulation dealing with a system of PDEs with 15 variables. In difference of time step sizes and mesh refinement levels are applied to investigate the convergence of numerical solutions.

Table 5.13: The parameters for SuS in numerical simulation II

Reactions	Parameters	Values	Units
PGAL $\rightleftharpoons$ DHAP	D_{PGAL}	6.930×10^{-6}	$m^2\ s^{-1}$
	D_{DHAP}	6.930×10^{-6}	$m^2\ s^{-1}$
	$V_{25max,1}$ (PGAL)	0.3	
	$V_{25max,2}$ (DHAP)	0.1	
	$K_{m25,1}$ (PGAL)	0.5	mM
	$K_{m25,2}$ (DHAP)	0.5	mM
DHAP + PGAL $\longrightarrow$ FBP	D_{FBP}	5.242×10^{-6}	$m^2\ s^{-1}$
	V_{26max}	0.42	
	$K_{m26,1}$ (DHAP)	0.3	mM
	$K_{m26,1}$ (PGAL)	0.4	mM

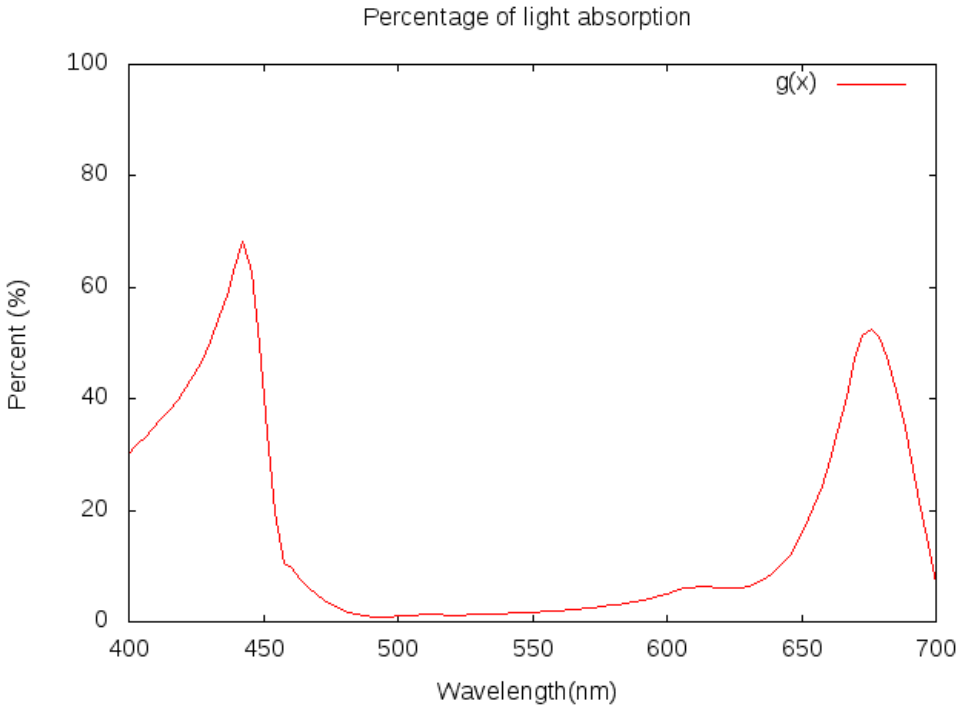

Figure 5.3: Example of the percentage of light absorption.

Results of numerical simulation I

The numerical simulation for light dependent reaction illustrates the concentration of each chemical species in the 2D domain at the specific time.

The numerical simulation has run on Ubuntu 14.04 LTS platform 64-bit, Disk 140.7 GB, Memory 3.9 GiB, Processor Intel Core i7 CPU 950 3.07GHz×8, and Graphics Quadro NVS 290/PCIe/SSE2.

Figure 5.2 shows the computational domain with locally refined mesh. The calculation has evaluated at the time step (dt) = 0.05 s for 400 iterations. The computational times for this case is nearly 2 minutes (112 s). The numerical results show the concentrations of each chemical species at different points in time. P_i, ATP, and NADPH are diffuse-transport only inside the sub-domain Ω_1. Figure 5.4 illustrates the concentration of P_i in the chloroplast (Ω_1) which is decreasing in time. In another hand, ATP and NADPH are increasing in time (see also Figures 5.5 and 5.6).

For the dynamical products of LDR and some substances, we consider the summation of the concentration of chemical species per the area of Ω_1 as shown in Figure 5.7.

Numerical simulation II

From the previous simulation, we have been developed and analyzed a numerical simulation for light dependent reaction. Similarly to the first simulation, we continue to consider the system with the coupling process that operate in multi-compartments. In this simulation, we not only deal with the light independent reactions but also include the process of photorespiration, starch and sucrose synthesis into the system. According to the chemical reactions, the photorespiration process is performed in four sub-domains except vacuole. Due to our research questions, the chemical species that we are focus on in this case consists of CO_2, PGAL, DHAP, starch, and sucrose. We are interesting in the dynamical product of the carbon reaction (PGAL and DHAP), starch reaction (starch) inside the chloroplast. The dynamical consumption of carbon reaction (CO_2) inside and outside chloroplast are important to discuss. Since the chemical reactions of the sucrose synthesis is take place in the cytoplasm and then the final product is transport into the vacuole. In this situation, we may consider that the sucrose is not converted the another form and only

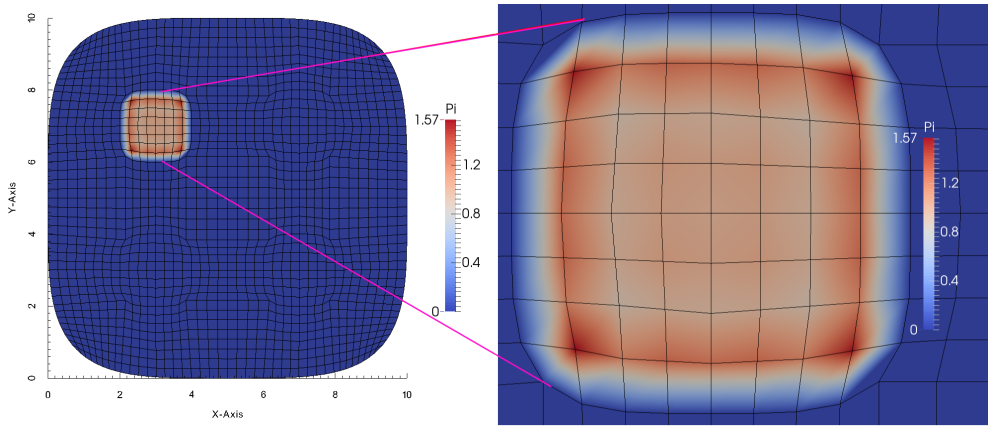

(a) Numerical result for P_i in Ω_1

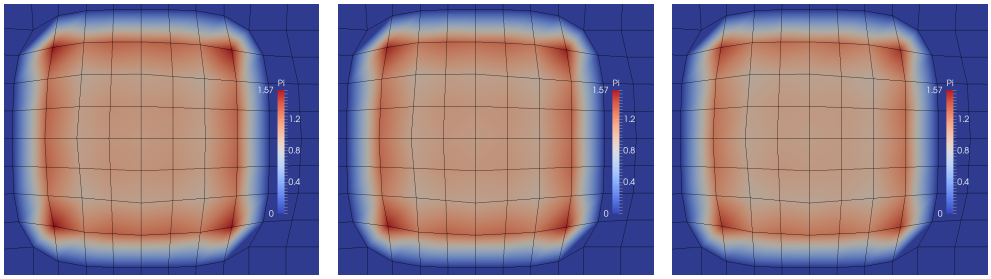

(b) ι=1 (c) ι=50 (d) ι=100

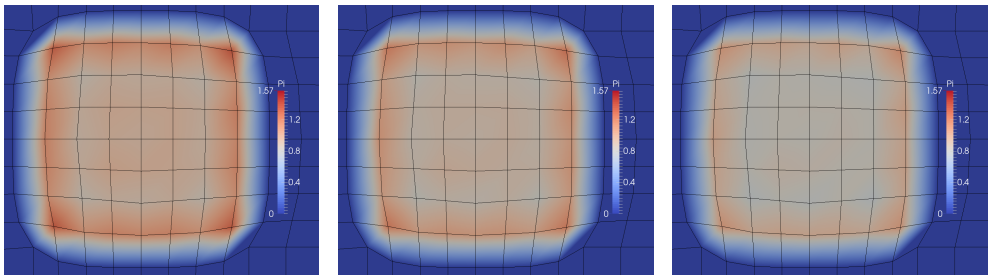

(e) ι=150 (f) ι=200 (g) ι=250

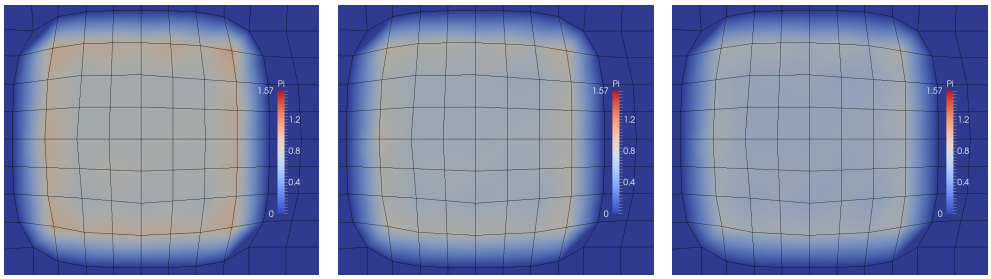

(h) ι=300 (i) ι=350 (j) ι=400

Figure 5.4: Numerical simulation I, diffusion-transport of P_i in Ω_1 at the iterations ι = 1, 50, 100, 150, 200, 250, 300, 350, and 400.

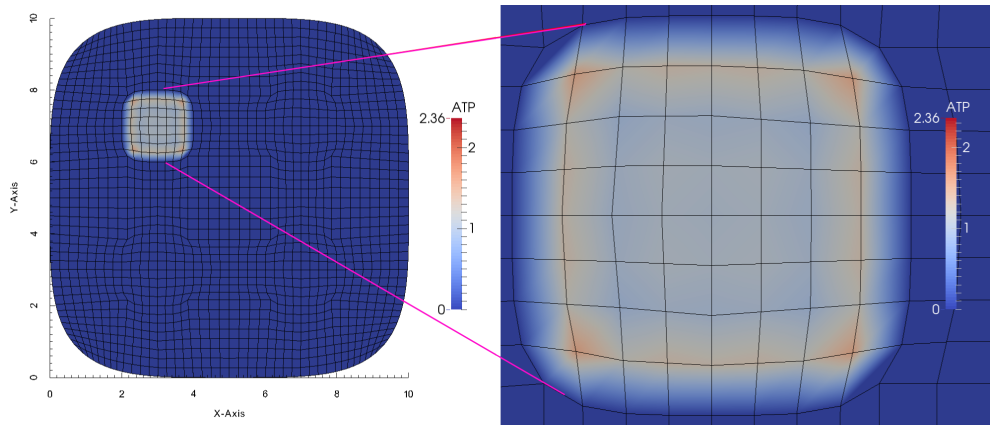

(a) Numerical result for ATP in Ω_1

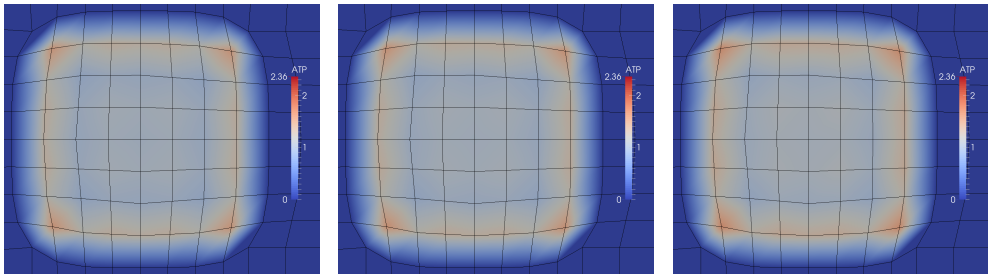

(b) ι=1 (c) ι=50 (d) ι=100

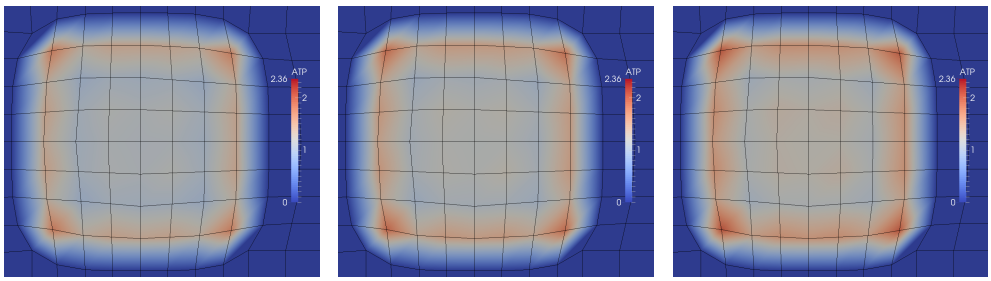

(e) ι=150 (f) ι=200 (g) ι=250

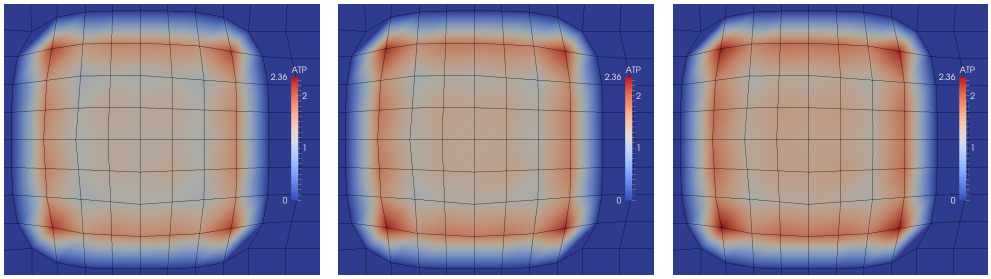

(h) ι=300 (i) ι=350 (j) ι=400

Figure 5.5: Numerical simulation I, diffusion-transport of ATP in Ω_1 at the iterations ι = 1, 50, 100, 150, 200, 250, 300, 350, and 400.

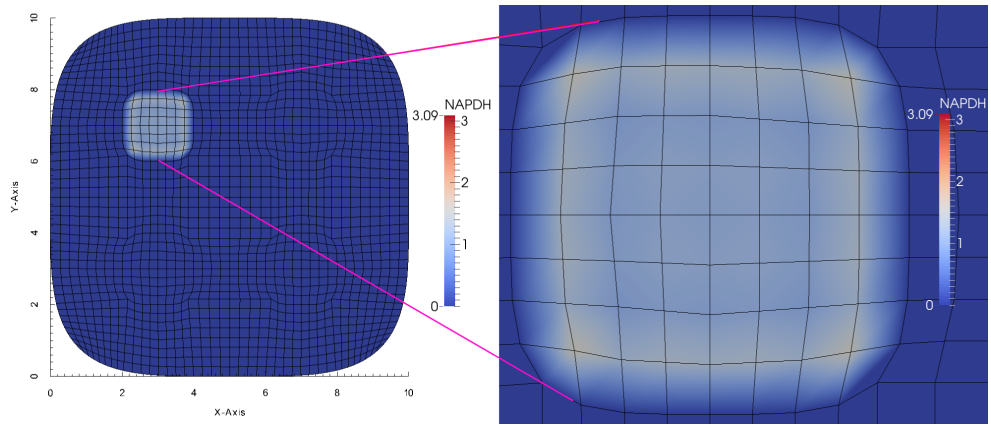

(a) Numerical result for NADPH in Ω_1

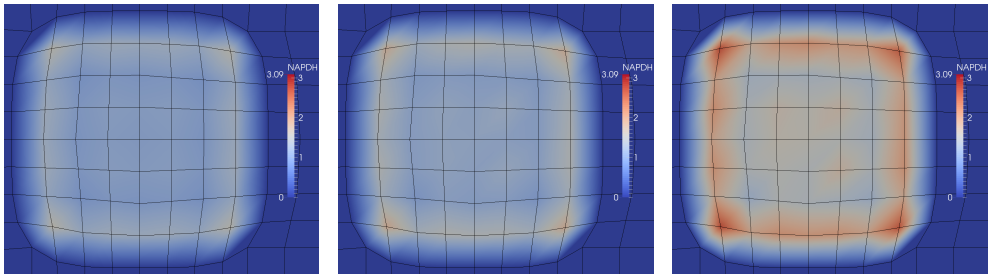

(b) ι=1 (c) ι=50 (d) ι=100

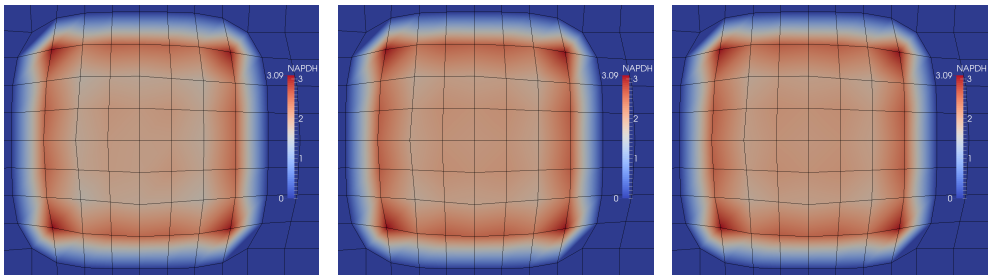

(e) ι=150 (f) ι=200 (g) ι=250

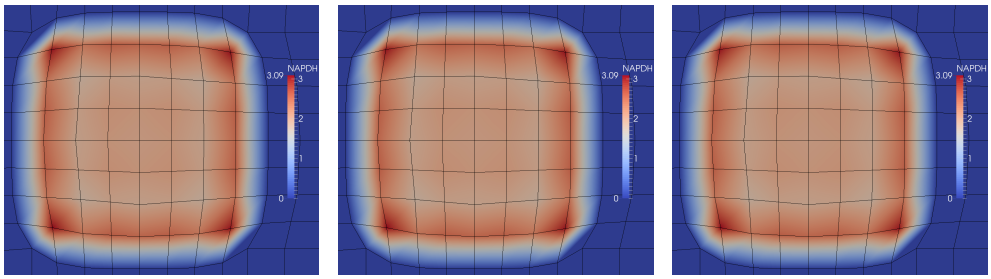

(h) ι=300 (i) ι=350 (j) ι=400

Figure 5.6: Numerical simulation I, diffusion-transport of the NADPH in Ω_1 at the iterations ι = 1, 50, 100, 150, 200, 250, 300, 350, and 400.

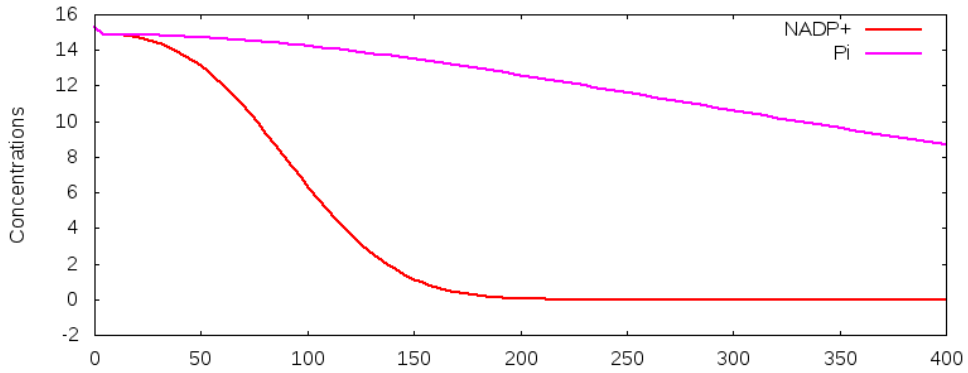

(a) Concentration of $NADP^+$ and P_i in Ω_1

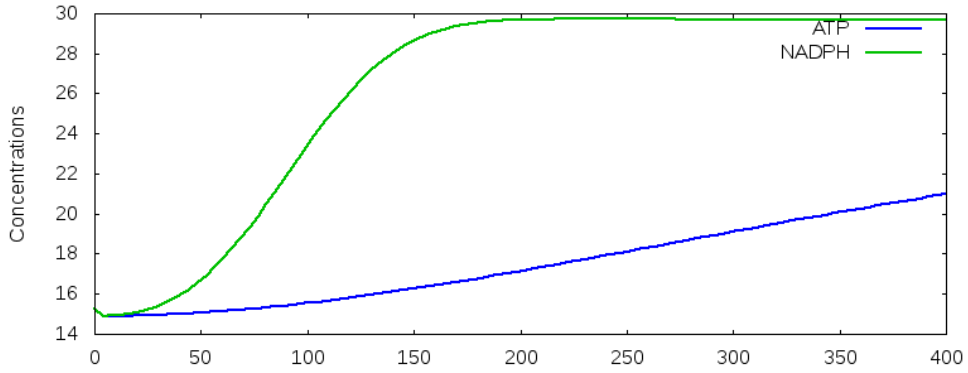

(b) Concentration of NADPH and ATP in Ω_1

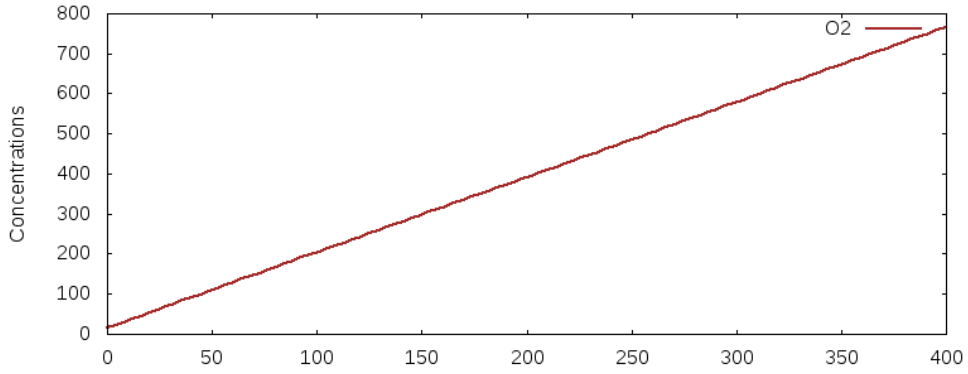

(c) Concentration of O_2 in Ω_1

Figure 5.7: Numerical simulation I, summation of the concentration u_i per area of Ω_1 (a) $NADP^+$ and P_i (b) ATP and NADPH (c) O_2, in 20 s (400 iterations, time step 0.05), respectively.

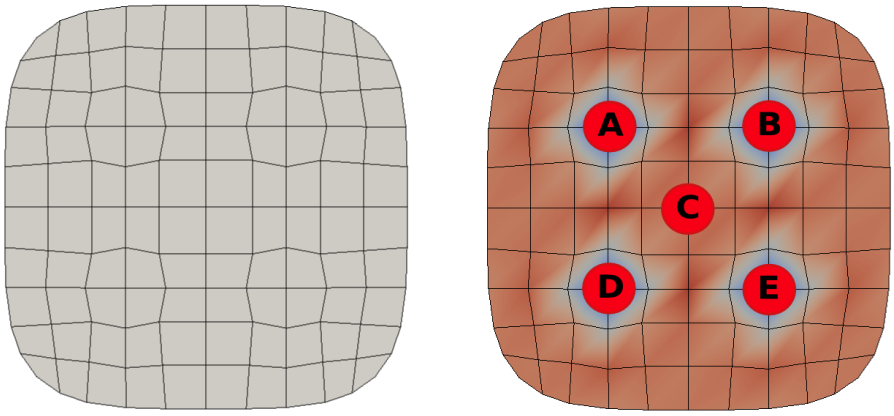

Figure 5.8: Mesh refinement for the numerical simulation II

stored inside the vacuole. So that the chemical species that we interesting in this part is also the dynamical product of the sugar reactions (sucrose). For this numerical simulation, the parameters are listed in Tables 5.7 to 5.14.

This computer simulation dealing with a system of PDEs with 84 variables together with 21×2 transmission conditions. So that the difference of time step sizes are applied to investigate the convergence of numerical solutions. However the system is so large, the mesh refinement levels is consider only at level one.

Results of numerical simulation II

The numerical simulation for full system illustrates the concentration of each chemical species in the 2D domain at the specific time. For 120 iterations, $dt = 1$, and 1 level of the mesh refinement, the computational time is reach to 10 hours. Due to the limitation of the mesh refinement, a sub-compartment contain only one point inside at the center. In this case, we consider the concentration of the chemical species i only at the center of the sub-domain (see also Figures 5.8 to 5.12).

In numerical simulation II, the calculation was not so clear because of the limitation of the mesh refinement. Next step, we will study the sensitivity analysis of the full models. After that, we will consider the reduced model and will perform the numerical simulation.

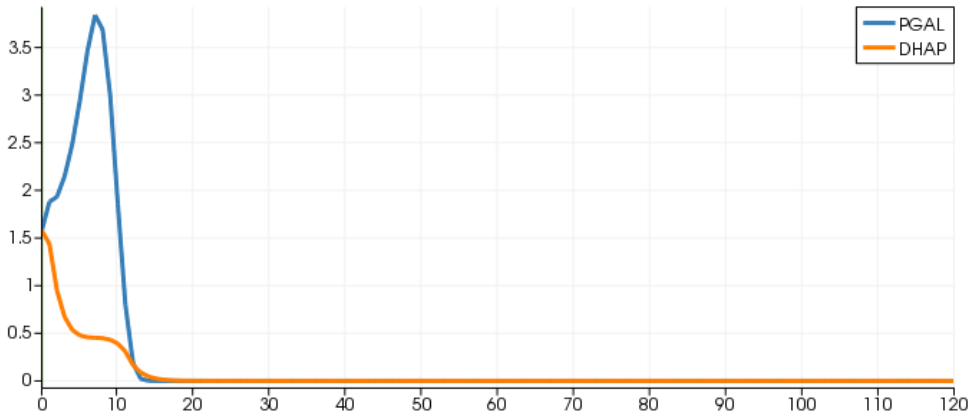

(a) Concentration of PGAL and DHAP at point A

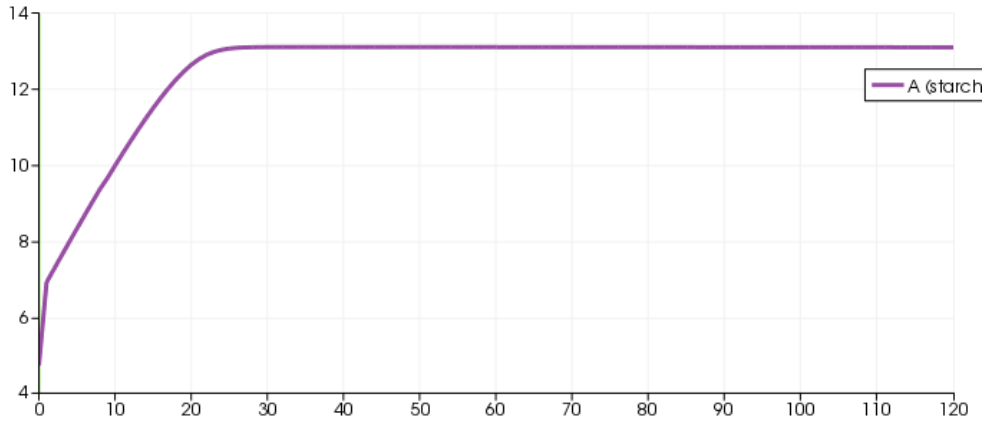

(b) Concentration of starch at point A

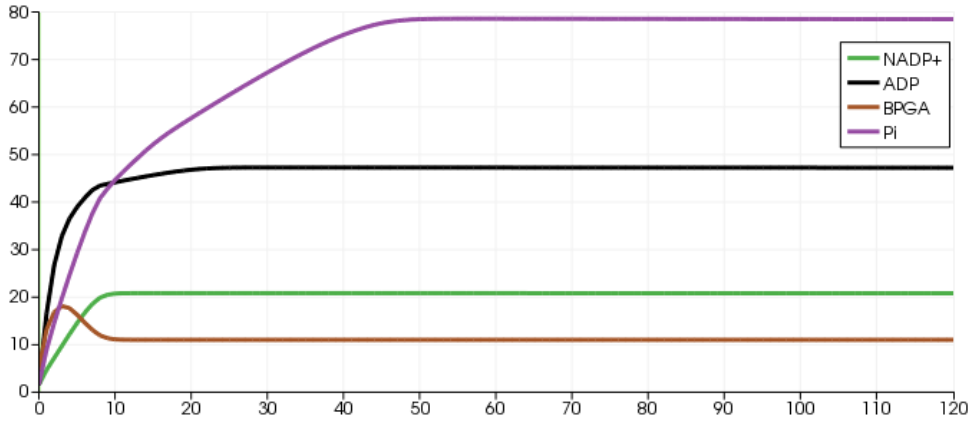

(c) Concentration of $NADP^+$, ADP, BPGA, and P_i at point A

Figure 5.9: Numerical simulation II, the concentration of (a) PGAL and DHAP, (b) starch, (c) $NADP^+$, ADP, BPGA, and P_i in Ω_1 at point A in 2 minutes (120 iterations, time step 1), respectively.

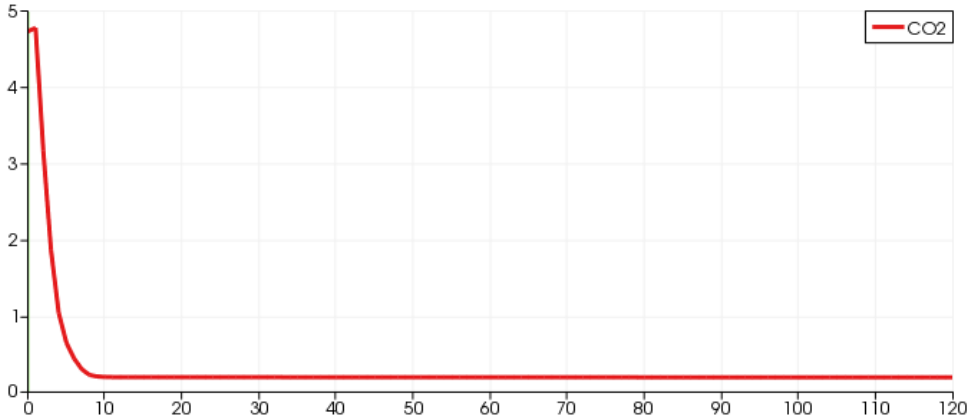

(a) Concentration of CO_2 at point A

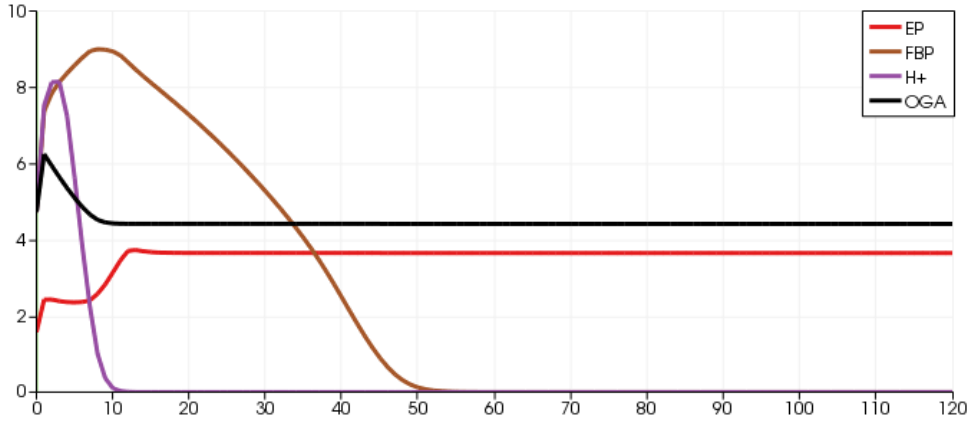

(b) Concentration of FB, FBP, HP, and OGA at point A

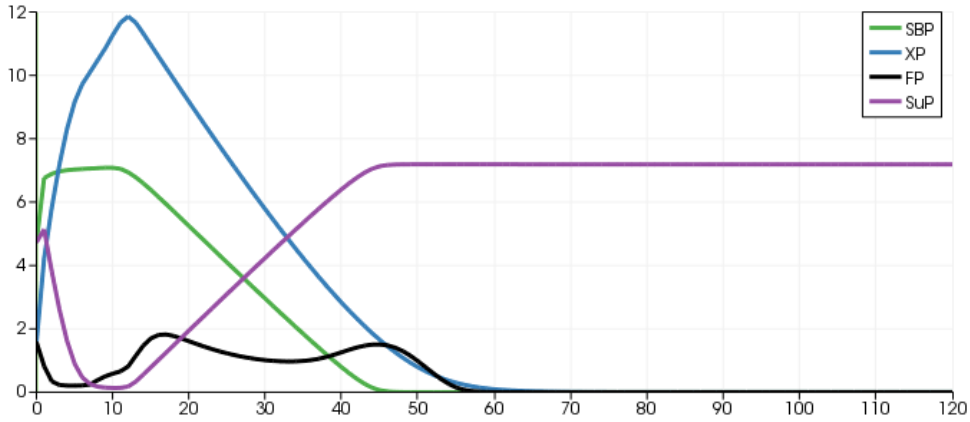

(c) Concentration of FP, XP, SBP, and SuP at point A

Figure 5.10: Numerical simulation II, the concentration of (a) CO_2, (b) FB, FBP, H^+, and OGA, (c) SBP, XP, FP, and SuP in Ω_1 at point A in 2 minutes (120 iterations, time step 1), respectively.

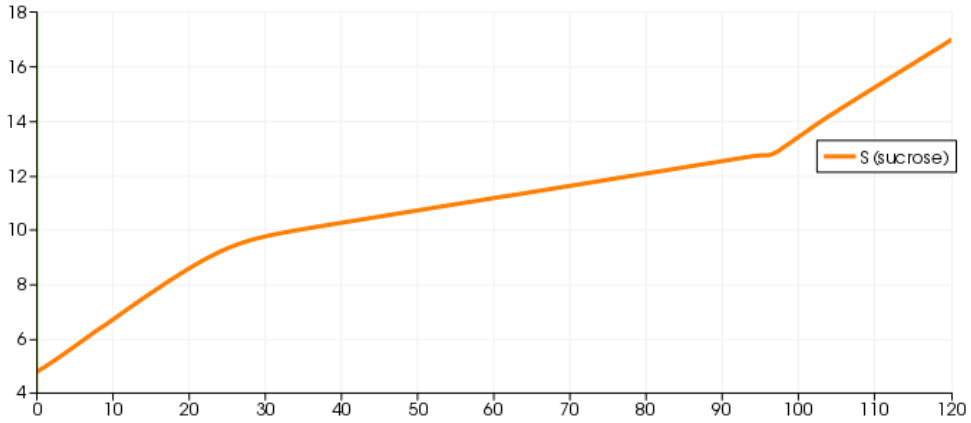

(a) Concentration of sucrose at point C (in cytoplasm, Ω_0)

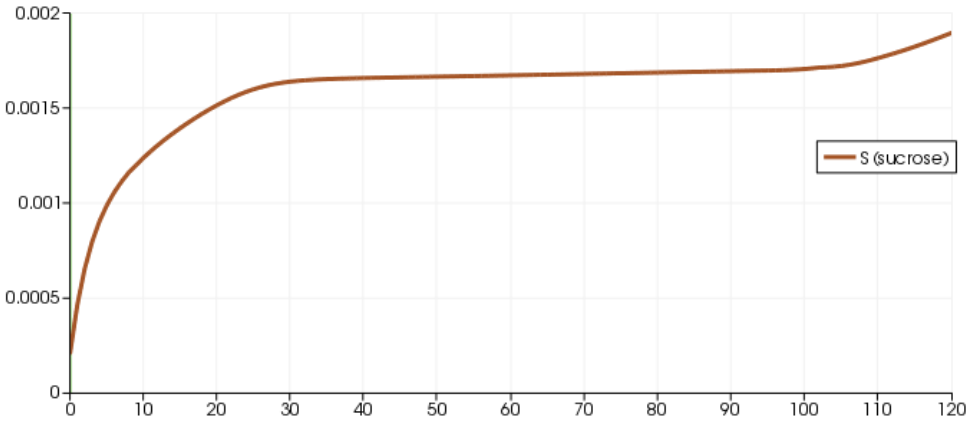

(b) Concentration of sucrose at point D (in vacuole, Ω_4)

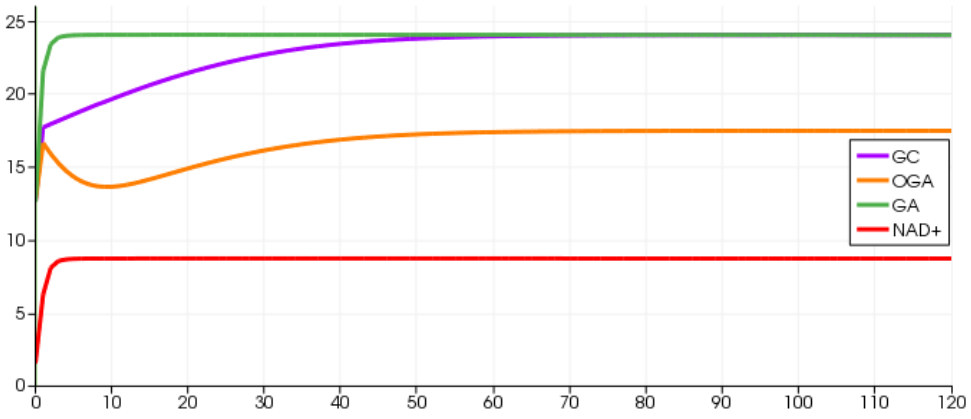

(c) Concentration of GC, OGA, GA, and NAD^+ at point E (in peroxisome, Ω_3)

Figure 5.11: Numerical simulation II, the concentration of (a) sucrose at point C in Ω_0, (b) sucrose at point D in Ω_4, (c) GC, OGA, GA, and NAD^+ at point E in Ω_3, in 2 minutes (120 iterations, time step 1), respectively.

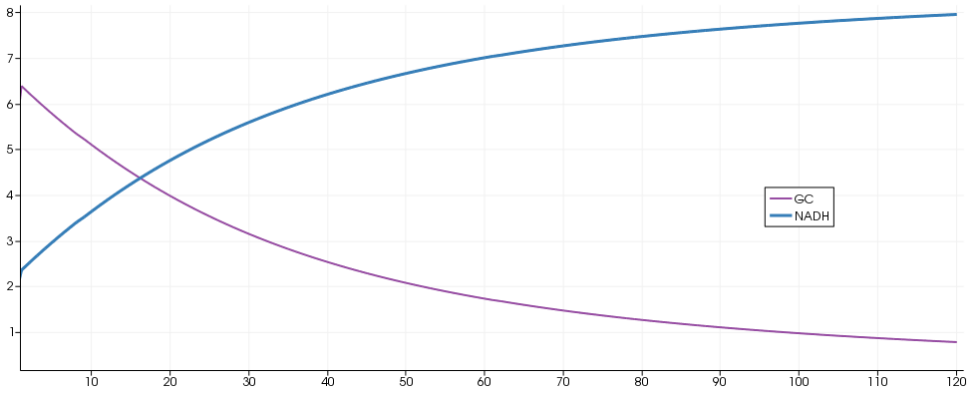

(a) Concentration of GC and NADH at point B

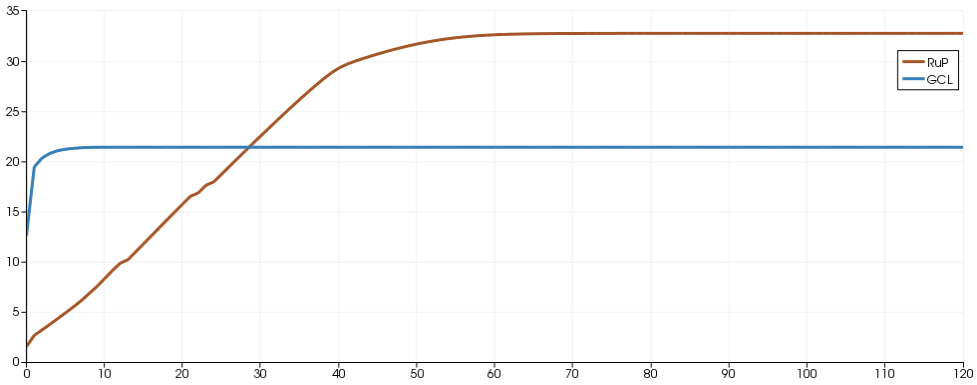

(b) Concentration of RuP and GCL at point A

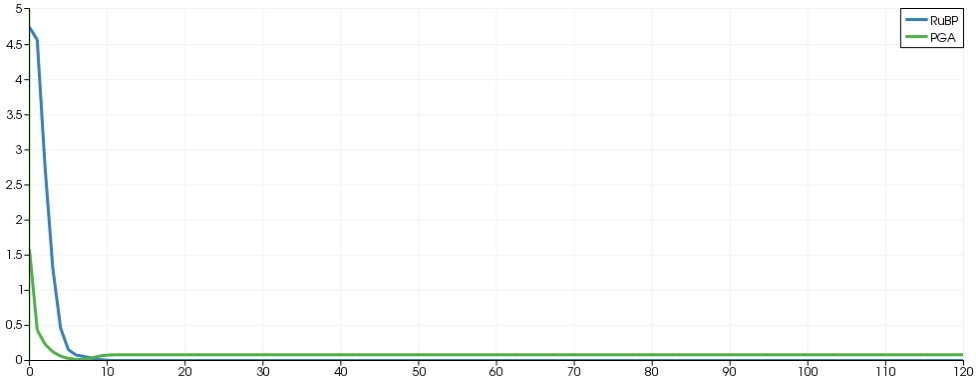

(c) Concentration of RuBP and PGA at point A

Figure 5.12: Numerical simulation II, the concentration of (a) GC and NADH at point B, (b) RuP and GCL at point A, (c) RuBP and PGA at point A in Ω_4 and Ω_1 in 2 minutes (120 iterations and time step = 1), respectively.

Sensitivity Analysis

In this section, we devote to the sensitivity analysis of the system of differential equation. The sensitivity analysis is implemented by the Kinetic PreProcessor (KPP) [48]. KPP is a software tools to generate the building blocks needs for the direct and adjoint sensitivity analysis of chemical kinetic systems. The KPP software is capable with the several computer languages: C, Fortran77, Fortran90, and Matlab. However, in this work we focus on Fortran77. For the numerical experiments we consider the third-oder third-stage L-stable method, *ROS3_DDM*, as the solver. The sensitivities are defined as the derivatives of the solution with respect to the parameters: initial values, and chemical reaction rate coefficients. In this work, we concentrate on the sensitivity of the solutions depending on the reaction rate coefficient.

Input: KPP basically handles two types of files: kinetics description files and auxiliary files (see also in [48–50] for more details). In order to compile with KPP software, it requires 4 of the root files with the suffix .kpp, .spc, .eqn, and .def. File *root.kpp* includes the declaration of the project name, the integrator, the selected computer language, the driver, the Jacobian matrix, the Hessian matrix, the stoichiometry matrix, and the double precisions. File *root.def* includes the parts of initial conditions, the calculation loop control, and the screen printed out. This file also connects to the chemical species files and the chemical reactions files. File *root.spc* contains the lists of the atoms: chemical species variable (DEFVAR) and fixed species (DEFFIX). File *root.eqn* includes the chemical kinetic mechanism, set of the chemical reactions, together with their rate coefficient. *Compile & Run*: To run the model with KPP, we can simply use the command "kpp root.kpp" in the terminal shell windows. Next, compile and run the Fortran77 code with the following command: *make -f Makefile_foot*. and *./root.exe* respectively.

Output: As the successfully compile and run, KPP produces root.map, root.dat, root.map, root_result.m, library files, and other related files. File *root.map* includes the overviews of the project including the options, parameter details, species, and subroutines. File *root.dat* shows the solutions of the ODEs for each variable in each time step. The numerical results of sensitivities analysis of solution depending on the rate coefficients are lists in the file *root_result.m*.

In this work, we have been studied the sensitivity analysis of the system of ordinary differential equations (ODEs) for the full chemical system includ-

ing light-dependent reactions (LDR), light-independent reactions (LIR), photorespiration process (PR), and starch synthesis (StS), and sucrose synthesis (SuS). In this case we consider the sensitivities analysis of solutions depending on the rate coefficients and the initial conditions. Remark that the studies of the sensitive of the solutions that depend on the spaces are not involved in this part. Due to the set of parameters and the chemical reactions, we perform sensitivity analysis with KPP tool. For the full network of C_3 photosynthesis, the system of ODEs contains 49 chemical reactions (rate constants) and 59 chemical species (variables). In KPP library, the chemical reaction terms are based on the law of mass action kinetics. As the results, the sensitive of the solution at the final time for each variables with respect to the reaction rates and the initial conditions are calculated. For some chemical species, the sensitivities of the solution at the final times depending on the reaction rate is not so large. So that there are some parts in the network that have small impacts to the system.

The reduced system

In this section, we introduce the reduced system of chemical network. According to the reaction-diffusion model in Chapter 3, the system consists of the Calvin cycle, photorespiration process (PR), and starch synthesis (StS), and sucrose synthesis (SuS). In the previous sections, sensitivity analysis for the system of ordinary differential equations suggest that there are some part of the network are possible to reduced. In our research questions, we interested in the dynamical product of carbon and carbohydrate reactions. For the light-independent reactions (LIR), photorespiration process, and starch synthesis, we focus on the concentration of PGAL, DHAP, and starch. However, [21,22,30] introduced the lumping of PGAL and DHAP in form of triose phosphate (TP):

$$[\mathrm{TP}] = [\mathrm{PGAL}] + [\mathrm{DHAP}].$$

So that the final target for LIR and PR is TP.

By the numerical sensitivity analysis with KPP tools before we calculate the sensitivities of the solutions depending on the reaction rate coefficient. The results show that there are some chemical species not so sensitive w.r.t the rate constants. Therefore, we reduced the system by lumping for some variables. The lumping and reduced of the system of chemical network are illustrated in Figure 5.13.

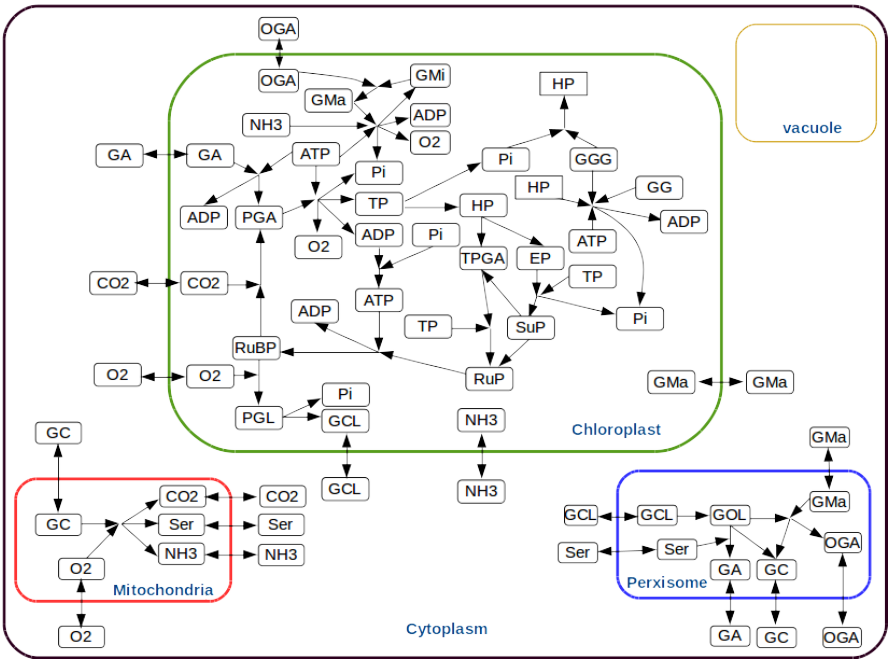

Figure 5.13: Reduced system contains 20 chemical reactions and 24 species.

Numerical simulation III: the reduced system

From the reduced chemical system, we setting up the model, the initial-boundary conditions, and the transmission conditions in the same approach as the full system. Then we perform the numerical for the reduced model in the same technique as the numerical simulation I and II. The numerical simulation for a reduced system illustrates the concentration of each chemical species in the 2D domain at the specific time. In this case, the computer simulation is dealing with a system of PDEs for 44 variables together with 21×2 transmission conditions. The difference of time step sizes and the levels of the mesh refinement are applied to investigate the convergence of numerical solutions.

Results of numerical simulation III

For time step 10 s, various mesh refinement levels are applied for the numerical simulation III (see also in Figure 5.14 and Table 5.17). However, we focus on the numerical simulation for 90 iterations, $dt = 10$, and 3 levels of the mesh refinement. As the results, the computational time of this case is reach to 35 minutes. The concentration of some chemical species are shown in Figures 5.15 to 5.25. Figures 5.17 and 5.18 show the concentrations of a

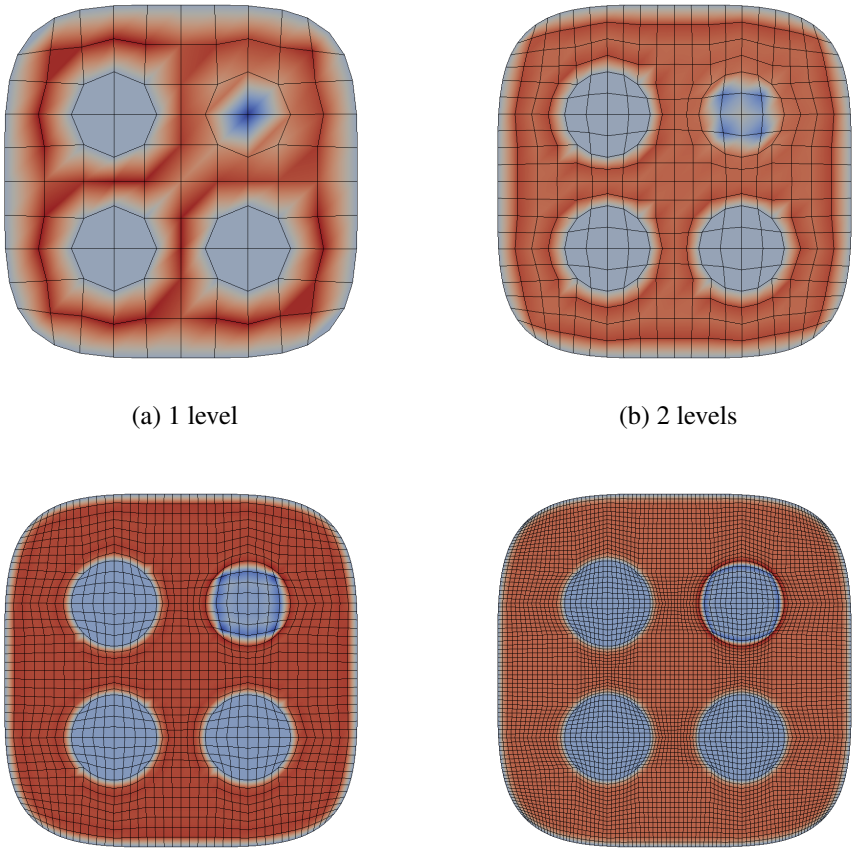

(a) 1 level (b) 2 levels

(c) 3 levels (d) 4 levels

Figure 5.14: Numerical simulation III, mesh refinement in a difference levels.

transmission specie (OGA) in the peroxisome (Ω_3) and in the cytoplasm (Ω_0) at the same iterations: $\iota = 1$, 10, 30, 50, and 90. The diffusion-transport of GMa in Ω_0, Ω_1, and Ω_3 are shown in Figure 5.19. Due to photorespiration, the concentration of GMa is rapidly increase in Ω_1 and decrease in Ω_3. In cytoplasm (Ω_0), the concentration of GMa is nearly constant except near the boundary and the interfaces.

For the dynamical products of LIR, PR, StS, and some other substances, we consider the summation of the concentration of chemical species per the area of the sub-domain (see also Figure 5.21 to Figure 5.25).

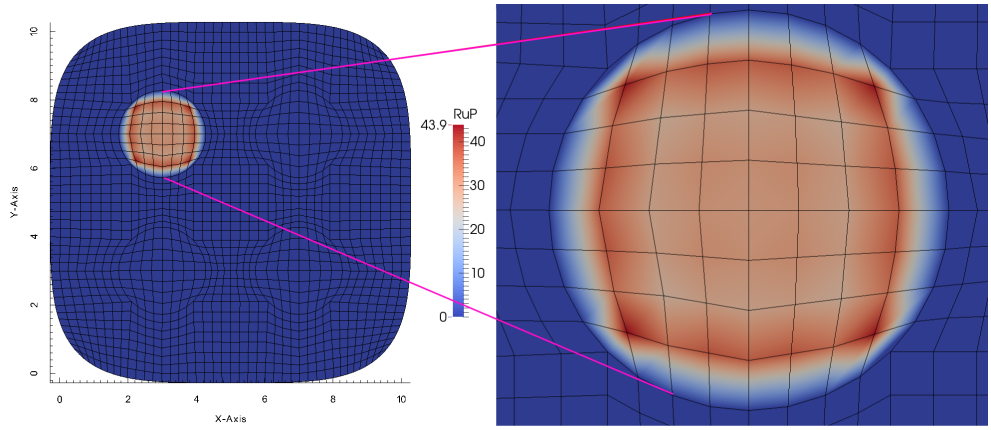

(a) zoom in the Ω_1

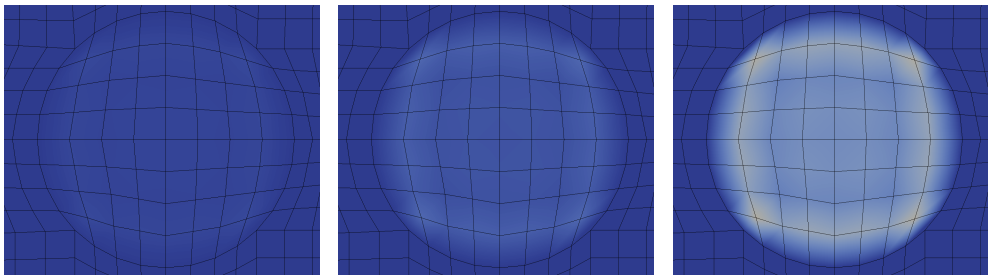

(b) ι=1 (c) ι=10 (d) ι=20

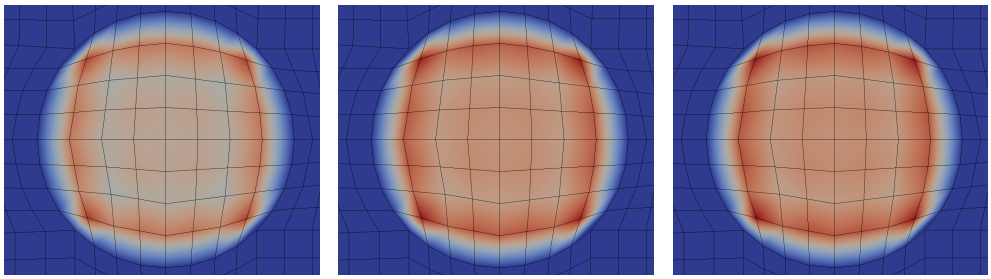

(e) ι=30 (f) ι=40 (g) ι=50

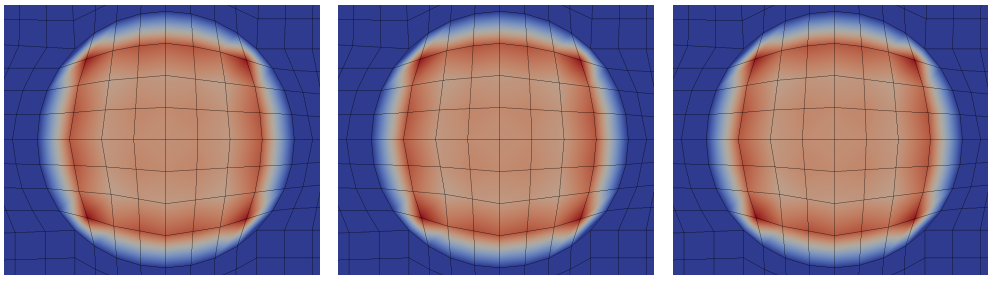

(h) ι=60 (i) ι=70 (j) ι=90

Figure 5.15: Numerical simulation III, diffusion-transport of RuP in Ω_1 at the iterations ι = 1, 10, 20, 30, 40, 50, 60, 70, and 90.

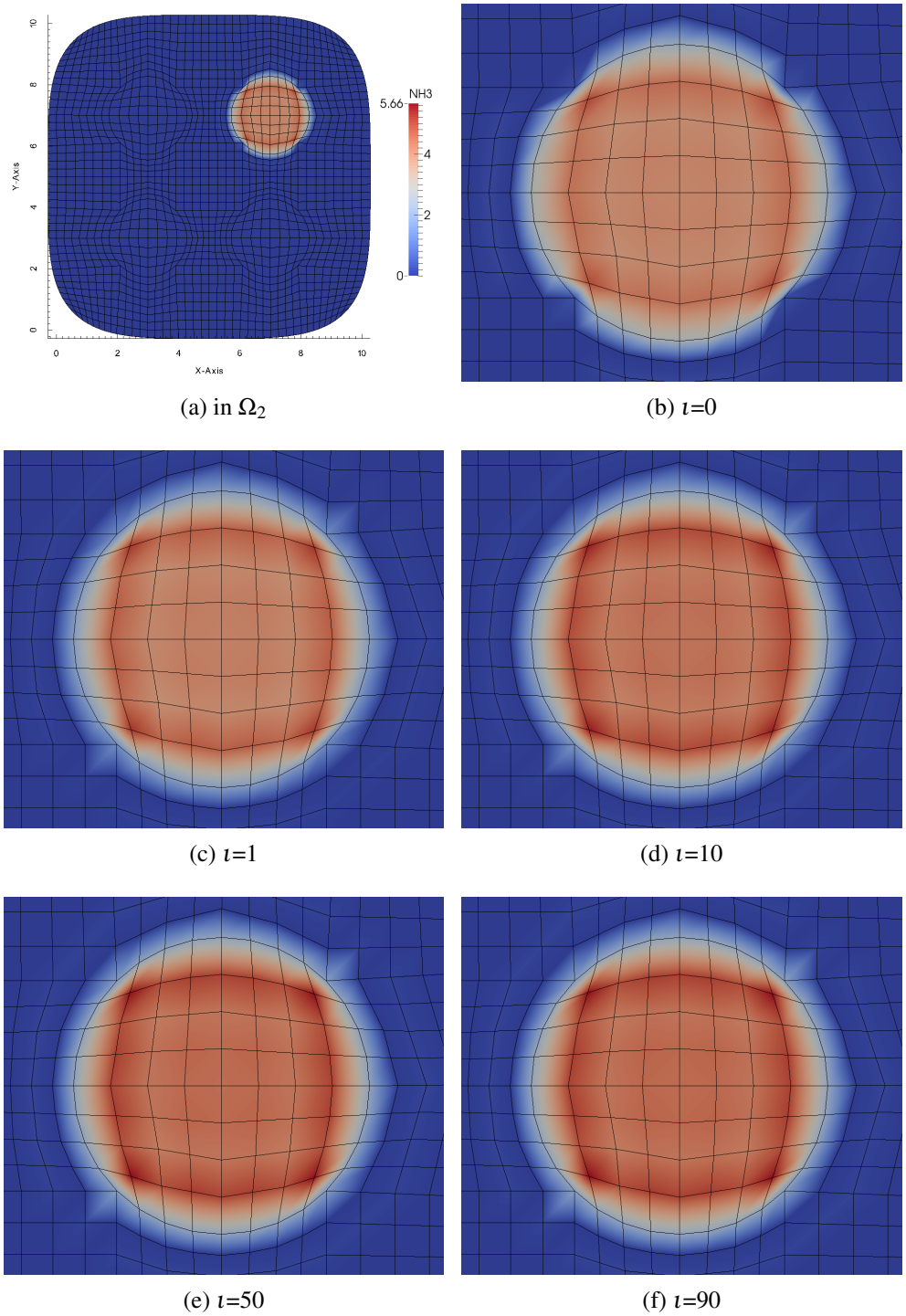

(a) in Ω_2 (b) ι=0

(c) ι=1 (d) ι=10

(e) ι=50 (f) ι=90

Figure 5.16: Numerical simulation III, diffusion-transport of NH_3^+ in Ω_2 at the iterations $\iota = 0$, 1, 10, 50, and 90, which have less change.

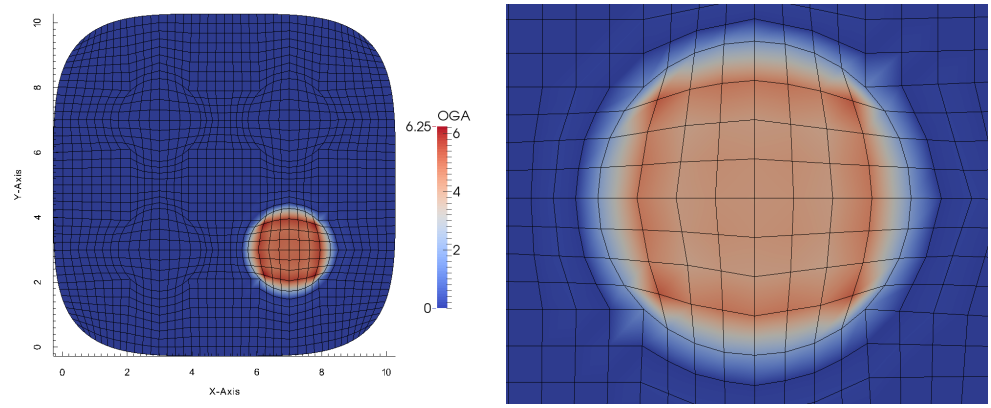

(a) in Ω_3 (b) ι=1

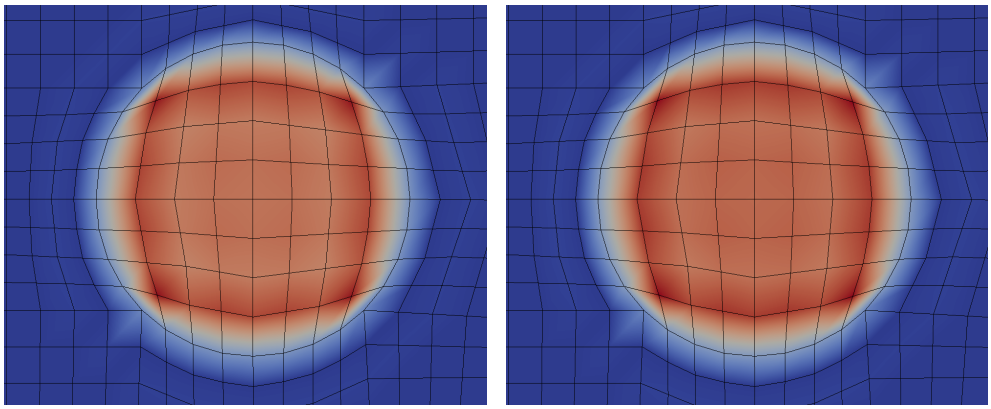

(c) ι=10 (d) ι=30

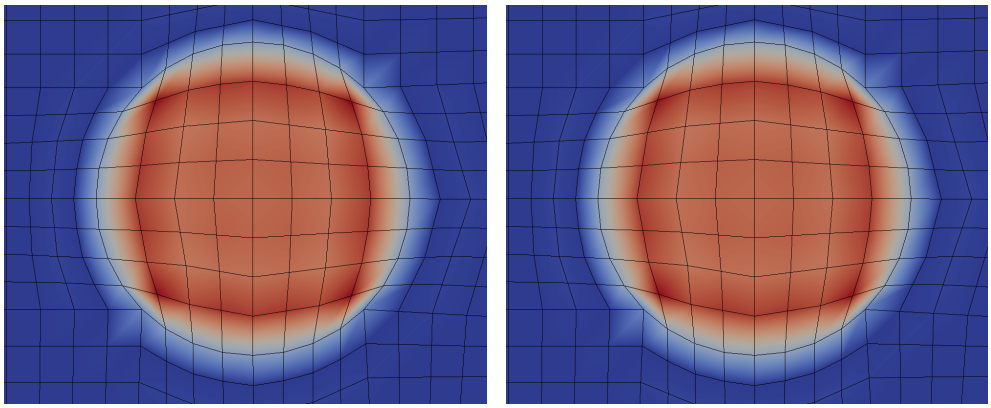

(e) ι=50 (f) ι=90

Figure 5.17: Numerical simulation III, diffusion-transport of OGA in Ω_3 at the iterations ι = 0, 1, 10, 50, and 90, which is fast increase in the beginning.

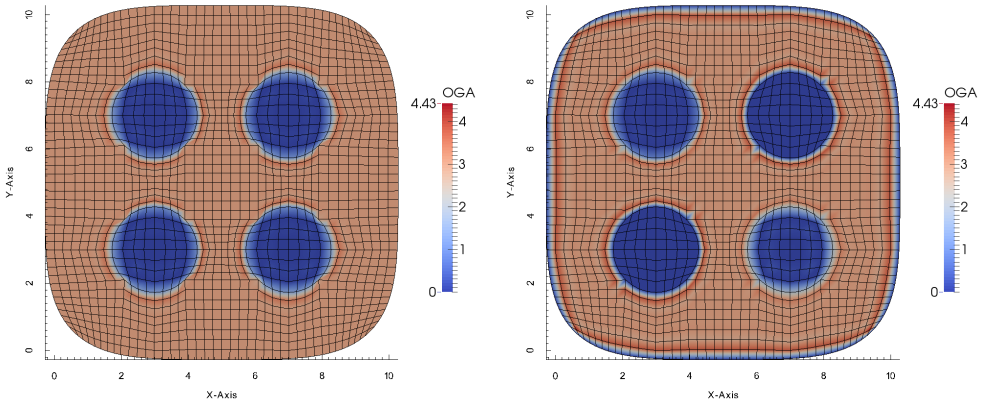

(a) ι=1 (b) ι=10

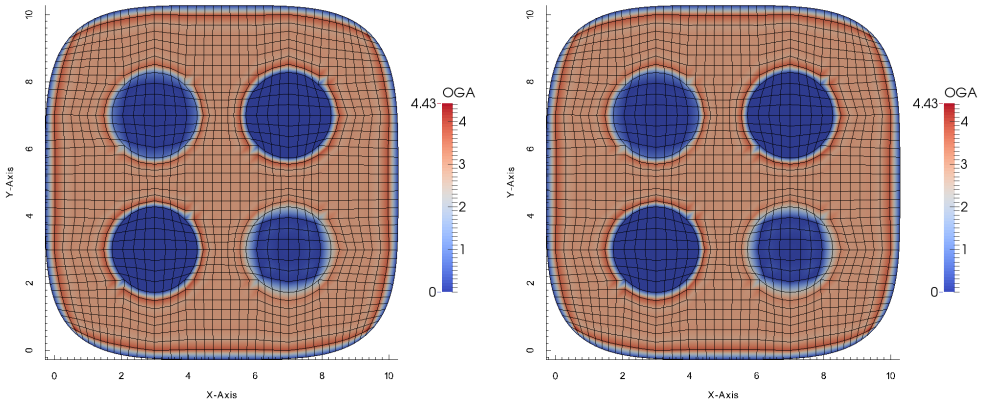

(c) ι=30 (d) ι=50

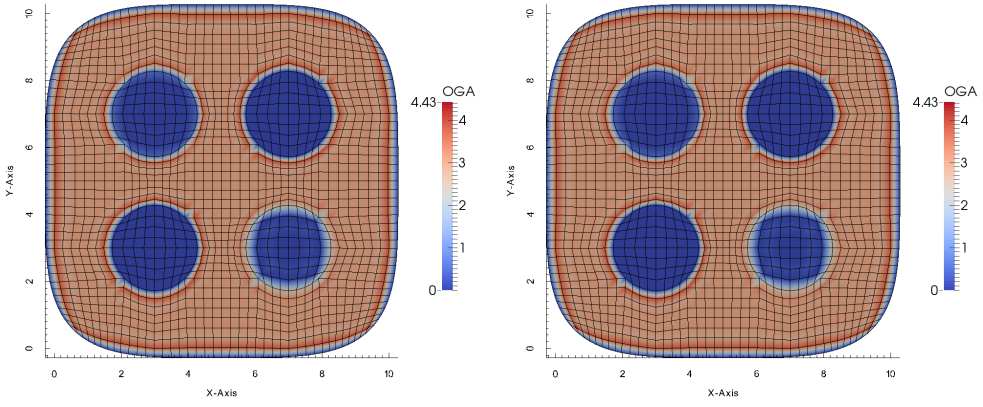

(e) ι=80 (f) ι=90

Figure 5.18: Numerical simulation III, diffusion-transport of the transmission species (OGA) in Ω_0 at the iterations ι = 1, 10, 30, 50, 80, and 90. The concentration of OGA in cytoplasm is almost constant except near the boundary and interfaces.

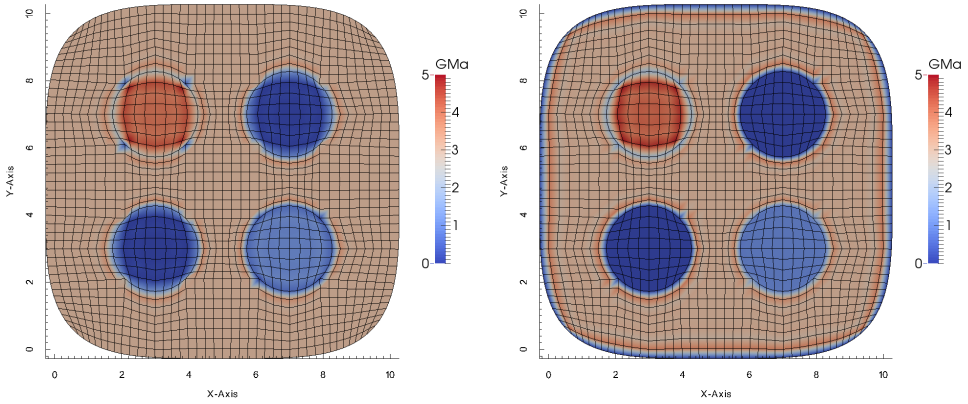

(a) ι=0 (b) ι=1

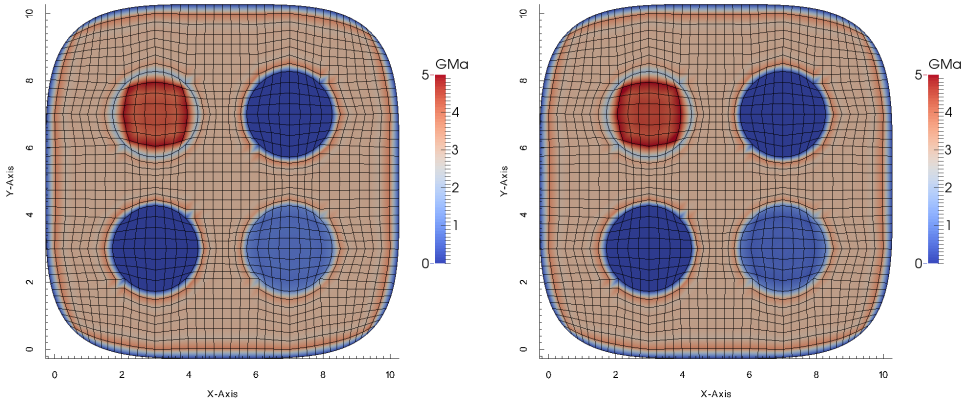

(c) ι=3 (d) ι=5

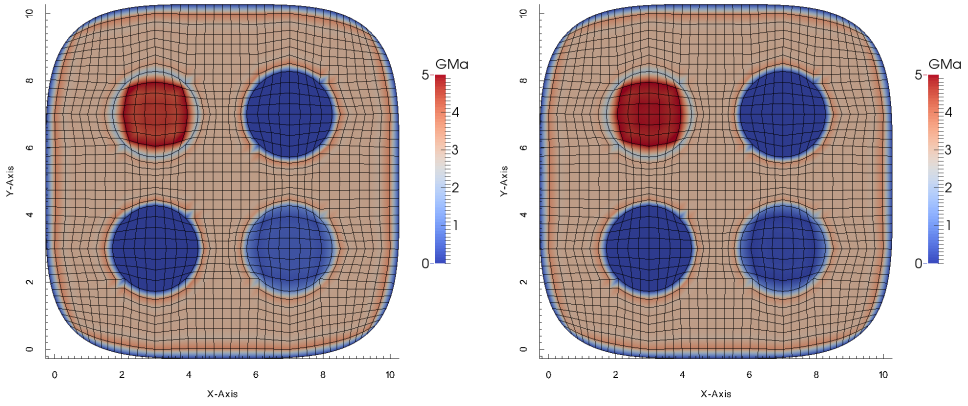

(e) ι=7 (f) ι=15

Figure 5.19: Numerical simulation III, diffusion-transport of GMa in Ω_0, Ω_1, and Ω_3 at the iterations $\iota = 0, 1, 3, 5, 7, 15$. There are small changes after the time step 15 because the concentration of GMa is reach to the steady state.

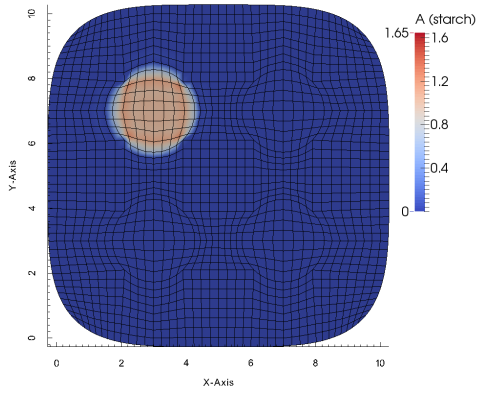

(a) in Ω_1

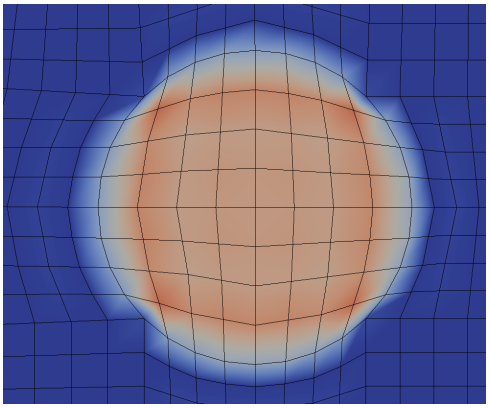

(b) ι=1

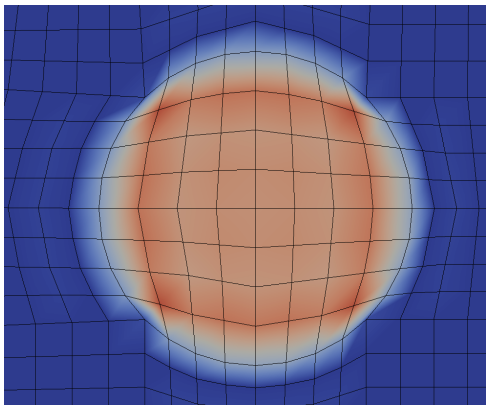

(c) ι=10

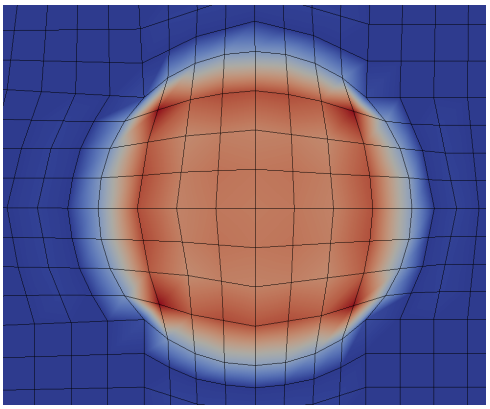

(d) ι=30

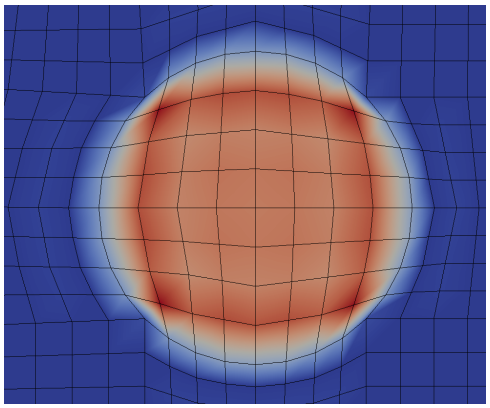

(e) ι=50

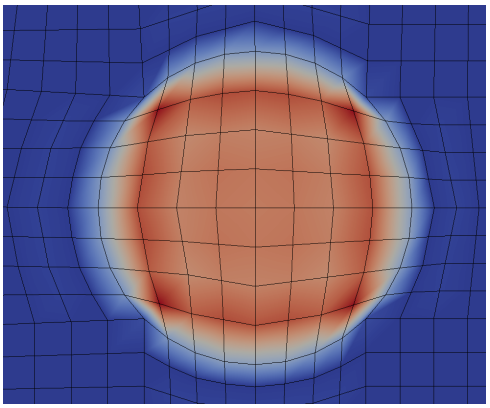

(f) ι=90

Figure 5.20: Numerical simulation III, diffusion-transport of starch in Ω_1 at the iterations ι = 1, 10, 30, 50, 90.

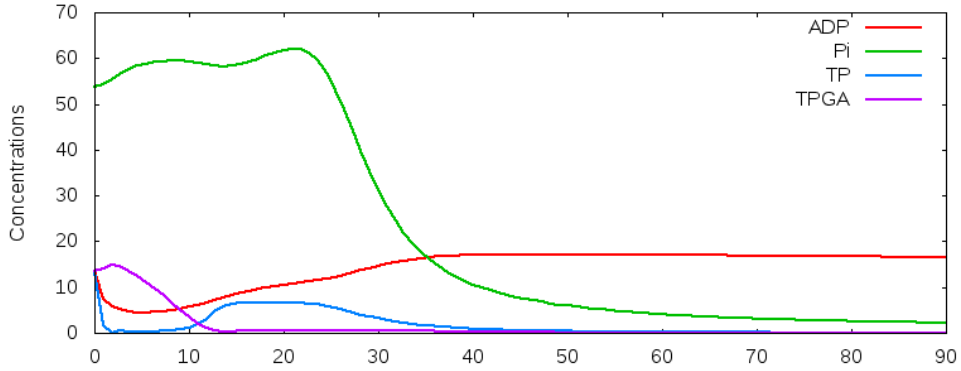

(a) Concentration of ADP, Pi, TP, and TPGA in Ω_1

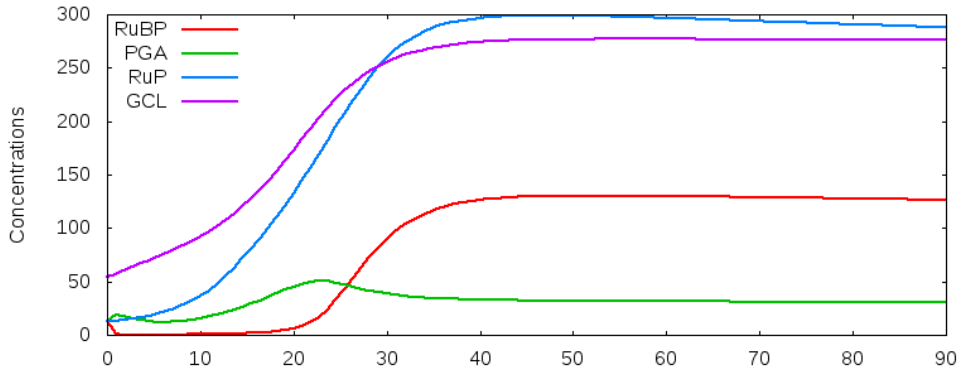

(b) Concentration of RuBP, PGA, RuP, and GCL in Ω_1

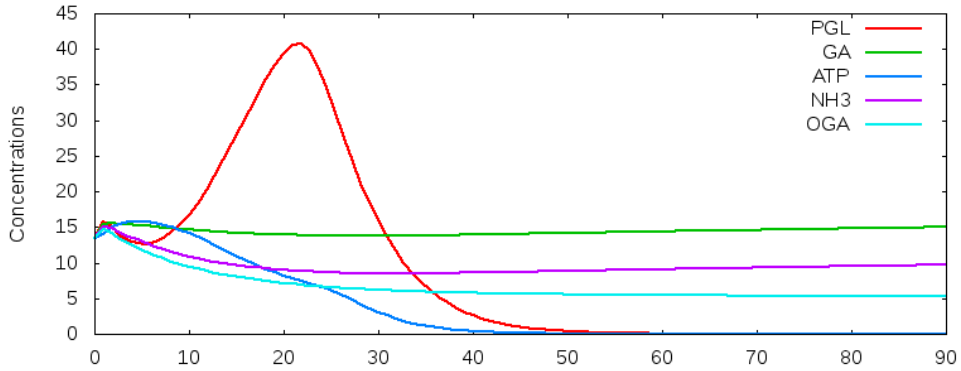

(c) Concentration of PGL, GA, ATP, NH_3^+, and OGA in Ω_1

Figure 5.21: Numerical simulation III, summation of the concentration u_i per area of Ω_1 (a) ADP, Pi, TP, and TPGA (b) RuBP, PGA, RuP, and GCL, (c) PGL, GA, ATP, NH_3^+, and OGA, in 15 minutes (90 iterations, time step 10), respectively.

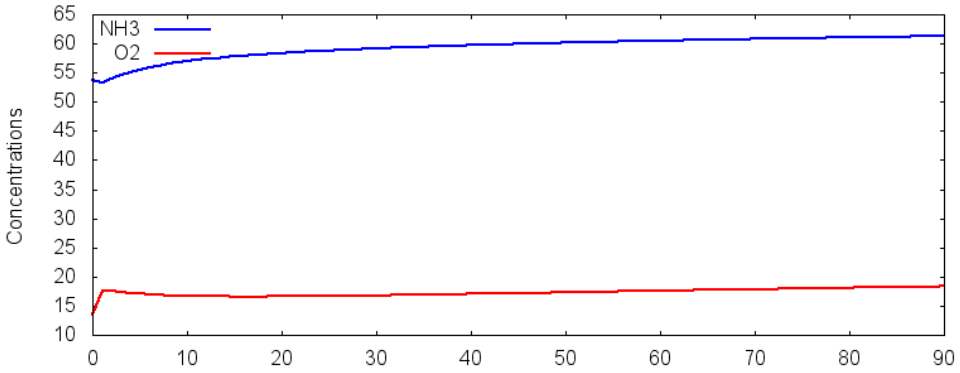

(a) Concentration of NH_3^+ and O_2 in Ω_2

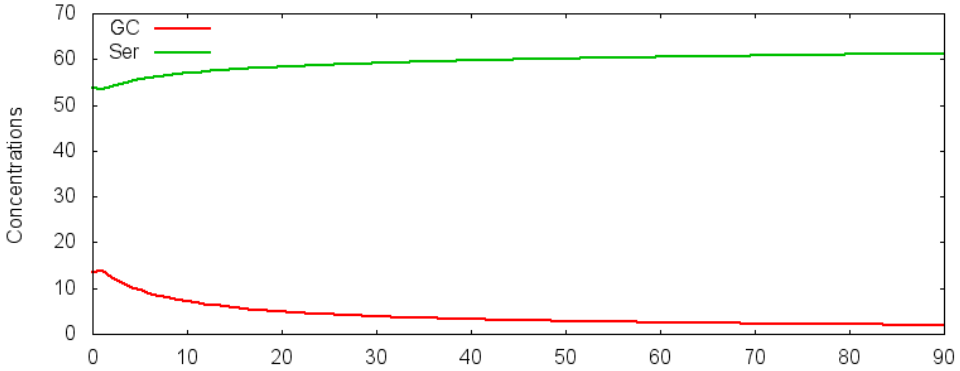

(b) Concentration of GC and Ser in Ω_2

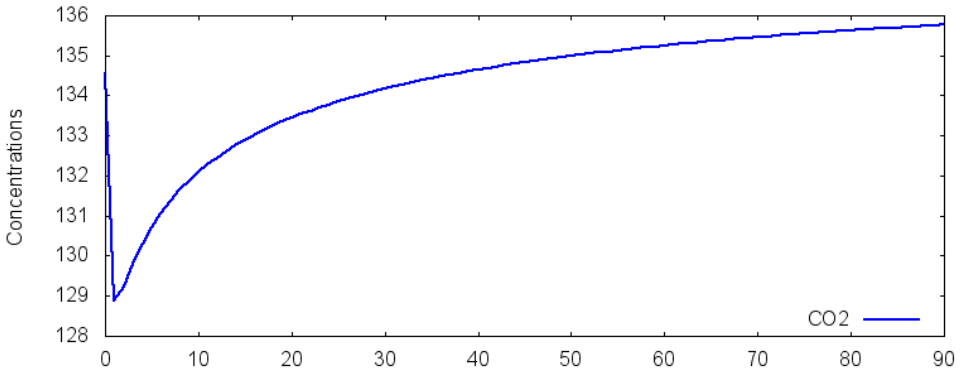

(c) Concentration of CO_2 in Ω_2

Figure 5.22: Numerical simulation III, summation of the concentration u_i per area of Ω_2 (a) NH_3^+ and O_2 (b) GC and Ser (c) CO_2, in 15 minutes (90 iterations, time step 10), respectively.

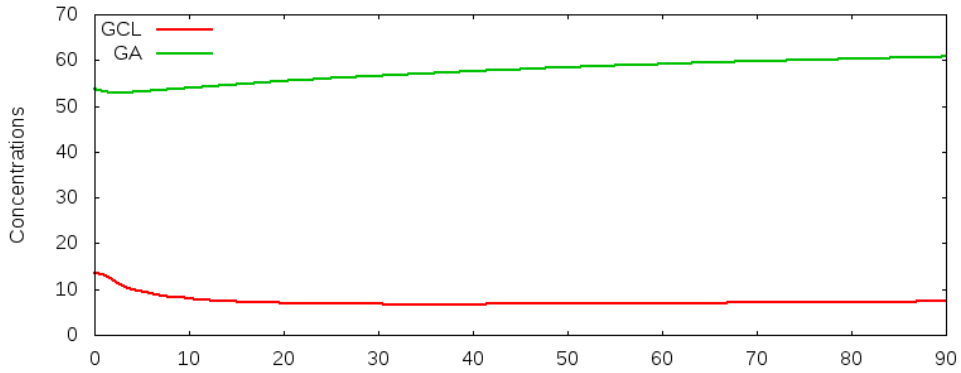

(a) Concentration of GCL and GA in Ω_3

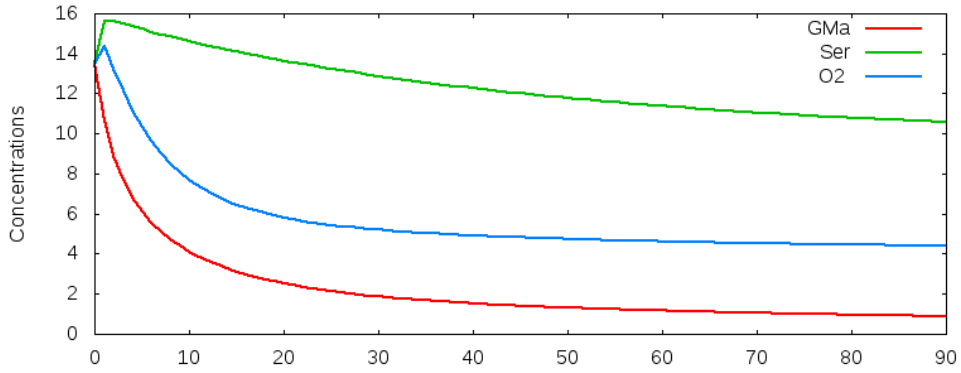

(b) Concentration of GMa, Ser, and O_2 in Ω_3

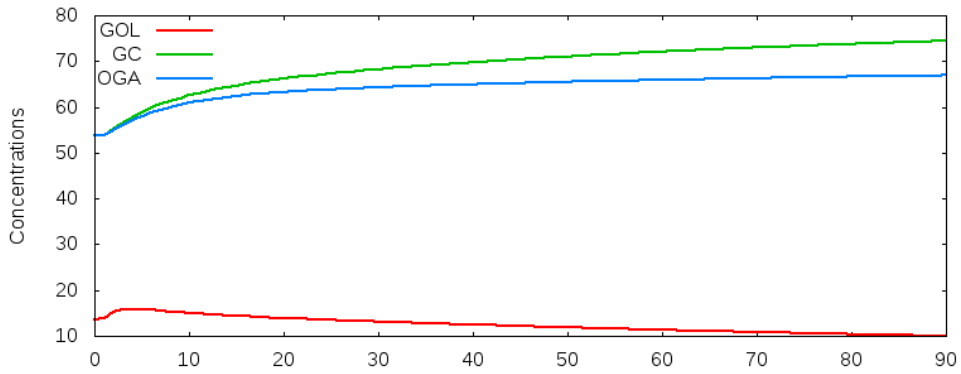

(c) Concentration of GOL, GC, and OGA in Ω_3

Figure 5.23: Numerical simulation III, summation of the concentration u_i per area of Ω_3 (a) GCL and GA (b) GMa, Ser and O_2 (c) GOL, GC and OGA, in 15 minutes (90 iterations, time step 10), respectively.

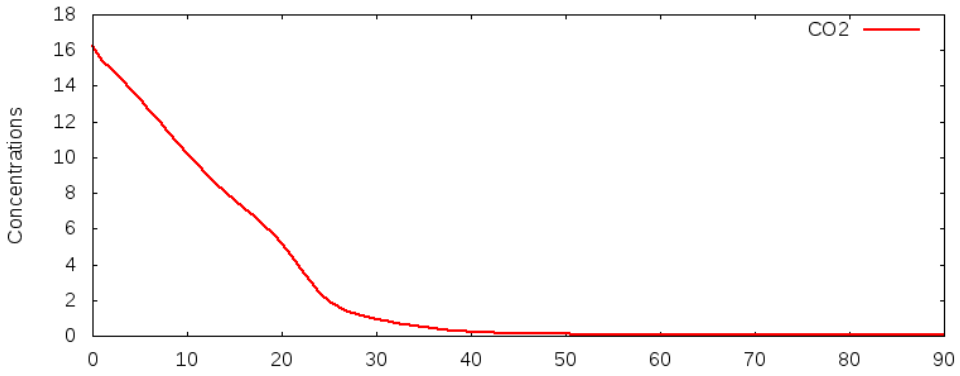

Figure 5.24: Numerical simulation III, summation of the concentration CO_2 per area of Ω_1 in 15 minutes (90 iterations, time step 10).

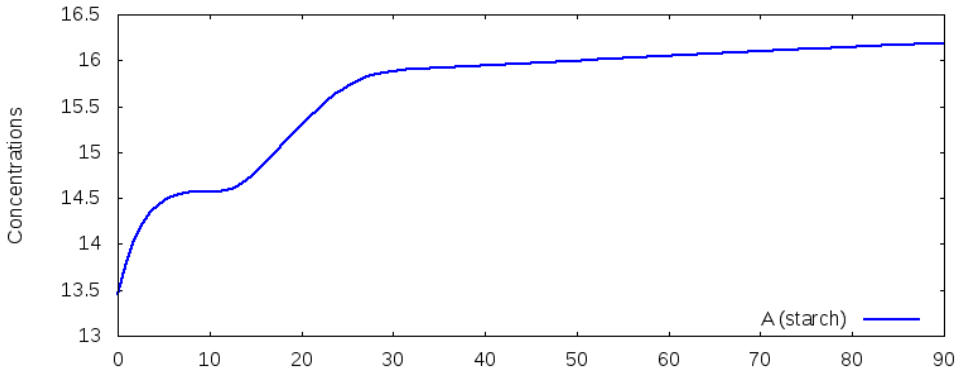

Figure 5.25: Numerical simulation III, summation of the concentration A (starch) per area of Ω_1 in 15 minutes (90 iterations, time step 10).

Table 5.14: The parameters for SuS in numerical simulation II (Cont'd)

$FBP + H_2O \longrightarrow FP + P_i$	D_{FP}	5.822×10^{-6}	$m^2\ s^{-1}$
	D_{P_i}	1.393×10^{-5}	$m^2\ s^{-1}$
	V_{27max}	0.21	
	$K_{m27,1}$ (FBP)	0.2	mM
$FP + ATP \longrightarrow FBP + ADP$	D_{ATP}	4.428×10^{-6}	$m^2\ s^{-1}$
	D_{ADP}	4.764×10^{-6}	$m^2\ s^{-1}$
	V_{28max}	0.2	
	$K_{m28,1}$ (FP)	0.5	mM
	$K_{m28,2}$ (ATP)	0.2	mM
$FP + PP_i \longrightarrow FBP + P_i$	D_{PP_i}	1.048×10^{-5}	$m^2\ s^{-1}$
	V_{29max}	0.4	
	$K_{m29,1}$ (FP)	0.3	mM
	$K_{m29,2}$ (PP_i)	0.2	mM
$FP + ATP \longrightarrow FTBP + ADP$	D_{FTBP}	5.216×10^{-6}	$m^2\ s^{-1}$
	V_{30max}	0.25	
	$K_{m30,1}$ (FP)	0.2	mM
	$K_{m30,2}$ (ATP)	0.2	mM
$FTBP + H_2O \longrightarrow FP + P_i$	V_{31max}	0.3	
	$K_{m31,1}$ (FTBP)	0.2	mM
$FP \longrightarrow GSP$	D_{GSP}	5.841×10^{-6}	$m^2\ s^{-1}$
	V_{32max}	0.2	
	$K_{m32,1}$ (FP)	0.1	mM
$GSP \longrightarrow GP$	D_{GP}	5.822×10^{-6}	$m^2\ s^{-1}$
	V_{33max}	0.15	
	$K_{m33,1}$ (GSP)	0.15	mM
$GP + UDP \longrightarrow UDPG + PP_i$	D_{UDP}	4.860×10^{-6}	$m^2\ s^{-1}$
	D_{UDPG}	4.232×10^{-6}	$m^2\ s^{-1}$
	V_{34max}	0.25	
	$K_{m34,1}$ (GP)	0.2	mM
	$K_{m34,2}$ (UDP)	0.2	mM
$UDPG + FP \longrightarrow UDP + SSP$	D_{SSP}	4.773×10^{-6}	$m^2\ s^{-1}$
	V_{35max}	0.2	
	$K_{m35,1}$ (UDPG)	0.15	mM
	$K_{m35,2}$ (FP)	0.2	mM
$SSP + H_2O \longrightarrow S + P_i$	D_S	5.202×10^{-6}	$m^2\ s^{-1}$
	V_{36max}	0.25	
	$K_{m36,1}$ (SSP)	0.3	mM

Table 5.15: The parameters for ζ_i^j in simulation I-III, we consider that the permeabilities are only depends on the chemical species (i).

Chemical species	Values
CO_2	1.0×10^{-1}
NH_4^+	0.5×10^{-1}
GC	1.0×10^{-1}
SR	1.0×10^{-1}
GCL	1.2×10^{-1}
O_2	1.5×10^{-1}
GMa	1.0×10^{-1}
OGA	1.7×10^{-1}
GA	0.4×10^{-1}
PGAL	0.2×10^{-1}
DHAP	0.2×10^{-1}
S	1.5×10^{-1}

Table 5.16: The coefficients of the function $\alpha(\lambda)$.

s	Wavelengths	a_s	b_s	c_s	d_s
1	$400 \leqslant \lambda < 440$	-3.13×10^4	2.29×10^2	-5.61×10^{-1}	4.58×10^{-4}
2	$440 \leqslant \lambda \leqslant 460$	-2.28×10^7	1.52×10^4	-3.37×10^1	2.50×10^{-2}
3	$460 < \lambda \leqslant 520$	1.56×10^4	-9.35×10^1	1.85×10^{-1}	-1.22×10^{-4}
4	$520 < \lambda \leqslant 600$	-1.36×10^3	7.62	-1.42×10^{-2}	8.85×10^{-6}
5	$600 < \lambda \leqslant 670$	-7.00×10^4	3.40×10^2	-5.51×10^{-1}	2.97×10^{-4}
6	$670 < \lambda \leqslant 700$	-8.38×10^5	3.63×10^3	-5.23	2.51×10^{-3}

Table 5.17: For reduced model, the computational informations of the numerical simulation with a various of mesh refinement levels (90 iterations, time step 10).

Mesh refinement levels	1	2	3	4
Computational times (minutes)	6	20	35	136
Number of cells	100	400	1600	6400
Number of points	121	441	1681	6561
Memory usages (MB)	0.057	0.22	0.78	2.9

Chapter 6

Conclusion and outlook

6.1 Conclusion

To investigate the influences of photorespiration reaction and related factors on the rate of photosynthesis, this thesis developed a mathematical model for photosynthesis of a C_3 plant leaf cell. The model describes the diffusion, transport, and related chemical reactions in a multi-component flow in a single cell. Our model consists of a system of non-linear partial differential equations based on biochemical and physiological assumptions. In this model, a complex system of the light-dependent reaction, the light-independent reaction, the photorespiration reaction, the starch synthesis, and the sucrose synthesis are all taken into account.

The mathematical model consists of two parts: the light-dependent and the reaction-diffusion model. The light-dependent model describes the process of light absorption, water photolysis, electron transport chain, generation of ATP, and formulation of NADPH. The generation rate of ATP for the light-depend reaction is not only depend on the chemical reaction, but also depend on the proton gradient. The reaction-diffusion model describes the complex network of Calvin cycle, photorespiration reaction, starch synthesis, and sucrose synthesis in details. In photorespiration process, multi-chemical species are take place in 3 difference organelles including chloroplast, mitochondria, and peroxisome. Therefore, we consider the transmission problem for the reaction-diffusion equations. Due to the structure network, the mathematical model focuses on 5 sub-domains including chloroplast, mitochondria, perox-

isome, cytoplasm, and vacuole. The appropriate initial-boundary conditions are derived for each of the sub-models. Since some chemical species move across the interface, we assume that the flux of substances though interfaces is proportional to the jump of the concentrations.

In this work, we developed a computer algorithm for converting chemical reaction to a system of reaction-diffusion equations. The computer program are implements with *Perl* script. The program consists of three modules working together, including a sub-module for extracting a chemical component, a sub-module for forming chemical reaction terms, and a sub-module for setting up a system of reaction-diffusion equations, respectively. To set up a system of reaction-diffusion equations for the large chemical network, this computer tool produce a good result without human mistake, save time, and user- friendly manual.

Based on the mathematical model, a variational formulation of the light-dependent model and the reaction-diffusion model is derived. The transmission conditions are necessary for the variational formulation. Therefore, those formulations has to be changed.

The numerical simulations of this model are performed by using the finite element method library Gascoigne 3D. The software is a C++ library for the solution of partial differential equations. The computer simulation for photosynthesis of a C_3 plant leaf cell focuses on 2 sub-models: the light-dependent model and the reaction-diffusion model. Spatial discretization is based on the Galerkin finite element method. Time discretization is performed by implicit backward Euler scheme. A 2 dimensional cell and its organelles of a C_3 plant are represented in a squircle shape. The numerical simulation for photosynthesis of a plant leaf cell illustrates the concentration of each chemical species in the 2D domain at a specific time. Various of time step sizes and mesh refinement levels are applied to investigate the convergence of numerical solutions.

As the results of the simulations, the multi-component diffuse and transport in the multi-compartment of a C_3 plant leaf cell. For the numerical simulation I, the dynamical productions of the light-dependent reactions: O_2, NADPH, ATP, agreed with the biological observation. The concentration of NADPH and ATP increases in the beginning of the simulation and are reach to the steady state. Due to our model, the concentration of O_2 increases in time and is seen not close to any steady state. For the light-independent reaction and

starch synthesis, the consumption of CO_2 rapidly decreases in the very short time of the beginning of the simulation. For the numerical simulation II, the concentration of PGAL reaches to up 2 local maximums and decreases to zero afterwards. In the numerical simulation III, the concentration of triose phosphate is decreased in the beginning, then reaches to 1 local maximum, and decreases to zero afterward. In numerical simulation II, the concentration of starch is increase and reach to steady state. In numerical simulation III, the concentration of starch is increase in time. For the sucrose synthesis in numerical simulation II, the concentration of sucrose in cytoplasm and vacuole is continuously increasing in time. However, we do not consider the sucrose synthesis in numerical simulation III.

In Figures 5.12 and 5.21, we see that the dynamics of RuP and GCL are not different. The concentration of RuP and GCL increases and reaches their steady state. However, the dynamics of RuBP and PGA from numerical simulation II and III are not similar. In numerical simulation III, the concentration of PGA reaches one local maximum and later decreases and reaches a steady state. In numerical simulation II, the PGA and RuBP concentrations both decrease in time. In contrast, from numerical III the concentration of RuBP decreases in the beginning, then increases and reaches a steady state. Nevertheless, others chemical species for each of the numerical simulations, which we are not mention here, are also possibles to be discussed in detail. From the mathematical models and the numerical simulation I - III, the dynamics of the products in the light reaction, the carbon reaction, the starch reaction, and the sucrose reaction are agreed with the biological observation.

Finally, we receive answers to our research questions. Moreover, the mathematical model and the numerical simulation for photosynthesis in C_3 a plant leaf cell produced reasonable results and are suitable for further studies.

6.2 Outlook

Based on the results of our work described above, we consider the following directions of research as particularly exciting:

- **Mathematical Modeling for photosynthesis of C_3 plants:**
  Since the fixed interface domain is developed in this work, a development of the mathematical model for a free boundary in a single cell is

very interesting.

For a simpler model, a lumping and reduced chemical system without losing the crucial biochemical and physiological informations stills required.

The model for a C_3 plant has to be extended from a single cell to a leaf tissue, using analytical and numerical upscaling methods.

- **Mathematical Analysis:**
  In this thesis we concentrated our investigation on the modelling and simulations. The results are positive and therefore the precise mathematical analysis of the existence of unique, nonnegative solutions is a necessary next step. Since we have systems of diffusion-reaction equations with different diffusion coefficients and nonlinear reaction terms this problem requires an independent theoretical investigation. Nevertheless, simpler sub-problems are challenges to current research.

- **Numerical Simulation for photosynthesis of C_3 plants:**
  The simulations have to be extended from 2 dimensions to 3 dimensions. Since transmission problems are involved, the numerical methods need more attention. Parallel methods are offering a realistic chance to improve the computational performance.

- **Mathematical Modeling and Simulation for photosynthesis of C_4 and CAM:**
  Based on the diversity of plants, plant physiology and biochemistry, this model is a good start to develop the mathematical model and numerical simulation for photosynthesis of C_4 and crassulacean acid metabolism (CAM) plants.

  For C_4 plants, the photosynthesis processes are divided between mesophyll and bundle sheath cells. There are two steps of C_4 photosynthesis that occur in the mesophyll cells: The light-dependent reactions and a preliminary carbon reaction into a molecule called malate. CO_2 is released from malate in the bundle sheath cells, where it is fixed again by rubisco and the Calvin cycle. The PEP, phosphoenolpyruvate carboxylase enzyme, is then recycled back into the mesophyll cells.

  In CAM plant leaves, the stomata remain close during the day to reduce evapotranspiration, but open at night to collect CO_2. The CO_2 is stored as the four-carbon acid malate in vacuoles at night. In the daytime, the

malate is transported to chloroplasts where it is converted back to CO_2, which is then used during photosynthesis.

- **Applications:**
  A possible application for this model is study growth and development of the industrial crops and plants, for example sugarcane, corn, bamboo, cassava, soy bean, rubber, and oil palm.

List of Figures

List of Tables

Appendix A

Calculus of several variables

In this section (Appendices A.1 to A.3), we give the formulation of the governing equations that concern with two mechanisms: reaction and diffusion. First, we will start with the brief explanation of the reaction kinetics of the chemical species. Second, we will give a short description of the diffusion mechanism. Third, we will investigate the derivation of the Reaction-Diffusion Equations (RDEs) which is applied in Chapter 3.

A.1 Reaction process

There are various possible ways to generate a chemical reaction term. However in this section we will give the description for two approaches called Law of Mass Action Kinetics (MAK) and the Michaelis–Menten Kinetics (MMK) (see also in [51] for more details and informations).

Law of Mass Action Kinetics

Law of mass action stats that the rate of any chemical reaction is proportional to the product of the masses of the reacting substances, with each mass raised to a power equal to the coefficient that occurs in the chemical equation [52].

Consider a following chemical reaction, molecular species S_i undergoing the single irreversible reaction

$$a_1 S_1 + \cdots + a_I S_I \xrightarrow{k} b_1 S_1 + \cdots + b_I S_I,$$

together with a_i, $b_i \in \mathbb{N}$ and a positive real chemical reaction constant k.

According to the law of mass action kinetics, the rate of reactions v (forward reaction rate) for the concentrations n_i of chemical species i is represented by $v = k\prod_{j=1}^{I} n_j^{a_j}$. For the reversible reaction

$$a_1S_1 + \cdots + a_IS_I \underset{k_r}{\overset{k_f}{\rightleftharpoons}} b_1S_1 + \cdots + b_IS_I,$$

where $a_i \neq b_i \in \mathbb{N}$ and $k_f, k_r \in \mathbb{R}^+$, the chemical reaction rate is given by $v = v_f - v_r$ where $v_f = k_f\prod_{j=1}^{I} n_j^{a_j}$ and $v_r = k_r\prod_{j=1}^{I} n_j^{b_j}$.

Michaelis–Menten Kinetics

To start with MMK, we consider the enzyme-catalyzed reactions in the following scheme

$$E + S \underset{k_{-1}}{\overset{k_1}{\rightleftharpoons}} ES,$$
$$ES \xrightarrow{k_2} P + E.$$

By applying the steady-state approximation to the complex ES:

$$\frac{d[ES]}{dt} = k_1[E][S] - (k_{-1} + k_2)[ES] = 0,$$

then we have

$$[ES] = \frac{k_1[E][S]}{k_{-1} + k_2}. \tag{A.1}$$

The mass balance expression for the enzyme is represented in the form

$$E_t = [E] + [ES]. \tag{A.2}$$

Combining the equations (A.1) and (A.2) and eliminating $[E]$, then we got

$$[ES] = \frac{k_1E_t[S]}{k_{-1} + k_2 + k_1[S]}. \tag{A.3}$$

The rate of chemical reactions is defined by

$$v = \frac{d[P]}{dt} = k_2[ES],$$

or

$$v = \frac{k_1k_2E_t[S]}{k_{-1} + k_2 + k_1[S]},$$

So that the chemical reaction rate that obey on the Michaelis–Menten kinetics which is usually written in the form

$$v = \frac{V_m[S]}{K_m + [S]}, \tag{A.4}$$

where $V_m = k_2 E_t$ represents the maximum rate achieved by these chemical reactions and $K_m = (k_{-1} + k_2)/k_1$ is the Michaelis–Menten constants.

A.2 Diffusion process

In this work, we assume that the diffusion of materials within the domain follows the classical diffusion process so called the Fick's law of diffusion.

Fick's Law

First of all, we consider the density function $u(x,t)$ where $x \in \Omega$ is the location and t is the time. Then, we also assume that Ω is the open subset in $\mathbb{R}^n$ where $n \geq 1$ is the *n-th* dimensional space in the Cartesian coordinate system. The movement of $u(x,t)$ is call the *flux* of the density.

According to the fact that a solute will move from high concentration regions to low concentration regions across a concentration gradient, the Fick's first law of diffusion describes the diffusive flux $\mathscr{J}$ of the concentration under the assumption of steady state in terms of its gradient.

From *high to low* principle, the flux which is a vector always decrease in the direction of $u(x,t)$. Therefore, the flux of the solute in an inhomogeneous phase can be represent as

$$\mathscr{J}(x,t) = -D(x)\nabla_x u(x,t) \tag{A.5}$$

where $D(x)$ is called diffusion coefficient at the position x and ∇_x is the gradient operator

$$\nabla_x f(x) = \left(\frac{\partial f}{\partial x_1}, \frac{\partial f}{\partial x_2}, \ldots, \frac{\partial f}{\partial x_n} \right).$$

A.3 Derivation of Reaction-Diffusion Equations

Base on the balance laws, we consider the general case that involve both reaction and diffusion processes in a domain $\Omega \in \mathbb{R}^n, n = 2$. Suppose that τ is a small time interval, the domain Ω is open, bounded, and smooth together with it's boundary $\partial\Omega$. Moreover, let $\mathscr{S}$ be a surface that enclose an arbitrary volume $\mathscr{V} \subset \Omega$ and n be an outward normal direction at the boundary. According to the general conservation equation, we see that

$$\int_{\mathscr{V}} [u(x,t+\tau) - u(x,t)]\, d\mathscr{V} = \int_t^{t+\tau} \left[-\int_{\mathscr{S}} \mathscr{J} \cdot n d\mathscr{S} + \int_{\mathscr{V}} f(x,t') d\mathscr{V} \right] dt', \tag{A.6}$$

where $u(x,t)$ is a concentration of a chemical specie at position $x \in \mathbb{R}^2$ at time t, $\mathscr{J}$ represents the flux of the population density, f is the source of the material that depend on u,x,t. By dividing equation (A.6) with τ and taking the limit as $\tau \to 0$, we have

$$\lim_{\tau\to 0} \int_{\mathscr{V}} \left[\frac{u(x,t+\tau) - u(x,t)}{\tau} \right] d\mathscr{V} \quad = \quad \lim_{\tau\to 0} \frac{1}{\tau} \int_t^{t+\tau} \left[-\int_{\mathscr{S}} \mathscr{J} \cdot n d\mathscr{S} + \int_{\mathscr{V}} f(x,t') d\mathscr{V} \right] dt',$$

So that, the appendix A.3 become

$$\int_{\mathscr{V}} \frac{\partial u(x,t)}{\partial t} d\mathscr{V} = -\int_{\mathscr{S}} \mathscr{J} \cdot n d\mathscr{S} + \int_{\mathscr{V}} f(x,t) d\mathscr{V}. \tag{A.7}$$

From the Divergence theorem in multi-variable calculus

$$\int_\Omega \nabla \cdot u dx = \int_{\partial\Omega} u \cdot n da \tag{A.8}$$

to the flux integral in appendix A.3, we have

$$\int_{\mathscr{S}} \mathscr{J} \cdot n d\mathscr{S} = \int_{\mathscr{V}} \nabla \cdot \mathscr{J}\, d\mathscr{V}. \tag{A.9}$$

Combining equations (A.5), (A.7) and (A.9), then interchanging the order of integration and differentiation, we got

$$\int_{\mathscr{V}} \left[\frac{\partial u(x,t)}{\partial t} + \nabla \cdot \mathscr{J} - f(u,x,t) \right] d\mathscr{V} = 0. \tag{A.10}$$

Since the choice of the volume $\mathscr{V}$ is arbitrary, then

$$\frac{\partial u(x,t)}{\partial t} + \nabla \cdot \mathscr{J} - f(u,x,t) = 0, \tag{A.11}$$

hold for any (x,t).

$$\frac{\partial u(x,t)}{\partial t} = \nabla \cdot (D_u(x)\nabla u(x,t)) + f(u,x,t). \tag{A.12}$$

In this work we consider in the case of the diffusion coefficients of the chemical specie u is a constant ($D_u \in \mathbb{R}^+ \cup \{0\}$), so that the equation (A.12) become

$$\frac{\partial}{\partial t}u(x,t) = D_u \Delta u(x,t) + f(u,x,t), \tag{A.13}$$

where

$$\Delta u = div(\nabla u) = \sum_{i=1}^{n} \frac{\partial^2 u}{\partial x_i^2}, \quad n = 3$$

is the Laplace operator. It is easy to see that when there is no reaction occurs, the equation (A.13) is the Diffusion equation:

$$\frac{\partial}{\partial t}u(x,t) = D_u \Delta u(x,t)). \tag{A.14}$$

Appendix B

Supplement tools

B.1 The algorithm chemToRDE

In this section, we developed a computer algorithm for converting chemical reaction to reaction-diffusion equation [53]. The computer program are implement with *Perl* script.

Input

Consider the irreversible chemical reaction $\mathrm{aA} + \mathrm{bB} \xrightarrow{k} \mathrm{cC} + \mathrm{dD}$, we then defined the input of the program by `aA_+_bB_-_cC_+_dD`, where `a,b,c,d` are positive real numbers, `_` is a free space, and `A,B,C,D` are strings. Moreover for the reversible chemical reaction $\mathrm{eE} \underset{k_{-1}}{\overset{k_1}{\rightleftharpoons}} \mathrm{fF} + \mathrm{gG}$, we should provided `eE_-_fF_+_gG` and `fF_+_g-_eE` as the input. All of the chemical reaction equations are stored in an input file0.

A computer program

Since a set of chemical reactions, $\sum \alpha_{\mathrm{j}} \mathrm{U_j} \xrightarrow{k_h} \sum \alpha_{\mathrm{l}} \mathrm{U_l}$, can be written in the system of reaction-diffusion equations:

$$\partial_t u_i - D_i \Delta u_i = f_i(u), \quad i = i, \ldots, m, \quad u = (u_1, \ldots, u_m)$$

where u_i is a concentration of the chemical species i.

Suppose that CE is a chemical reaction equations including a substrate part (SP) and a product part (PP),
k is a chemical reaction rate of CE,
CS is a chemical specie,
σ is a stoichiometric coefficients of a CS,
CC is a chemical component,
s is a sign (- if CS is a substrate and + if CS is a product),
KR_{CC} is a kinetic rate of a chemical component, and
RDE is a reaction-diffusion equation.

The computer program consists of three functions working together. The sub-programs are cover the part of extracting a chemical component (Algorithm 1) , forming a chemical reaction terms (Algorithm 2), and forming a system of reaction-diffusion equations (Algorithm 3) respectively.

Algorithm 1 Extracting a chemical components

```
1:  function ChemicalComponents(CE, CS, k, s, σ, CC)
2:      for all CE do
3:          CC = 0
4:          store k in tmp
5:          if CS ∈ SP then s = -                    ▷ Store s in tmp
6:              search σ, CS in SP                   ▷ Store σ, CS in tmp
7:          else  s = +                              ▷ Store s in tmp
8:              search σ, CS in PP                   ▷ Store σ, CS in tmp
9:          end if
10:         tmp = {k, s, σ, CS}
11:         CC ← CC + tmp
12:     end for
13:     return CC                          ▷ The CC is chemical components
14: end function
```

To form a chemical reaction terms, we can easily apply some rule for the kinetic rate of a chemical components i.e. law of mass action kinetics, Michaelis-Menten kinetics (see also Algorithm 2).

Output

The output of the **chemToRDE** program is the list of the reaction-diffusion equations. By providing the good input file, the function **ReactionDiffu-**

Algorithm 2 Forming a chemical reaction terms

function CHEMICALREACTIONTERMS(CC, CS, k, s, σ, KR_{CC})
  for all CC **do**
    $KR_{CC} = 0$
    ChemicalComponents (CE, CS, k, s, σ, CC)
    $tmp \leftarrow s \cdot \sigma_{CC} \cdot k \cdot \prod [CS]^{\sigma_{CS}}$ ▷ Law of mass action kinetics
    $KR_{CC} \leftarrow KR_{CC} + tmp$
  end for
  return KR_{CC} ▷ The kinetic rate of a chemical components
  write output ▷ Write to file1
end function

sionEquations calling to the corresponding sub-program for extract the chemical component and construct the chemical reaction terms (see also Algorithm 3).

Algorithm 3 Forming a system of reaction-diffusion equations

function REACTIONDIFFUSIONEQUATIONS(CC, KR_{CC}, RDE)
  read input ▷ Read from file0
  for all CE **do**
    $CC = 0$
    search CS in CE
    $CC \leftarrow CC + CS$
    for all CC **do**
      $RDE = \partial_t [CC] - D_{CC} \Delta [CC]$
      $tmp = 0$,
      KR_{CC} = ChemicalReactionTerms (CC, CS, k, s, σ, KR_{CC})
      read input ▷ Read from file1
      sort KR_{CC} ▷ Collect all CC for the same species
      $tmp \leftarrow KR_{CC}$
      $RDE \leftarrow RDE + tmp$
    end for
    return RDE ▷ The reaction-diffusion equations
  end for
  write output ▷ Write to file2
end function

B.2 Example (a simple user manual)

In this sections, we give some simple example how to use this program and how to make it work. From the chemical reaction equations

$$12\,\mathrm{E} + 3\,\mathrm{S} \underset{k_{-1}}{\overset{k_1}{\rightleftharpoons}} \mathrm{ES},$$
$$5\,\mathrm{E} \xrightarrow{k_2} \mathrm{ES},$$

then the input file (.txt) should be represented the following information:

```
12E + 3S - ES
ES - 12E + 3S
5E - ES
```

By compile and running the *Perl* script with the simply command line "`perl chemToRDE`" (without quote) in a console (terminal) screen, finally the results will be show in the output file (.tex):

```
\partial_t [E] - D_{E} \Delta [E] =
-12 (k_1)[E]^{12}[S]^3 + (k_2)[ES] -5 (k_3)[E]^5
\partial_t [S] - D_{S} \Delta [S] =
- 3 (k_1)[E]^{12}[S]^3 + (k_2)[ES]
\partial_t [ES] - D_{ES} \Delta [ES] =
+ (k_1)[E]^{12}[S]^3 - (k_2)[ES] + (k_3)[E].
```

Working together with some commonly LaTeX softwares and editors, the above results of our program is directly converted to

$$\partial_t[E] - D_E\Delta[E] = -12(k_1)[E]^{12}[S]^3 + (k_2)[ES] - 5(k_3)[E]^5$$
$$\partial_t[S] - D_S\Delta[S] = -3(k_1)[E]^{12}[S]^3 + (k_2)[ES]$$
$$\partial_t[ES] - D_{ES}\Delta[ES] = +(k_1)[E]^{12}[S]^3 - (k_2)[ES] + (k_3)[E].$$

References

[1] R.E. Blankenship. *Molecular Mechanisms of Photosynthesis*. Blackwell Science, 2002.

[2] W.K. Smith, T.C. Vogelmann, and C. Critchley. *Photosynthetic Adaptation Chloroplast to Landscape*. Springer,, 2004.

[3] Öpik H., Rolfe S.A., and A.J. Willis. *The Physiology of Flowering Plants*. Cambridge University Press. Chapter 2.

[4] Lincoln Taiz and Eduardo Zeiger. *Plant Physiology*. Sinauer Associates, Sunderland, MA, 5th edition, 2010.

[5] Laisk A., H. Eichelmann, and Oja. C_3 photosynthesis in silico. *Photosynth. Res.*, 90:45–66, October 2006.

[6] von S. Caemmerer, G.D. Farquhar, and A. J. Bery. *Advanced in Photosynthesis and Respiration*. Springer, 2009. Chapter 9 A biochemical model of C_3 photosynthesis.

[7] Govaerts Y.M., Jacquemoud S., Verstraete M.M., and Ustin S.L. Three-dimensional radiation transfer modeling in a dycotyledon leaf. *Applied Optics*, 35:6585–6598, 1996.

[8] Berdnik V. V. and Mukhamedyarov R. D. Radiative transfer in plant leaves. *Optics and Spectroscopy*, 90(4):652–663, 2001.

[9] D. Tholen and X. G. Zhu. The mechanistic basis of internal conductance: a theoretical analysis of mesophyll cell photosynthesis and CO_2 diffusion. *Plant Physiology*, 156:90–105, 2011.

[10] Aalto T. and Juurola E. A three-dimensional model of CO_2 transport in airspaces and mesophyll cells of silver birch leaf. *Plant cell Environ*, 25:1399–1409, 2002.

[11] Evans J. R, Kaldenhoff R., Genty B., and Terashima I. Resistances along the CO_2 diffusion pathway inside leaves. *J. Exp. Bot.*, 60:2235–2248, 2009.

[12] Farquhuar G. D. and Sharkey T.D. Stomatal conductance and photosynthesis. *Ann. Rev. Plant Physiol*, 33:317–345, 1982.

[13] Park S. Nobel. *Physicochemical and Environmental Plant Physiology*. Academic Press, 3rd edition, 2004.

[14] Jeff Hardin, Gregory Bertoni, and Lewis J. Kleinsmith. *Becker's world of the cell*. Pearson International Edition, 8th edition, 2012.

[15] F. Frost Blackman. Optima and limiting factors. *Annals of Botany*, pages 281–295, April 1905.

[16] F. Frost Blackman and Gabrielle L. C. Matthaei. Experimental researches in vegetable assimilation and respiration. iv.–a quantitative study of carbon-dioxide assimilation and leaf-temperature in natural illumination. *Proceedings of the Royal Society of London B: Biological Sciences*, 76(511):402–460, 1905.

[17] G. D. Farquhar, S. Von Caemmerer, and J. A. Berry. A biochemical model of photosynthetic CO_2assimilation in leaves of C_3 species. *Planta*, 149:78–90, 1980.

[18] O. Kull and B. Kruijt. Leaf photosynthetic light response: A mechanistic model for scaling photosynthesis to leaves and canopies. *Functional Ecology*, 12(5):767–777, 1998.

[19] T. D. Sharkey. Photosynthesis in intact leaves of C_3 plants: physics, physiology and rate limitations. *Botanical Review*, 51:53–105, 1985.

[20] T. D. Sharkey, C. J. Bernacchi, G. D. Farquhar, and E. L. Singsaas. Fitting photosynthetic carbon dioxide response curves for C_3 leaves. *Plant, Cell and Environment*, 30(9):1035–1040, September 2007.

[21] Brian D. Hahn. A mathematical model of leaf carbon metabolism. *Annals of Botany*, 54:325–339, 1984.

[22] Brian D. Hahn. A mathematical model of the calvin cycle: Analysis of the steady state. *Annals of Botany*, 57:639–653, 1986.

[23] Brian D. Hahn. A mathematical model of photorespiration and photosynthesis. *Annals of Botany*, 60:157–169, 1987.

[24] Brian D. Hahn. Photosynthesis and photorespiration: Modelling the essentials. *Journal of Theoretical Biology*, 151(1):123–139, 123–139 1991.

[25] G. Pettersson and U. Ryde-Pettersson. A mathematical model of the calvin photosynthesis cycle. *European Journal of Biochemistry*, 175(3):661–672, August 1988.

[26] Mark G. Poolman, David A. Fell, and Simon Thomas. Modelling photosynthesis and its control. *Experimental Botany*, 51:319–328, 2000.

[27] Mark G. Poolman, Hülya Ölçer, Julie C. Lloyd, Christine A. Raines, and David A. Fell. Computer modelling and experimental evidence for two steady states in the photosynthetic calvin cycle. *European Journal of Biochemistry*, 268(10):2810–2816, May 2001.

[28] A. Laisk, H. Eichelmann, V. Oja, A. Eatherall, and D. A. Walker. A mathematical model of the carbon metabolism in photosynthesis. difficulties in explaining oscillations by fructose 2,6-bisphosphate regulation. *Proceedings of the Royal Society of London B: Biological Sciences*, 237(1289):389–415, 1989.

[29] Xin-Guang Zhu, Govindjee, Neil R. Baker, Eric de Sturler andDonald R. Ort, and S. P. Long. Chlorophyll a fluorescence induction kinetics in leaves predicted from a model describing each discrete step of excitation energy and electron transfer associated with photosystem ii. *Planta*, 223:114–133, 2005.

[30] Xin-Guang Zhu, Eric de Sturler, and Stephen P. Long. Optimizing the distribution of resources between enzymes of carbon metabolism can dramatically increase photosynthetic rate: a numerical simulation using an evolutionary algorithm. *Plant Physiology De Sturler E. & Long S.P.*, 145:513–526, 2007.

[31] Xin-Guang Zhu, Rafael Alba, and Eric de Sturler. A simple model of the calvin cycle has only one physiologically feasible steady state under the same external conditions. *Nonlinear Analysis: Real World Applications*, 10:1490–1499, 2009.

[32] Xin-Guang Zhu, Yu Wang, Donald R. Ort, and Stephen P. Long. e-photosynthesis: a comprehensive dynamic mechanistic model of C_3 photosynthesis: from light capture to sucrose synthesis. *Plant, Cell and Environment*, 36(9):1711–1727, September 2013.

[33] Laurence A. Moran, H. Robert Horton, K. Gray Scrimgeour, and Marc D. Perry. *Principle of biochemistry*. Pearson International Edition, 5th edition, 2012.

[34] Govindjee and R. Govindjee. Action spectra for the appearance of difference absorption bands at 480 and 520 mμ in illuminated chlorella cells and their possible significance to a two-step mechanism of photosynthesis. *Photochemistry and Photobiology*, 4(4):793–801, September 1965.

[35] Eugene I. Rabinowitch. *Photosynthesis and related processes,*, volume II. Interscience Publishers Inc., New York, 1951.

[36] Dmitriy Shevela, Roman Y. Pishchalinikov, Lutz A. Eichacker, and Govindjee. *Oxygenic Photosynthesis in Cyanobacteria*. Taylor & Francis, UK, 2013.

[37] Thomas Williams, Colin Kelley, and many others. Gnuplot 4.6: an interactive plotting program. http://gnuplot.sourceforge.net/, October 2013.

[38] Sandia National Labs, Kitware Inc, and Los Alamos National Labs. Paraview: Parallel visualization application. http://www.paraview.org/, 2005-2008.

[39] Thomas Richter. Introduction to gascoigne 3d high performance adaptive finite element toolkit. http://numerik.uni-hd.de/~richter/SS14/gascoigne/, April 2014.

[40] Roland Becker, Malte Braack, Thomas Dunne, Dominik Meidner, Thomas Richter, Michael Schmich, Winnifried Wollner, and Boris Vexler. Gascoigne3d: High performance adaptive finite element toolkit. http://www.gascoigne.de/, July 2002.

[41] Govindjee. *Bioenergetics of Photosynthesis*. Academic Press, London, 1975.

[42] Martin Kamen. *Primary Process of Photosynthesis*. Academic Press, New York, 1963.

[43] Peter Grunwald. Determination of effective diffusion coefficients - an important parameters for the efficiency of immobilized biocatalysts. *Biochemical Education*, 17(2):99–102, April 1989.

[44] AS Verkman. Solute and macromolecule diffusion in cellular aqueous compartment. *Trends Biochem. Sci.*, 27(1):27–33, January 2002.

[45] Hongbo Gao, Jeremy Metz, Nick A. Teanby, Andy D. Ward, Stanley W. Botchway, Benjamin Coles, Mark R. Pollard, , and Imogen Sparkes. In vivo quantification of peroxisome tethering to chloroplasts in tobacco epidermal cells using optical tweezers. *Plant Physiol*, 170(1):263–272, January 2016.

[46] Neil R. Baker. *Photosynthesis and the Environment*. Kluwer academic publishers, 2004. page 131.

[47] M. Ryczkowski. Changes of the viscosity of the central vacuolar sap during the development of the ovule. *Planta*, 55(4):357–364, October 1960.

[48] Valeriu Damiana, Adrian Sandub, Mirela Damianc, Florian Potrad, and Gregory R. Carmichael. The kinetic preprocessor kpp-a software environment for solving chemical kinetics. *Computers and Chemical Engineering*, 26(11):1567–1579, November 2002.

[49] Adrian Sandua, Dacian N. Daescub, and Gregory R. Carmichaelc. Direct and adjoint sensitivity analysis of chemical kinetic systems with kpp: Part i—theory and software tools. *Atmospheric Environment*, 37(36):5083–5096, November 2003.

[50] Adrian Sandua, Dacian N. Daescub, and Gregory R. Carmichaelc. Direct and adjoint sensitivity analysis of chemical kinetic systems with kpp: Ii—numerical validation and applications. *Atmospheric Environment*, 37(36):5097–5114, November 2003.

[51] Kenneth A. Connors. *Chemical Kinetics: The Study of Reaction Rates in Solution*. John Wiley & Sons, 1990.

[52] Encyclopaedia Britannica. Law of mass action. http://www.britannica.com/science/law-of-mass-action/, 2008.

[53] Ovidiu Pârvu. Guide: How to build ordinary differential equations corresponding to a set of chemical reactions or a petri net. http://brunel.ac.uk/~cspgoop/, October 2012.

[54] A. J. Davies. *The Finite Element Method: An Introduction with Partial Differential Equations*. Oxford university press, 2011.

[55] Lawrence C. Evans. *Partial differential equations*. Graduate studies in mathematics. American Mathematical Society, Providence (R.I.), 1998.

[56] Vidar Thomée. *Galerkin Finite Element Methods for Parabolic Problems*, volume Springer Series in Computational of *25*. Springer, 2006.

[57] Yifan Yang. *Mathematical Modeling and Simulation of the Evolution of Plaques in Blood Vessels*. PhD thesis, Ruprecht-Karls-Universität Heidelberg, 2014.